TECHNISCHE UNIVERSITÄT MÜNCHEN

Department Chemie
Lehrstuhl für Biotechnologie

Functional analysis of TPR cofactors of Hsp90

Veronika Haslbeck

Vollständiger Abdruck der von der Fakultät für Chemie der Technischen Universität München zur Erlangung des akademischen Grades eines Doktors der Naturwissenschaften genehmigten Dissertation.

Vorsitzender:		Univ.-Prof. Dr. Johannes Buchner
Prüfer der Dissertation:	**1.**	Priv.-Doz. Dr. Klaus Richter
	2.	Univ.-Prof. Dr. Andreas Bausch
	3.	Univ.-Prof. Dr. Michael Groll

Die Dissertation wurde am 19.06.2013 bei der Technischen Universität München eingereicht und durch die Fakultät für Chemie am 04.09.2013 angenommen.

SUMMARY

Aim of this thesis was to explore the cochaperone network of the molecular chaperone Heat Shock Protein 90 (Hsp90). Hsp90 has been discovered over 30 years ago in studies that analyzed the cellular reaction in fruit flies after heat shock where it appeared as a considerably enriched component of the heat stressed cytoplasm. Since then, many important signaling pathways and their operative proteins have been shown to directly depend on the chaperone. A vast number of cellular key players is processed or activated by Hsp90 and the help of its many cofactors. These so-called cochaperones bind at different interaction sites of the multi-domain protein Hsp90 and bring additional functions or certain client proteins to the chaperone module. This thesis is focused on a particular class of cochaperones which all contain a TPR domain to mediate binding to Hsp90.

Eukaryotic genomes encode an increasing number of TPR domain containing proteins according to their progression through evolution. Based on a bioinformatic approach, all TPR proteins from *C. elegans* were compiled and rated according to their probability to interact with Hsp90 and Hsp70. Subsequently, independent methods were applied for the detection of protein-protein interactions *in vitro* to validate the quality of the ranking. Generation and characterization of transgenic worms allowed the assignment of two uncharacterized open reading frames of *C. elegans* to well-studied human homologs. Finally, novel human TPR cochaperones could be identified by applying the same search algorithm on the human proteome. Hence, this study provides the first systematic approach to define the Hsp90 interacting TPRome in different organisms.

Another important TPR cochaperone, the protein phosphatase 5 (PP5), is a key player in the regulation of the protein phosporylation level in the cell. A high-throughput screen was performed that identified five compounds which are able to selectively increase PP5's activity up to 20-fold. The underlying mode of action was elucidated by crystal structures of a protein-activator complex as well as thorough enzymatic characterization. Studying the assembly of the nematode phosphatase cofactor with Hsp90 could further identify a new regulatory binding site in the protein complex.

In addition, the interplay between Hsp90 and its muscle-specific TPR cochaperone UNC-45 in muscle maintenance and motility of the living worm was investigated. Exploiting the small model organism *C. elegans* proved useful in studying the *in vivo* localization of both proteins, whereas *in vitro* characterization scrutinized the mode of binding between chaperone and cochaperone.

INDEX

***** These chapters are parts of accepted or submitted publications.

1. Introduction

1.1 Protein folding in the cell is assisted by molecular chaperones

A newly synthesized protein chain rearranges conformational states until its three dimensional structure, its so-called native state, is adopted. This conformation is defined by the one dimensional amino acid sequence that is encoded in the genome (Anfinsen, 1973; Anfinsen et al, 1961). In principle, interactions between the different residues of a polypeptide dictate the folding pathway and the formation of the secondary structure that leads to the final, usually globular fold of a protein. Several forces guide this process, like the formation of hydrogen bonds between H-bond donors and acceptors, Van der Waals interactions, electrostatic forces such as dipol-dipol interactions, but also the hydrophobic collapse that buries bulky non-polar residues and salt-bridged polar residues in the interior of the core of a globular protein to leave hydrophilic amino acids on the solvent exposed protein surface (Kiefhaber et al, 1991). The 3D structure is characterized by the angles Φ and Ψ connecting the Cα atoms with the peptide bonds of the protein backbone and the positioning of the side chains. The angles Φ and Ψ adopt values that are specific for the different secondary structure elements α-helix and β-sheet. The loops connecting different folding modules, however, are highly flexible and allow a huge variety of possibly folding intermediates until the final conformation is reached. One current hypothesis is that the protein undergoes these intermediate structures where subsequently new interactions are formed to guide the folding in a productive process to the native form (Dill & Chan, 1997).

In the cell, the nascent protein encounters a highly dense and crowded environment when it leaves the ribosome. The concentrated protein mixture as well as organelles and other macromolecules provide a diverse set of surfaces that can disturb the process of protein folding. Intermediate structures can expose hydrophobic patches that are burried in the final protein, but are sensitive to unproductive intra- or intermolecular interactions eventually causing protein misfolding or aggregation. To counteract this problem, so-called molecular chaperones evolved during evolution. Amongst them are the strictly conserved heat shock proteins Hsp90 and Hsp70 (Bukau et al, 2000; Bukau et al, 2006; Richter et al, 2010). Both, Hsp90 and Hsp70, are highly abundant and essential in the eukaryotic cell. In general, chaperones help guiding proteins through their folding

intermediates by transient interactions without becoming part of their final native state (Gething & Sambrook, 1992; Hartl, 1996).

While Hsp70 is a more general chaperone interacting rather unspecific with many different proteins, the clients of Hsp90 are more defined though large in number (www.picard.ch/downloads/Hsp90interactors.pdf). Interaction with Hsp90 can lead to conformational changes inducing ligand binding or full activation of the client. Therefore, client proteins of Hsp90 are supposed to be dependent of the chaperone in a certain state during their life cycle rather than during their initial folding process. A common feature of both Hsp70 and Hsp90, however, is the interplay of the chaperones with their so-called cochaperones that are able to modulate and fine-tune the chaperones' activities and may convey substrate specificity. Hsp90 as well as Hsp70 need to hydrolyze ATP while processing their substrates (Mayer & Bukau, 2005; Mayer et al, 2009). This enzymatic activity can be reduced or enhanced by certain cofactors such as Hop/Sti1, Aha1 for Hsp90 and the nucleotide exchange factors and J proteins for Hsp70, respectively. Cochaperones can be assigned into two groups, one containing only tetratricopeptide repeat domain (TPR domain) containing proteins and another group comprising all other cochaperones whose interaction with Hsp90 or Hsp70 is not dependent on a TPR domain interaction with the chaperones' C-terminal EEVD-motif (Rohl et al, 2013) (Figure 1.1). This thesis will focus on several TPR cofactors of Hsp90 and Hsp70 which will be introduced in the following sections.

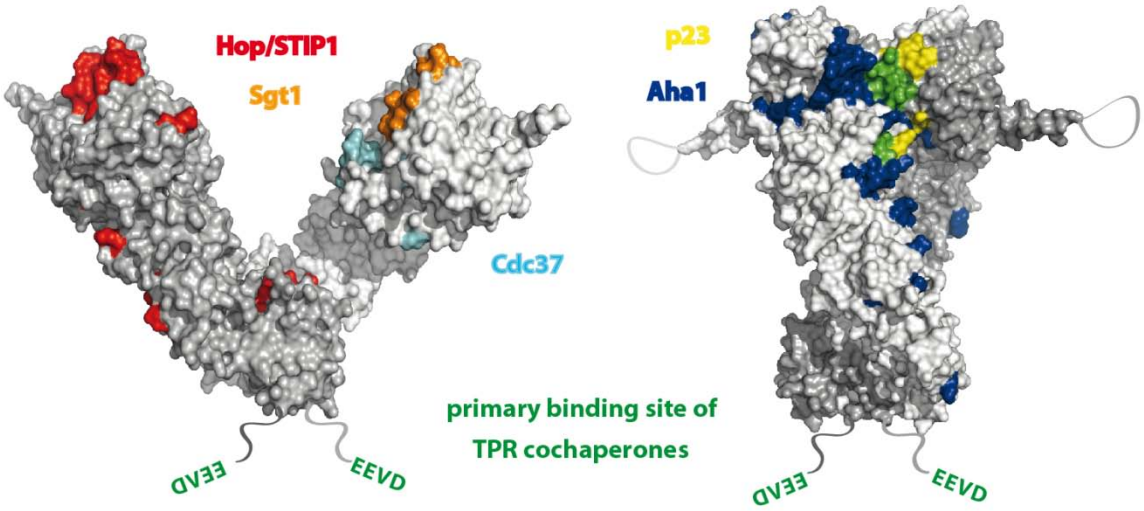

Figure 1.1. *Surface representation of open Hsp90 (PDB ID: 2IOQ, left) and closed Hsp90 (PDB ID: 2GC9, right) with the respective interaction sites for different TPR and non-TPR cochaperones indicated. Figure was adapted from(Rohl et al, 2013).*

1.2 TPR cochaperones modulate protein folding by Hsc70 and Hsp90*

*****This chapter is part of an article that was submitted for publication in the *Journal of Molecular Biology*.

The cytosolic chaperones Hsc70 and Hsp90 are molecular machines which convert the energy of ATP hydrolysis into conformational changes to support the folding and activation of substrate proteins (Mayer & Bukau, 2005; Mayer et al, 2009). They are not evolutionary related but share a common motif at the C-terminus which mediates the interaction with cofactors. In case of Hsp90, this motif is the strictly conserved amino acid sequence MEEVD, while in case of Hsc70/Hsp70, the motif is either IEEVD or LEEVD. The EEVD-motif is recognized by the TPR domain, which is used as protein-protein interaction module in an evolutionary conserved set of cofactors (D'Andrea & Regan, 2003). A TPR domain consists of 3 tetratrico peptide repeats with each folding into a helix-turn-helix module (Figure 1.2). In humans, the group of TPR cochaperones include the peptidyl-prolyl isomerases (PPIases) FKBP5, FKBP4, PPID and AIP, the myosin-interacting proteins UNC45A and UNC45B and the phosphatase PP5 (Bell & Poland, 2000; Ebong et al, 2011; Liu et al, 2008; Silverstein et al, 1997). Also the proteins STI1P, STUB1, ST13 and TTC4 contain TPR domains, which interact with the C-terminus of Hsc70 or Hsp90 (Crevel et al, 2008; Frydman & Hohfeld, 1997; Hohfeld et al, 1995; Murata et al, 2001; Scheufler et al, 2000). The binding of STI1P to Hsp90 regulates the ATP turnover, and brings the chaperones Hsc70 and Hsp90 into close proximity within one protein complex (Hessling et al, 2009; Prodromou et al, 1999; Schmid et al, 2012). The TPR containing PPIases which are specific for Hsp90 participate in the activation of substrate proteins by Hsp90 (Koren et al, 2011; Sivils et al, 2011). The same applies to the serine/threonine phosphatase PP5 which dephosphorylates Hsp90, its cochaperones and clients (Vaughan et al, 2008; Wandinger et al, 2006; Zhang et al, 2009).

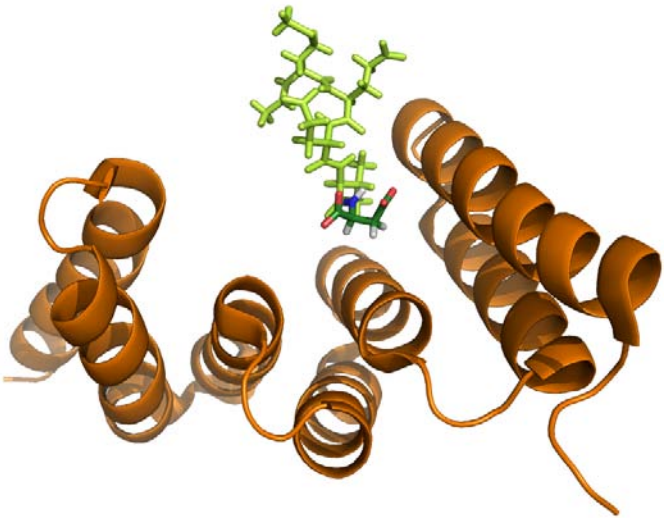

Figure 1.2. *The crystal structure of the TPR domain of human PP5 was solved in complex with the C-terminal MEEVD-motif of human Hsp90 (Cliff et al, 2006) (2BUG). The TPR domain is depicted in orange and the MEEVD-peptide in grey with the last Asp as the two carboxylate clamp-residue colored by element.*

Usually, the affinities of the EEVD-motif to TPR domains are in the range of 50 nM to 1 µM. Available crystal structures show that the peptide ligand is bound in an elongated stretch in a groove lined by the α-helices of the TPR domain (Cliff et al, 2006; Scheufler et al, 2000). In the case of PP5, the recognition of the MEEVD-peptide was reported to stabilize and compact the TPR domain representing a coupled folding and binding mechanism (Cliff et al, 2005). Other studies demonstrated that TPR domains can be folded and structured also in the absence of their peptide ligands (Cortajarena et al, 2010). The binding appears to rely mostly on the fixation of the VD-motif at the end of the C-terminal stretch (Carrello et al, 2004; Ramsey et al, 2009). Generally, a positively charged carboxylate clamp of the TPR binding groove complexes the C-terminal aspartate residue of the EEVD-motif and thereby ensures complex formation (Brinker et al, 2002; Russell et al, 1999; Scheufler et al, 2000). So far, a discrimination between Hsc70 and Hsp90 interacting TPR domains based on the sequence is not possible. It is likely that the TPR domain only represents one binding interface, while specificity for one chaperone might be determined by residues outside the peptide-TPR interaction (Brinker et al, 2002). An *in silico* approach to identify novel cochaperones based on the carboxylate-clamp residues was reported for the genome of *Arabidopsis thaliana* (Prasad et al, 2010). However, no proteome-wide approaches have been made to identify potential chaperone interacting TPR domains from the over 70 TPR proteins in nematodes and over 200 TPR proteins encoded in the human genome.

Beyond the established TPR containing cofactors of Hsp70 and Hsp90, a vast number of proteins are postulated to contain TPR domains based on a reliable prediction pattern for the TPR motif. Some of these proteins are known to employ their TPR domains for interactions with proteins outside the chaperone system. In general, the highly conserved TPR fold serves as a protein-protein interaction tool enabling protein assembly. The proteins Cdc16, Cdc23 and Cdc27 bind to the anaphase-promoting complex by means of their TPR domains (Schreiber et al, 2011). Another example is the *O*-Glc-NAc-transferase (OGT). Here, the TPR domain acts as docking site for substrates of the enzymatic domain of OGT (Iyer & Hart, 2003; Kreppel & Hart, 1999). The ligands for many uncharacterized TPR proteins though remain unknown and likewise their affinity to Hsc70 and/or Hsp90.

1.3 The TPR cofactor protein phosphatase 5 is an Hsp90-dedicated phosphatase*

*****This chapter is part of an article that will be submitted for publication.

Protein phosphatases are functional counterparts of kinases and are an integral part of cellular signal transduction. Collectively, both act as molecular check points within a wide spectrum of signaling cascades. Protein phosphatase 5 (PP5) belongs to small pool of intracellular protein phosphatases. It shares a high degree of homology within the phosphatase domain to PP1, PP2A and PP2B/PP3, all members of the phosphoprotein phosphatase (PPP) family. In contrast to the latter phosphatases, PP5 is composed of an N-terminal tetratricopeptide repeat (TPR) domain and a C-terminal αJ subdomain. The contact between those two locks the enzyme in an autoinhibited state (Chen et al, 1994; Yang et al, 2005) (Figure 1.3). While other PPP family members are modulated by the interaction of various subunits to control catalytic activity and substrate specificity of the holoenzyme (Moorhead et al, 2009), PP5's regulatory elements are encoded on the same polypeptide.

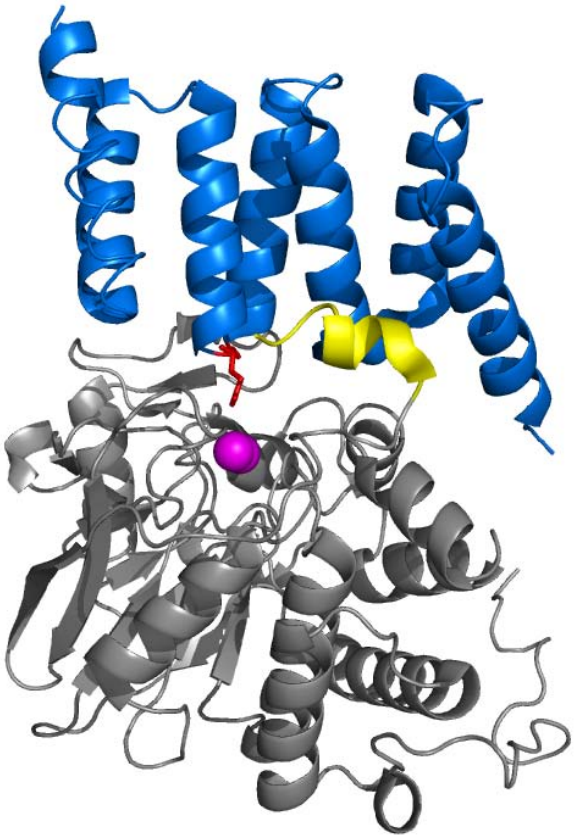

Figure 1.3. *The full-length crystal structure of human PP5 was solved by (Yang et al, 2005) (1WAO). The TPR domain is colored in blue, the catalytic phosphatase domain in grey, as well as the C-terminal αJ domain in yellow. The* Mn^{2+} *ions of the catalytic center are depicted in magenta and the inhibitory Glu76 sticking into the active site in red.*

In contrast to other PPP family members that are stimulated by accessory subunits, PP5 is an Hsp90-regulated enzyme (Ramsey & Chinkers, 2002; Yang et al, 2005). In the absence of the molecular chaperone Hsp90 PP5 exhibits only low basal activity. The C-terminal helix of PP5, the so-called αJ subdomain, binds the N-terminal TPR domain of PP5 and locks the enzyme in a latent state. In this conformation, residues of the TPR domain and αJ helix are positioned in a way that limits substrate entry to the active site of the phosphatase core domain (Yang et al, 2005). PP5 forms high affinity complexes with Hsp90 (Chen et al, 1996; Silverstein et al, 1997). In particular, the C-terminal MEEVD-peptide of Hsp90 is recognized by the phosphatase's TPR domain with low micromolar affinity and thereby, stabilizes the structure of the TPR domain of PP5 (Cliff et al, 2006). Hsp90-PP5 complexes have also been described in yeast and nematodes (Gaiser et al, 2010; Wandinger et al, 2006). This interaction consequently causes the release of the intramolecular contacts between TPR and αJ domain of autoinhibited PP5 and opens the active site access. Upon complex formation with Hsp90, the phosphatase activity of PP5

is fully activated and thus, diverse Hsp90-interacting proteins, e.g. Cdc37, can be dephosphorylated with increased rates (Vaughan et al, 2008; Wandinger et al, 2006). Cdc37 is a kinase-dedicated Hsp90 co-chaperone that delivers immature kinases to the Hsp90 chaperone machinery. Its dephosphorylation by PP5 represents a critical step within the activation of kinase clients of Hsp90 (Vaughan et al, 2008). It has been suggested that Hsp90 may enhance the phosphatase activity of PP5 also towards Hsp90-attached phosphate residues. This mode of action permits a PP5-dependent control of the Hsp90-chaperone machinery (Wandinger et al, 2006).

PP5 is localized in the cytosol and nucleus and is predominantly found in the brain (Bahl et al, 2001; Chen et al, 1994; Galigniana et al, 2002). This protein is known to be involved in various cellular processes, ranging from steroid hormone receptor regulation, cell cycle control to neuronal degeneration. Early studies have identified PP5 as part of Hsp90-glucocorticoid receptor (GR) complexes (Silverstein et al, 1997). Later, PP5 was shown to affect the translocation of the hormone-activated complex into the nucleus and to directly dephosphorylate GR complexes (Davies et al, 2005; Dean et al, 2001; Wang et al, 2007). After DNA-damage or during cell cycle control, PP5 is able to dephosphorylate the kinases ASK1 and DNA-PKcs. In addition, PP5 is associated with the G1/S-phase checkpoint regulators ATM and ATR (Ali et al, 2004; Hinds & Sanchez, 2008; Morita et al, 2001; Wechsler et al, 2004; Zhang et al, 2009). Hyperphosphorylation of the human microtubule-associated protein tau has been suggested to be crutial in the pathogenesis of tauopathies such as Alzheimers's disease (AD). Tau is phosphorylated by a variety of protein kinases and hyperphosphorylation promotes its dissociation from axonal microtubules (Brunden et al, 2009; Mandelkow & Mandelkow, 2012). Hyperphosphorylated tau can be dephosphorylated by PP5 and other PPP family members (Liu et al, 2005a; Liu et al, 2005b). Interestingly, activity levels of PP5 have been found to be reduced in AD brains (Liu et al, 2005a). These findings imply that enhanced phosphatase activities, including that of PP5, may cause beneficial effects in AD and other human tauopathies.

Despite the important cellular functions of protein phosphatases, only a few small molecule inhibitors, which are highly selective for certain members of the PPP family, have been identified yet (McConnell & Wadzinski, 2009). Arachidonic acid and its derivatives have been found to stimulate PP5, but the physiological relevance remains elusive (Cher et al, 2010; Kang et al, 2001; Ramsey & Chinkers, 2002). Efforts to analyze

the underlying mode of activation have suggested a crucial involvement of the PP5 TPR domain which releases the autoinhibition of the enzyme upon binding of arachidonic acid (Cher et al, 2010). Contrarily, synthetic small molecule activators that target PP5 have not been identified so far.

1.4 Hsp90 and its TPR cofactor Unc45 are important for correct muscle development

* This chapter is part of an article published in *Biochimica et Biophysica Acta Molecular Cell Research* (Haslbeck et al, 2012).

The TPR-containing cofactor of Hsp90, Unc45, has long been known to be involved in the maintenance of motility. In fact, this cofactor had originally been discovered in 1974 in large scale screens of mutated *C. elegans* strains by Sydney Brenner as allele e286 (Brenner, 1974). This allele was shown to be responsible for a motility defect, resulting in the assignation of the ’unc–‘ identifier, which relates to the ’uncoordinated’ movement of the nematodes. Further characterization of the strain *unc-45(e286)* showed that the unc-phenotype was inducible and reversible by temperature shifts during larval stages (Epstein & Thomson, 1974). Later, a point mutation in the myosin binding UCS domain of Unc45 (L822F) was assigned to the allele e286 (Barral et al, 1998). The TPR protein is attached to and implicated in the correct assembly of thick filaments in the nematode muscle cells (Ao & Pilgrim, 2000; Venolia & Waterston, 1990). In *C. elegans* the 95 striated body wall muscle cells form one of the largest tissues in the adult organism (Moerman & Fire, 1997). Muscle cells are positioned in double rows in four longitudinal quadrants. In adult nematodes Unc45 is expressed intensively in muscle cells (Venolia et al, 1999).

Extensive studies by the Straehle group and others highlighted Hsp90 and Unc45 both being relevant for the formation of myosin fibers also in zebrafish (Bernick et al, 2010; Du et al, 2008; Wohlgemuth et al, 2007). Truncation of Hsp90a.1 in zebrafish completely disrupts thick and thin filament organization (Codina et al, 2010; Hawkins et al, 2008). It is noteworthy that a high degree of specialization of the Hsp90a isoform has taken place in this organism. Although both are expressed in skeletal and cardiac muscles, only knockdown of Hsp90a.1 develops a muscular phenotype with immotile embryos and disorganized myofibrils. Depletion of Hsp90a.2, however, has almost no effect on

myofibrillogenesis (Etard et al, 2007; Hawkins et al, 2008). An Unc45 mutant in zebrafish was initially named *steif*, relating to the stiffness of the body structure in the event of Unc45 loss (Behra et al, 2002), a phenotype that closely resembles knockdown of the muscle specific Hsp90a.1 (Etard et al, 2007). Studies in this model system revealed a surprising plasticity of Hsp90a.1 and Unc45, which both change their subcellular localization upon muscle lesion (Etard et al, 2008). Apparently, Unc45 and Hsp90 are retained at the Z-line in a highly dynamic state and move to become associated to the A-band after damage (Figure 1.4). This study highlights a potential repair function of fiber-bound Unc45 and Hsp90, which is obvious in response to lesions, but also might be constantly required under normal growth conditions as well. Also the protein levels of Unc45 are tightly regulated. Hoppe and coworkers could identify a CHIP-dependent degradation pathway of Unc45 in nematodes. The E3/E4-ligase CHIP was initially identified as a cochaperone of Hsp70 that also interacts with Hsp90 (Ballinger et al, 1999; Murata et al, 2001). The *C. elegans* ortholog CHN-1 was shown to be responsible for the polyubiquitylation of Unc45 *in vivo* together with the E4 conjugating factor UFD-2 (Hoppe et al, 2004). Hence, another member of the Hsp90 network is directly responsible for the regulation of Unc45.

A systematic RNAi screen targeting muscle development in *Drosophila melanogaster* confirmed the conserved role of Hsp90 and its cofactor Unc45. The muscular depletion of Hsp90 or Unc45 was lethal in early development. Both knockdowns cause defects in myofibril organization (Schnorrer et al, 2010). A recent study affirmed by rescue experiments that the cochaperone Unc45 is indispensible for myosin fibril organization in the fly muscle (Lee et al, 2011).

The function of Unc45 is not restricted to muscle cells, though. In zebrafish, mouse and human two Unc45 isoforms have been identified which are differentially expressed in either various tissues (Unc45a or general cell GC-Unc45) or exclusively in cardiac or skeletal muscle cells (Unc45b or striated muscle SM-Unc45) (Etard et al, 2007; Price et al, 2002; Wohlgemuth et al, 2007). In most tissues of higher eukaryotic organisms like zebrafish the Unc45a isoform is responsible to safeguard non-muscular myosin, which is needed for general cellular processes like cytokinesis and cell migration (Edwards & Kiehart, 1996). This distinction is not found in nematodes and *Drosophila* (Etheridge et al, 2002; Hutagalung et al, 2002; Price et al, 2002). Here, beyond its function in muscle cells, the sole Unc45-paralog additionally cooperates with the non-muscle myosin II

(NMY-2) in early embryogenesis to establish polarity and ensure correct cytokinesis (Kachur et al, 2004; Kachur et al, 2008).

It is still unclear how Unc45 and Hsp90 work together. At the N-terminus, Unc45 contains a TPR-domain with close homology to the TPR-domains shared by several other Hsp90 cochaperones (Venolia et al, 1999). *In vitro* studies indicate that Unc45 binds to Hsp90 via this domain (Barral et al, 2002). It additionally contains a UCS (**U**nc-45/**C**RO1/**S**he4p) domain at its C-terminus, which was shown to be responsible for type II myosin binding and Hsp90-dependent folding of the myosin motor domain. Furthermore, Hsp90 stabilizes the myosin motor domain and prevents its aggregation *in vitro* (Barral et al, 2002; Liu et al, 2008; Srikakulam et al, 2008) and it was shown that a complex of Unc-45, Hsp90 and the myosin II protein Unc-54 can be detected *in vitro* (Barral et al, 2002).

In muscular cells it remains an open question, whether the involvement of Hsp90 is required at the assembled myofibrils, or whether Hsp90 and Unc45 cooperate to chaperone the folding of monomeric myosin proteins. Cooperation of both proteins may not be a conserved feature in yeast, as the Unc45 homolog She4p lacks the Hsp90-interacting TPR-domain. She4p appears to work independently of Hsp90 to chaperone myosins (Toi et al, 2003; Wesche et al, 2003). Thus, it is possible that this very specific activity of Hsp90 is a feature arising together with the development of a highly specialized muscular tissue in metazoans.

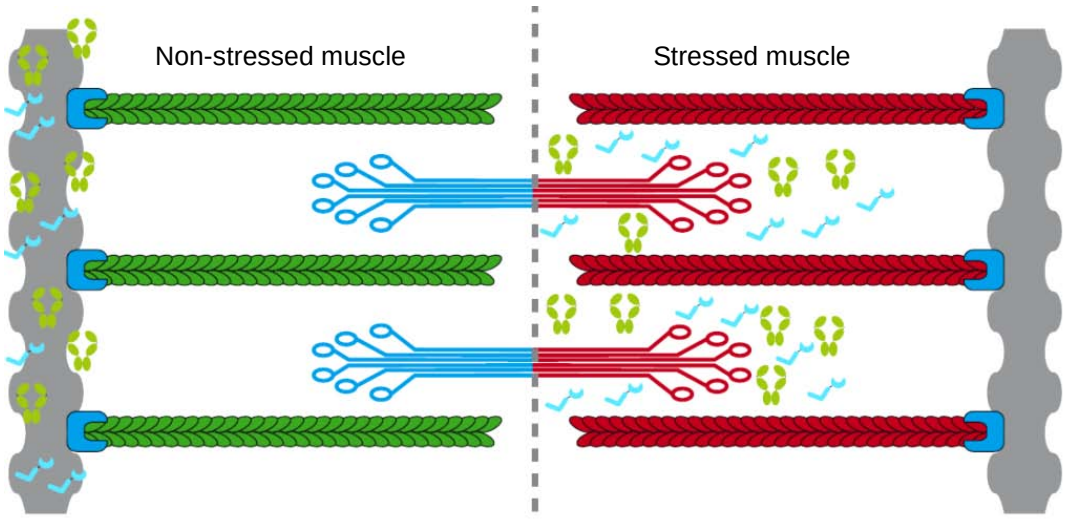

Figure 1.4. *Schematic localization of Hsp90 and UNC-45 in the muscle cell. Non-stressed (left) and stressed (right) conditions are depicted with either Hsp90 (light green) and UNC-45 (light blue) associated to the Z-line (grey) or, in case of muscular stress, tranlocating to the A-band. The figure was taken from (Haslbeck et al, 2012).*

1.5 The model organism *C. elegans* allows *in vivo* and *in vitro* analysis of the Hsp90-cochaperone system

* This chapter is part of an article published in *Biochimica et Biophysica Acta Molecular Cell Research* (Haslbeck et al, 2012).

The Hsp90-cochaperone network has been studied in yeast and mammalian cell culture for many years. These systems lack, however, the individual impact of either Hsp90 or its cofactors on the different tissues and cell types of metazoans. Exploiting the simple model organism *C. elegans* allows monitoring of disruptions within the Hsp90 system *in vivo* and the consequences these inflict on the growth and development of the model system. Genome-wide approaches have been performed to identify homozygous nematode knockout strains for non-essential genes and heterozygous or temperature-sensitive strains for essential genes (Barstead & Moerman, 2006; Duverger et al, 2007; Gengyo-Ando & Mitani, 2000). Furthermore, dsRNA encoding plasmids have been generated for close to 90% of the nematode genes as well as a wealth of knockdown data on a genome wide level are available (Kamath et al, 2003; Rual et al, 2004). These studies show that several of the cofactors, like p23 and Hop/Sti1, can be knocked out without lethal effect on the organism (Barstead & Moerman, 2006; Song et al, 2009). Mutations in CHIP or Unc45 instead generate developmental phenotypes (Epstein & Thomson, 1974; Khan & Nukina, 2004). Based on these resources, it is possible to connect *in vivo* and *in vitro* approaches, by rescuing a phenotype through the expression of either the wildtype protein or a modified version. In this way, the functionality of a mutant protein is addressable in selected tissues simply by generating trangenic nematode strains carrying tissue-specific promoters.

Another way to analyze protein activities *in vivo* is the overexpression of fluorescently tagged proteins to observe their subcellular localization. One such example is the cofactor p23 in *C. elegans*. This protein apparently is not essential under normal growth conditions as homozygous knockout strains were successfully generated. Overexpressed fluorescently-tagged p23 nevertheless compromises muscle structure and accumulates at the myofibrillar lattice (Meissner et al, 2011). These microscopically observable effects might consequently be utilized to study protein functions in the cellular environment and address the impact of an introduced mutation.

The available collections of nematode cDNAs further allow studying the proteins and their functionality in the absence of the complex organism. Genome-wide two-hybrid

experiments revealed networks of protein-protein interactions for the *C. elegans* proteome (Li et al, 2004). Studying these online accessible networks for *C. elegans* reveals a wealth of information on potential cofactors and client proteins of the Hsp90 system. The direct biochemical analysis of purified proteins has already been performed for several of the nematode Hsp90 cofactors. Studies aimed at understanding the biochemical mechanism of the cofactor Hop/Sti1, which despite the absence of the N-terminal TPR and DP1 domains appears functional in most aspects regarding the interaction with Hsp90 (Gaiser et al, 2009). It further has been shown, that the activity of the cofactors like CDC-37 and PPH-5 concerning the interaction with Hsp90 and the influence on the enzymatic turnover is well conserved (Gaiser et al, 2010). Additionally, the binding of SGT-1 and FKB-6 to the highly conserved C-terminal MEEVD-motif of Hsp90 was confirmed, implying that also TPR-containing cofactors interact with Hsp90 in a conserved manner (Richardson et al, 2007; Worrall et al, 2008).

While large parts of the biochemistry may be conserved between yeast, the metazoan model proteins and human proteins, the wealth of well observable traits in combination with the potential to study protein functionality in the living model system of *C. elegans* provides a platform that allows addressing the mechanistic aspects of protein-protein interactions and their influence on the organismal development.

1.6 Objectives of the thesis

1.6.1 Identification of TPR cofactors by TPRome analysis of *C. elegans*

Eukaryotic genomes encode diverse set of TPR domain containing proteins. Amongst these various interactors of the Hsp90/Hsc70 chaperone system can be found. However, the binding partner or any functional information for many uncharacterized TPR proteins is still missing. Therefore, the so-called TPRome of *C. elegans* was analyzed in this study using the software HMMER3.0 to predict the binding potential of each TPR protein to the Hsp90/Hsc70 chaperone system. By ranking of all TPR proteins a threshold was postulated for the distinction of TPR cochaperones versus non chaperone-interacting TPR proteins. *In vitro* and *in vivo* analysis of three uncharacterized ORFs of *C. elegans* should then support the computational approach and validate the prediction. The aim of this project was to develop a fast method to identify chaperone-interacting cofactors from any

annotated genome. Therefore, the prediction and *in vitro* characterization should be expanded to promising candidates of the human TPRome.

1.6.2 Activator screen and characterization of the nematode protein phosphatase 5

The nematode homolog of human PP5 is a clinically very interesting target and its activation might prove beneficial for the treatment of various neurodegenerative diseases or cancer. Different screening approaches for this protein have been established, but could only provide weakly binding activating substances. One aim of this thesis was to identify new potent PP5 activators with potential *in vivo* efficacy. Therefore, a synthetic library was screened for compounds that enhance PP5 activity. The characterization of small molecule effectors of PP5 and their mode of action should provide a strategy for a selective activation of this phosphatase. Furthermore, the interplay between the protein phosphatase 5 and Hsp90 is not fully understood to date. A thorough analysis of nematode PPH-5 activation by Hsp90 as well as protein-protein interaction studies was performed in this work to elucidate the tight regulation mechanism that Hsp90 imposes onto its dedicated phosphatase.

1.6.3 Analysis of the Hsp90-UNC-45 interaction

The implications of the Hsp90 TPR cofactor UNC-45 in muscle development have been studied for many years. Advanced microscopy techniques taking advantage of temporal and spatial resolution methods allowed the analysis of protein localization of Hsp90 and UNC-45 *in vivo* and their migration in response to muscle lesion. However, data concerning the interaction sites between the TPR protein and the molecular chaperones Hsp90 and Hsc70 are still a matter of debate. In the last part of the thesis *in vitro* experiments with the purified proteins UNC-45, Hsp90 and Hsc70 should clarify the role of the TPR domain regarding chaperone interactions. Generation of a transgenic nematode expressing Hsp90-YFP(li) and UNC-45-CFP in muscles will allow further studies of the proteins' interplay in the living nematode.

2. Materials and methods

2.1 Materials

2.1.1 Strains and organisms

Table 2.1.1. *Strains and organisms.*

	description	**origin**
***E. coli* strains**		
E. coli XL1 DH10B	F-*mcr*A Δ(*mrr-hsd*RMS-*mcr*BC) ϕ80*lac*Z ΔM15 Δ *lac*X74 recA1 *end*A1 *ara*D139 Δ(*ara*,*leu)*7697 *gal*U *gal*Kλ- *rps*L *nup*G *ton*A	Stratagene
E. coli BL21 (DE3)	F- *ompT* hsdS(rB-mB-) dcm+ *Tet*r gal1 (DE3) *end*A *Hte [argU ileY leuW*camR]	Stratagene
E. coli HT115 (DE3)	for RNAi experiments with *C. elegans*	CGC
E. coli OP50	for feeding of *C. elegans*	CGC
***C. elegans* strains**		
N2	wild type strain	CGC
YFP-DAF-21/UNC-45-CFP	stable, double injected (plasmids #67 and #79) transgenic nematode	this work
C34B2.5-YFP/CFP-HSP-1	stable, double injected (plasmids #69 and #71) transgenic nematode	this work
ZK370.8-YFP	stable, single injected (plasmid #73) transgenic nematode	this work

2.1.2 Plasmids

Table 2.1.2. *Plasmids.*

#	**name**	**plasmid for**	**origin**
1	pET28-PPH-5	PPH-5 (*C. elegans*) expression	Dr. Klaus Richter (TUM)
2	pET28-C34B2.5	C34B2.5 (*C. elegans*) expression	this work
3	pET28-C34B2.5-F29S	C34B2.5-F29S variant expression	this work
4	pET28-C34B2.5-F29A	C34B2.5-F29A variant expression	this work
5	pET28-C34B2.5-K22S	C34B2.5-K22S variant expression	this work
6	pET28-C34B2.5-E85G	C34B2.5-E85G variant expression	Dr. Klaus Richter (TUM)
7	pET28-C34B2.5-aa1-119	C34B2.5 deletion variant expression	this work
8	pET28-C34B2.5-aa1-139	C34B2.5 deletion variant expression	this work
9	pET11-C34B2.5	C34B2.5 His-tag free expression	this work
10	pAS-C34B2.5	yeast-two-hybrid bait C34B2.5	Julia Eckl (TUM)
11	pAS-C34B2.5-F29A	yeast-two-hybrid bait C34B2.5-F29A	Julia Eckl (TUM)
12	pAS-C34B2.5-K22S	yeast-two-hybrid bait C34B2.5-K22S	Julia Eckl (TUM)
13	pET28-F52H3.5	F52H3.5 (*C. elegans*) expression	this work
14	pET28-F52H3.5-C163R	F52H3.5 variant expression	Dr. Klaus Richter (TUM)
15	pET28-C33H5.8	C33H5.8 (*C. elegans*) expression	this work
16	pET28-C33H5.8-aa1-116	C33H5.8 deletion variant expression	this work
17	pET28-C33H5.8-aa1-122	C33H5.8 deletion variant expression	this work
18	pET28-SUMO-C33H5.8	SUMO-C33H5.8 fusion del. var. exp.	
19	pET28-ADPR-1	ADPR-1 (*C. elegans*) expression	this work
20	pET28-ADPR-1-aa272-408	ADPR-1 deletion variant expression	this work
21	pET28-ZK370.8	ZK370.8 (*C. elegans*) expression	this work
22	pET28-ZK370.8-aa34-554	ZK370.8 deletion variant expression	this work
23	pET28-ZK370.8-aa1-164	ZK370.8 deletion variant expression	this work
24	pET28-ZK370.8-aa34-164	ZK370.8 deletion variant expression	this work
25	pET28-ZK370.8-aa34-167	ZK370.8 deletion variant expression	this work
26	pET28-SUMO-ZK370.8-aa34-554	SUMO-ZK370.8 fusion del. var. exp.	
27	pET28-UNC-45	UNC-45 (*C. elegans*) expression	this work
28	pET28-UNC-45-aa1-114	UNC-45 deletion variant expression	this work

29	pET28-UNC-45-aa1-126	UNC-45 deletion variant expression	this work
30	pET28-CHN-1-aa1-122	CHN-1 deletion variant expression	this work
31	pET28-PPH-5	PPH-5 (*C. elegans*) expression	Dr. Klaus Richter (TUM)
32	pET28-PPH-5-aa21-124	PPH-5 deletion variant expression	this work
33	pET28-PPH-5	PPH-5 deletion variant expression	this work
34	pET28-PPH-5-aa21-141	PPH-5 deletion variant expression	this work
35	pET28-PPH-5-aa1-485	PPH-5 deletion variant expression	this work
36	pET28-PPH-5-aa1-490	PPH-5 deletion variant expression	this work
37	pET28-PPH-5-aa184-313	PPH-5 deletion variant expression	this work
38	pET28-PP5	PP5 (*R. norvegicus*) expression	this work
39	pET28-PP5-aa166-499	PP5 (*R. norvegicus*) del. var. exp.	this work
40	pET28-PP5-aa170-499	PP5 (*R. norvegicus*) del. var. exp.	this work
41	pET28-PP5-aa16-499	PP5 (*R. norvegicus*) del. var. exp.	this work
42	pET28-PP5-aa1-491	PP5 (*R. norvegicus*) del. var. exp.	this work
43	pET28-PP5-aa1-483	PP5 (*R. norvegicus*) del. var. exp.	this work
44	pET28-SMA-4	SMA-4 (*C. elegans*) expression	this work
45	pET28-Smad4	Smad4 (*H. sapiens*) expression	this work
46	pET28-Ask1-aa655-960	Ask1 (*H. sapiens*) del. var. exp.	this work
47	pET28-Ask1-aa655-1064	Ask1 (*H. sapiens*) del. var. exp.	this work
48	pET28-WDTC1	WDTC1 (H. sapiens) expression	this work
49	pET28-WDTC1-aa346-490	WDTC1 (*H. sapiens*) del. var. exp.	this work
50	pET28-TTC12-aa98-224	TTC12 (*H. sapiens*) del. var. exp.	this work
51	pET28-LONRF3N-aa213-396	LONRF3N (*H. sapiens*) del. var. exp.	this work
52	pET28-TTC9-aa20-220	TTC9 (*H. sapiens*) del. var. exp.	this work
53	pET28-Y71G12B.27	Y71G12B.27 (*C. elegans*) expression	this work
54	pET28-DAF-21	DAF-21 (*C. elegans*)	Dr. Klaus Richter (TUM)
55	pET28-DAF-21N-YFP-DAF-21C	YFP fusion between aa230 and aa231	this work
56	pET28-YFP-DAF-21	YFP fusion N-terminal of DAF-21	this work
57	pET28-Hsp90β-aa538-724	Hsp90β (*H. sapiens*) del. var. exp.	this work
58	pET28-Hsp90β-aa563-724	Hsp90β (*H. sapiens*) del. var. exp.	this work
59	L4440-daf-21	daf-21-cDNA for gene knock-down	Thermo Fischer Scientific
60	L4440-unc-45	unc-45-cDNA for gene knock-down	Thermo Fischer Scientific
61	L4440-C33H5.8	C33H5.8-cDNA for gene knock-down	Thermo Fischer Scientific
62	L4440-C34B2.5	C34B2.5-cDNA for gene knock-down	Thermo Fischer Scientific
63	L4440-F52H3.5	F52H3.5-cDNA for gene knock-down	Thermo Fischer Scientific
64	L4440-F26D10.3	F26D10.3-cDNA for gene knock-down	Thermo Fischer Scientific
65	L4440-unc-45-bp1-440	unc-45-cDNA bp1-440 for knock-down	this work
66	pPD95.79m	modified pPD95.79 vector	Dr. Klaus Richter (TUM)
67	pPD95.79m-YFP-DAF-21	YFP fusion N-terminal of DAF-21 under muscular promotor for injection	this work
68	pPD95.79m-DAF-21N-YFP-DAF-21C	YFP fusion between aa230 and aa231 of DAF-21 under muscular promotor for injection	this work
69	pPD95.79m-C34B2.5::C34B2.5-YFP	C-terminal YFP fusion of C34B2.5 under C34B2.5 endogenous promotor for injection	Dr. Klaus Richter (TUM)
70	pPD95.79m-C34B2.5::C34B2.5-CFP	C-terminal CFP fusion of C34B2.5 under C34B2.5 endogenous promotor for injection	this work
71	pPD95.79m-C34B2.5::CFP-HSP-1	N-terminal CFP fusion of HSP-1 under C34B2.5 endogenous promotor for injection	this work
72	pPD95.79m-C33H5.8::C33H5.8-YFP	C-terminal YFP fusion of C33H5.8 under C33H5.8 endogenous promotor for injection	this work
73	pPD95.79m-ZK370.8::ZK370.8-YFP	C-terminal YFP fusion of ZK370.8 under ZK370.8 endogenous promotor for injection	this work
74	pPD95.79m-ZK370.8::ZK370.8-CFP	C-terminal CFP fusion of ZK370.8 under ZK370.8 endogenous promotor for injection	this work
75	pPD95.79m-PPH-5::PPH-5-YFP	C-terminal YFP fusion of PPH-5 under PPH-5 endogenous promotor for injection	this work
76	pPD95.79m-PPH-5::PPH-5-CFP	C-terminal CFP fusion of PPH-5 under PPH-5 endogenous promotor for	this work

		injection	
77	pPD95.79m-PPH-5::YFP	YFP under PPH-5 endogenous promotor for injection	this work
78	pPD95.79m-PPH-5::CFP	CFP under PPH-5 endogenous promotor for injection	this work
79	pPD30.38-UNC-45-CFP	C-terminal CFP fusion of UNC-45 under muscular promotor for injection	this work
80	pET28-YFP-PPH-5	N-terminal YFP fusion to PPH-5	this work
81	pET28-YFP-ZK370.8-aa34-554	N-terminal YFP fusion to ZK370.8-aa34-554	this work
82	pET28-YFP-Smad4	N-terminal YFP fusion to huSmad4	this work
83	pET28-CFP-DAF-21	N-terminal CFP fusion to DAF-21	this work
83	pET28-ScDia2-TPR	Dia2-aa1-169 (*S. cerevisiae*)	this work
84	pET28-ScSwa2-TPR	Swa2-aa362-527 (*S. cerevisiae*)	this work

2.1.3 Chemicals

Table 2.1.3. *Chemicals.*

name	**origin**
Acrylamide (38%, 2% Bisacrylamide)	Roth (Karlsruhe, Germany)
Agarose, ultra pure	Roth (Karlsruhe, Germany)
Ammoniumperoxodisulfate (APS)	Roche (Mannheim, Germany)
Ampicillin	Roth (Karlsruhe, Germany)
Adenosin-5'-triphosphate (ATP) disodium salt	Roche (Mannheim, Germany)
Radioactive ATP	Hartmann Analytics (Braunschweig, Germany)
Agar Agar	Serva (Heidelberg, Germany)
Agarose	Serva (Heidelberg, Germany)
Bacto Agar	Difco (Detroit, USA)
Bacto Tryptone	Difco (Detroit, USA)
Bacto Yeast Extract	Difco (Detroit, USA)
Bromphenolblue S	Serva (Heidelberg, Germany)
Protease Inhibitor Mix HP	Serva (Heidelberg, Germany)
5-(and-6)-Carboxyfluorescein succinimidyl ester (FAM)	Invitrogen (La Jolla, USA)
Cholesterol	Sigma (St. Louis, USA)
Coomassie Brilliant-Blue R-250	Serva (Heidelberg, Germany)
Coomassie Protein Assay Reagent	Pierce (Rockford, USA)
5,5’ Dithio-bis-Nitrobenzoic acid (DTNB)	Sigma (St. Louis, USA)
1,4-Dithiothreitol (DTT)	Roth (Karlsruhe, Germany)
Deoxynucleoside triphosphates (dNTPs)	Roche (Mannheim, Germany)
Dimethyl sulfoxide (DMSO)	Sigma (St. Louis, USA)
ECL-Westernblot Detection System	GE Healthcare (Munich, Germany)
Ethylendiamintetraacidic acid (EDTA)	Merck (Darmstadt, Germany)
Ethidiumbromide	Sigma (St. Louis, USA)
Formaldehyde, 37% p.A.	Roth (Karlsruhe, Germany)
Glutaraldehyd, 25% in water	Serva (Heidelberg, Germany)
Glycerol, 99 %	ICN, Costa Mesa, USA
Glycine	Roth (Karlsruhe, Germany)
HEPES	ICN (Costa Mesa, USA)
Imidazole	Sigma (St. Louis, USA)
Isopropanol	Roth (Karlsruhe, Germany)

Isopropyl-β-D-thiogalaktopyranosid (IPTG)	Roth (Karlsruhe, Germany)
Kanamycin	Roth (Karlsruhe, Germany)
LB medium	Serva (Heidelberg, Germany)
β-Mercaptoethanol, pure	Merck (Darmstadt, Germany)
Milk powder	Roth (Karlsruhe, Germany)
NADH	Roche (Mannheim, Germany)
Peptides (AEEDASRMEEVD, GGAGGPTIEEVD)	Biomatik (Cambridge, Ontario, Canada)
Phosphoenolpyruvate (PEP)	Sigma (St. Louis, USA)
P5SA-1 (5638-0063)	ChemDiv (San Diego, California, USA)
P5SA-2 (C301-7823)	ChemDiv (San Diego, California, USA)
P5SA-3 (E635-0056)	ChemDiv (San Diego, California, USA)
P5SA-4 (G199-1264)	ChemDiv (San Diego, California, USA)
P5SA-5 (G839-0123)	ChemDiv (San Diego, California, USA)
Sodiumdodecylsulfate (SDS)	Roth (Karlsruhe, Germany)
Stain G	Sigma-Aldrich (Hamburg, Germany)
N,N,N´,N´-Tetramethylethylendiamine (TEMED)	Roth (Karlsruhe, Germany)
Polyoxyethylen-Sorbitan-monolaurat (Tween 20)	Merck (Darmstadt, Germany)
Protease inhibitor Mix FY, G, HP, M	Serva (Heidelberg, Germany)
TEMED	Roth (Karlsruhe, Germany)
Tris-(Hydroxymethyl)-aminomethane (Tris)	Roth (Karlsruhe, Germany)
Urea	Merck (Darmstadt, Germany)

2.1.4 Enzymes and standards

Table 2.1.4. *Enzymes and standards.*

device	**origin**
Restriction enzymes	New England Biolabs (Beverly, USA)
T4-Ligase	Promega (Madison, USA)
GoTaq DNA polymerase	Roche (Mannheim, Germany)
Pfu polymerase	Promega (Madison, USA)
Pyruvate kinase (PK)	Roche (Mannheim, Germany)
Trypsin	Sigma-Aldrich (Hamburg, Germany)
Low range molecular weight standard	BioRad Laboratories (München, Germany)
1 kb DNA-ladder	New England Biolabs (Beverly, USA)
ECL detection system	GE Healthcare (Freiburg Germany)
Roti Mark, prestained	Roth (Karlsruhe, Germany)

2.1.5 Kits, chromatography and other devices

Table 2.1.5. *Kits, chromatography and other devices.*

device	**origin**
Wizard Plus SV Miniprep DNA Purification System	Promega (Madison, USA)
Centricon microconcentrators	Millipore (Bedford, USA)
Blotting paper	Whatman
Immobilon-P membrane (PVDF)	Roth (Karlsruhe, Germany)

Dialysis tubes Spectra/Por (6-8 kDa)	Spectrum (Huston, USA)
Cuvettes, plastic, 1 mL	Brand
Sterile filter 0.2 µm	Zefa (München, Germany)
Ni-NTA (5 ml)	GE Healthcare (Freiburg Germany)
Q-Sepharose (150 mL)	GE Healthcare (Freiburg Germany)
Resource-Q (6 mL)	GE Healthcare (Freiburg Germany)
Superdex 75 Prep Grade (130 mL)	GE Healthcare (Freiburg Germany)

2.1.6 Media

Table 2.1.6. *Media.*

LB_0:	20	g/L			LB_0 medium adjust to 1 L with H_2O, autoclave
NGM (nematode growth medium):	7.5	g			peptone
	3	g			NaCl
	17	g			agar adjust to 1 L with H_2O, autoclave, cool to 55 °C
	25	ml	1	M	KH_2PO_4, pH 6.0
	1	ml	1	M	$CaCl_2$
	1	ml	1	M	$MgSO_4$
	1	ml	5	mg/mL	cholesterol
SOB:	0.5	% (w/v)			yeast extract
	2	%			tryptone
	10	mM			NaCl
	2.5	mM			KCl
	10	mM			$MgCl_2$
	10	mM			$MgSO_4$ adjust to 1 L with H_2O, autoclave
TB:	10	mM			HEPES/KOH or HCl, pH 6.7
	15	mM			$CaCl_2$
	250	mM			KCl
	55	mM			$MnCl_2$, add after adjusting pH sterilize by filtration with 0.45 µm

2.1.7 Buffers

Table 2.1.7. *Buffers.*

Molecular biology buffers:			
TAE (50x):	2	M	Tris/acetate, pH 8.0
	50	mM	EDTA
BJ (10x) :	50	% (v/v)	glycerol
	10	mM	EDTA, pH 8.0
	0.2	% (w/v)	bromphenoleblue
	0.2	% (w/v)	xylencyanol
Protein chemical buffers:			
SDS running buffer (10x):	250	mM	Tris/HCl, pH 6.8
	2	M	glycine
	1	% (w/v)	SDS
Laemmli sample buffer (5x):			
	312.5	mM	Tris/HCl, pH6.8
	10	% (w/v)	SDS
	25	% (v/v)	β-mercaptoethanol
	50	% (v/v)	glycerol
	0.05	% (w/v)	bromphenolblue
separating gel buffer (4x):	250	mM	Tris/HCl, pH 8.8
	0.8	% (w/v)	SDS
stacking gel buffer (2x):	250	mM	Tris/HCl, pH 6.8

	0.4	% (w/v)	SDS
Fairbanks A:	2.5	g	Coomassie Brilliant Blue R 250
	250	mL	ethanol
	80	mL	acetic acid
			adjust to 1 L with H_2O
Fairbanks D:	250	mL	ethanol
	80	mL	acetic acid
			adjust to 1 L with H_2O
Protein purification buffers:			
Ni-NTA:			
equilibration buffer:	40	mM	HEPES/KOH, pH 7.5
	20	mM	KCl
elution buffer:	40	mM	HEPES/KOH, pH 7.5
	20	mM	KCl
	400	mM	imidazole
denaturing buffer :	40	mM	HEPES/KOH, pH 7.5
	20	mM	KCl
	8	M	urea
	1	mM	DTT
Q Sepharose and Resource Q:			
low-salt-buffer:	40	mM	HEPES/KOH, pH 7.5
	10	mM	KCl
	1	mM	DTT
	1	mM	EDTA
high-salt-buffer:	40	mM	HEPES/KOH, pH 7.5
	1	M	KCl
	1	mM	DTT
	1	mM	EDTA
Size exclusion chromatography:			
SEC buffer:	40	mM	HEPES/KOH, pH 7.5
	300	mM	KCl
	1	mM	DTT
Final dialysis buffer			
(for protein storage):	40	mM	HEPES/KOH, pH 7.5
	20	mM	KCl
	1	mM	DTT

2.1.8 Equipment and computer programs

Table 2.1.8. *Equipment and computer programs.*

device	origin
Absorption Spectrophotometers	
Varian Cary 100 Bio UV-Vis-Spectrophotometer	Varian (Palo Alto, USA)
Circular dichroism spectropolarimeter	
Jasco J715 including PTC 343 Peltier temperature device	Jasco (Groß-Umstadt, Germany)
Fluorescence Spectrophotometer	
Spectrofluorometer: Jasco (with autopolarizers) with temperature adjustable cuvette holder	Spex (Edison, USA)
Analytical Ultracentrifuge	
XL-A equipped with absorbance and fluorescence detection systems	BeckmanCoulter (Krefeld, Germany) and AVIV Biomedical (Lakewood, USA)
Chromatography devices	
ÄKTA FPLC	GE Healthcare (Freiburg Germany)
HPLC devices	
HPLC-Device Pump System: PU-1580 Fluorescence Detector: FP-920 UV-Detector: UV-1575	Jasco (Großumstadt, Germany)
Gel electrophoresis devices	

Hoefer Mighty Small II	GE Healthcare (Freiburg, Germany)
Power amplifier	
LKB-GPS 200/400	Amersham Bioscience (Freiburg, Germany)
Pharmacia EPS 3500, 301 and EPS 1001	GE Healthcare (Freiburg, Germany)
Analytical Balance	
BP 121 S	Satorius (Göttingen, Germany)
BL 310	Satorius (Göttingen, Germany)
Centrifuges	
Rotina 46 R Centrifuge	Hettich (Tuttlingen, Germany)
Eppendorf-Centrifuge 5415 C	Eppendorf (Hamburg, Germany)
Avanti J25, JA-10 and JA-25.50-Rotor	Beckmann (Vienna, Austria)
Additional Equipment	
Eppendorf-Thermomixer	Eppendorf (Hamburg, Germany)
Magnetic stirrer Heidolph MR2000	Heidolph (Kehlheim, Germany)
pH-Meter - WTW	WTW (Weilheim, Germany)
Incubator	New Brunswick Scientific (Nürtingen, Germany)
Water bath Haake F6-K	Haake (Karlsruhe, Germany)
Cell Disruption Apparatus	Basic Z Constant Systems (Warwick, UK)
Computer Programs	
Adobe Photoshop CS2	Adobe Systems (San Jose, USA)
Adobe Illustrator CS2	Adobe Systems (San Jose, USA)
Microsoft Office 2007	Microsoft (Unterschleißheim, Germany)
Origin 8	OriginLab (Nothhampton, USA)
UltraScan 9.3	Borries Demeler (www.ultrascan.uthscsa.edu)
SedView	Hayes, Stafford
Pymol	Schrödinger
MacBiophotonics ImageJ [V1.43m]	Open Source
Microscopes	
Axiovert 200 inverted microscope	Carl Zeiss (Oberkochen, Germany)
MZ16FA stereo microscope	Leica Microsystems (Wetzlar, Germany)
Stemi stereo microscope	Carl Zeiss (Oberkochen, Germany)
TCS SP5 confocal microscope	Leica Microsystems (Wetzlar, Germany)

2.2 Methods

2.2.1 Molecular biology

2.2.1.1 Polymerase chain reaction (PCR)

Cloning of the respective genes and its variants was performed by using comercially available cDNA of *C. elegans* (Thermo Fisher Scientific, Lafayette, CO, USA) as template. The Pfu polymerase with the provided buffer was used for amplification of DNA. In general, the following setting was used for PCR reactions.

Table 2.2.1. *PCR.*

reaction mix:		
H_2O, sterile	83.5	µL
dNTPs (100 mM)	2	µL
Pfu polymerase	1	µL
Primer, each	1.5	µL
Pfu 10x buffer	10	µL
template	0.5	µL
reaction protocol:		
step 1 (melting)		95 °C, 5:00 min
step 2 (denaturation)		95 °C, 0:30 min
step 3 (annealing)		55-62 °C, 0:45 min
step 4 (elongation)		72 °C, 2:30 min
step 5		GOTO step 2-4, 25x
step 6		72 °C, 3:00 min
step 7		10 °C forever

2.2.1.2 Purification and storage of DNA

PCR products were purified using the Wizard Plus Gel Extraction Kit following the manufacturors centrifugation protocol. After digestion of DNA fragments or plasmid DNA the Wizard Plus Gel Extraction was used and for preparation of bacterial genomic DNA the Wizard Plus SV Minipreps DNA Purification System was used. DNA was stored in sterile H_2O at -20 °C.

2.2.1.3 Restriciton and ligation protocols

DNA was digested and ligated according the following protocols.

Table 2.2.2. *Restriciton and ligation protocols.*

restriction protocol		
H_2O, sterile	2	µL
PCR products or plasmid DNA (1 µg)	40	µL
high fidelity enzyme I (NEB)	1.5	µL
high fidelity enzyme II (NEB)	1.5	µL
NEB buffer 4	5	µL
		incubation at 37 °C for 3 h
ligation protocol:		
H_2O	7	µL (only for negative control instead of insert)
insert: digested PCR products (100 ng)	7	µL
vector: digested plasmid DNA (30 ng)	2	µL
ligase	1	µL
ligase-buffer	1.5	µL
		incubation at room temperature for 20 min

2.2.1.4 Sequencing

Plasmid DNA with a concentration ranging from 30 to 100 ng/µL was sent to GATC Biotech AG, Konstanz, Germany.

2.2.1.5 Storage and cultivation of *E. coli*

E. coli was cultivated at 37°C either on LB plates or LB liquid medium. Strain selection was performed by antibiotic resistance such as resistance to kanamycin (35 µg/mL) or ampicillin (100 µg/mL). Resistance genes were either coded on the plasmid or in the genome of the respective strain. Liquid cultures were inoculated 1:50 from fresh overnight (ON) cultures or by transferring single colonies from plates. Bacterial growth was monitored at 600 nm. For glycerol stocks 600 µL fresh ON culture were mixed with 300 µL of a sterile 87 % glycerol stock solution and transferred to -80 °C.

2.2.1.6 Preparation of chemical competent *E. coli* cells for transformation

This protocol is based on (Inoue et al, 1990). Ten large colonies were transferred of a fresh ON cultured plate into 250 mL SOB medium and incubated at 19 °C to an OD_{600} of 0.5 (approx. 24 h). After a cold shock of 10 minutes (min) on ice, cells were spinned down at 4000 rpm for 10 min at 4 °C. Cells were gently resuspended in 80 ml ice-cold TB medium and stored on ice for 10 min. After spinning the cells down, the pellet was resuspended in 20 ml ice-cold TB medium containing 1.4 mL DMSO. The cells were aliquoted to 100 µL, frozen in liquid nitrogen and stored at -80 °C.

2.2.1.7 Transformation of competent *E. coli* cells and amplification of plasmid DNA

100 µL of chemical competent *E. coli* cells were incubated with 50 ng of plasmid DNA on ice for 15 min. After a heat step at 42 °C for 60 sec, cells were left on ice for another 2 min. 700 µL LB_0 were added and the cells incubated at 37 °C for 45 min to let the resistance genes be transcribed and the antibiotics converting enzymes be synthesized. Cells were pelleted at 5000 rpm for 5 min and plated on selection media. Plates were incubated at 37 °C ON.

2.2.2 Working with *C. elegans*

2.2.2.1 Maintenance of *C. elegans*

C. elegans was treated and maintained as described extensively on www.wormbook.org. Worms were grown on OP50 seeded NGM-plates, incubated at 20 °C and junked onto fresh seeded NGM-plates when necessary.

2.2.2.2 RNAi experiments with *C. elegans*

RNAi is only found in eukaryotes including *C. elegans* and is the way of a cell to post-transcriptionally regulate the expression intensity of a gene. Two different types of RNA, microRNA (miRNA) and small interfering (siRNA) can bind specifically to target mRNAs and lead to their degradation. Responsible for RNAi and the executing tools are several proteins. The Dicer is an enzyme that cleaves double-stranded RNA, like siRNAs that include the target sequence, into short fragments of ~20 nucleotides. The leading strand of these fragments are then incorporated into the RNA-induced silencing complex (RISC) with its catalytic part, the RNase Argonaute. This process can spread systemically throughout the organism despite initially limited concentrations of siRNA.

RNAi experiments against Hsp90 and Hsc70 were performed as described before by feeding dsRNA-expressing *E. coli* HT115 (DE3) (Gaiser et al, 2009; Gaiser et al, 2011). The pL4440 plasmids used to deprive C34B2.5 or ZK370.8 were purchased from Open Biosystems, but did not result in phenotypes (Thermo Fisher Scientific, Lafayette, CO, USA). Respective clones of dsRNA expressing *E. coli* were grown in LB medium with 6 µg/mL tetracycline and 100 µg/mL ampicilline and dsRNA expression was induced by the addition of 1 mM IPTG. After 4 hours of incubation at 37 °C, bacteria were placed on NGM agar plates containing 50 µg/ml ampicillin, 6 µg/ml tetracycline, 1 mM IPTG and

5 µg/ml cholesterol. About 20 synchronized L1 larvae were grown on 6 cm plates at 20 °C and analyzed after several days. Synchronization of the larvae was performed as stated in the WormBook (www.wormbook.org).

2.2.2.3 Generation of transgenic nematodes

For the generation of strains carrying a C-terminal YFP or CFP fusion construct under its endogenous reporter a genomic fragment was cloned into the plasmid PD95.79. For the C34B2.5::C34B2.5-YFP strain the ORF of C34B2.5 with a 0.4 kb upstream fragment was cloned using the primers GGT TTT GCG GCC GCG AAT CGT CGA GAC TTT GAT GAT TTA CC and GGT TTT GCT AGC TGC ATT TTC CTC TTC TTT CTT TTC C and the template pL4440-C34B2.5 (Thermo Fisher Scientific, Lafayette, CO, USA). For the C34B2.5::Hsc70/HSP-1-YFP strain the coding sequence of F26D10.3 was cloned 3' to the C34B2.5 promoter using the primers GGT TTT GCT AGC ATG AGT AAG CAT AAC GCT GTT GGA ATC G and GGT TTT GCT AGC GTC GAC CTC CTC GAT CGT TGG. For ZK370.8::ZK370.8-YFP a 0.8 kb fragment upstream of the ORF ZK370.8 was cloned with the primers GGT TTT GCG GCC GCG CTA CGT ACG TAG GTT AGC TTG ACA C and GGT TTT CTG CAG CTG CCA CAC CGA TCA GCA C to the 5' end of PstI site in the first exon of ZK370.8 followed by the coding sequence of ZK370.8 using the primers GGT TTT CTG CAG CGA CAG TTG CAG GTG TAG GAT AC and GGT TTT GCT AGC ATA CAT ATCGAG CAT TTC AGC TGC ACG and the template pL4440-ZK370.8 (Thermo Fisher Scientific, Lafayette, CO, USA). In order to analyze the muscular association of Hsp90 a Hsp90-YFP fusion construct with YFP in the linker region of Hsp90 (between amino acid 230 and 231) was generated using the template pL4440-daf-21 (Thermo Fisher Scientific, Lafayette, CO, USA). This construct was inserted into the plasmid pPD30.38, leading to muscular expression under the control of the unc-54 promoter. Also, a muscular expressed UNC-45 fusion protein which contains CFP at the C-terminus was constructed using the template pL4440-unc-45 (Thermo Fisher Scientific, Lafayette, CO, USA) as template. Microinjections were carried out according to standard procedures (Mello et al, 1991) by injecting a solution of 100 mg/ml plasmid DNA into the distal gonads of young adult worms. Injections were performed on a Zeiss Axiovert 200 microscope (Zeiss Microimaging, Jena, Germany) equipped with an injection device (Eppendorf, Hamburg, Germany). Existence of fluorescent F1 progeny was observed using a Leica MZ-16FA (Leica Microsystems,

Wetzlar, Germany) fluorescence microscope. In order to obtain stable lines, fluorescent offspring were transferred to new NGM plates.

2.2.2.4 Expression pattern and localization analysis

A small drop of molten 2 % agar solution in M9 buffer (see www.wormbook.org) at 65 °C was placed on clean glass slides and another glass slide put on top with spacers in between to get defined agarose pads of around 1 mm of thickness. 2 µL of 5 mM tetramisole were placed onto the pad and several living adult worms transferred with a worm pick into the drop. A coverslip was placed above and sealed with silicone. Fluorescence images were generated using a Zeiss Axiovert 200 microscope equipped with a Hamamatsu C4742-95 camera (Hamamatsu, Herrsching, Germany). The expression patterns of the ORFs C34B2.5 and ZK370.8 and the localization of Hsp90-YFP(li) as well as UNC-45-CFP were studied by confocal microscopy using a Leica SP5 laser scanning microscope. CFP and YFP were excited, using the 458 nm and 514 nm lines of an Argon laser. For images with MitoTracker costaining worms were soaked in 5 nM MitoTracker CMXRos (M-7512, Invitrogen, La Jolla, USA) in M9 for 20 min and washed in M9 before mounting on an agar pad for imaging. Using this combination of dyes, YFP was excited at 488 nm of an Argon laser and MitoTracker CMXRos was excited at 633 nm of a HeNe laser. For imaging, 4% of the total laser power was deployed. Gain and offset were adjusted to fully exploit the dynamic range of the photomultipliers. Image adaptions, if necessary, were linear adaptation of contrast and brightness and were performed using ImageJ.

2.2.2.5 Evaluation of motility by thrashing assays

200 eggs of either N2 or CB286 worms were placed on OP50 seeded NGM plates and incubated at the indicated temperature. Temperature shifts were performed as stated in section 3.4.3. To analyze the motility of the worms, individual nematodes were placed in a drop of M9 buffer and body bends per minute were counted using a stereo microscope.

2.2.3 Protein chemical and biophysical methods

2.2.3.1 SDS-polyacrylamide gel electrophoresis (SDS-PAGE)

SDS-PAGE was performed in accordance to the protocol of (Laemmli, 1970). Gels were assembled by the following protocol. Each gel was run with 30 mA for 1 h. Gels were stained for 15 min in hot Fairbanks A solution and destained in hot Fairbanks D solution according to (Fairbanks et al, 1971).

Table 2.2.3. *SDS-PAGE.*

	12.5 % separating gel (µL)	**3 % stacking gel (µL)**
H_2O	4375	1875
separating gel buffer (4x)	2500	-
stacking gel buffer (2x)	-	2500
acrylamide (40 %)	3125	625
APS (10 %)	100	50
TEMED	10	5

2.2.3.2 Protein expression

The proteins purified in this thesis were expressed in the BL21-CodonPlus(DE3)-RIL strain which carries an additional plasmid encoding extra copies of the *argU, ileY* and *leuW* tRNA genes and enables efficient high-level expression of heterologous protein of AT-rich genomes in *E. coli*. Over-expression of proteins can deplete the pool of rare tRNAs and stall translation. BL21-CodonPlus strains encode tRNAs that most frequently limit translation of heterologous proteins. These tRNAs recognize the arginine codons AGA and AGG and the isoleucine codon CUA.

The pET28b system was used as expression vector with the regarding genes cloned after an N-terminal tag including a sequence of six histidines for Ni-affinity purification. Expression was performed on a 2-8 L scale. After inoculation and growth at 37 °C to an OD_{600} of 0.6, cells were incubated on ice for 45 min followed by the induction of the lac promotor and protein expression by addition of 1 mM IPTG. Cells were incubated at 20 °C over night and harvested at 6000 rpm and 4 °C for 15 min (JA 10 rotor).

2.2.3.3 Protein purification

All steps of protein purification were performed at 4 °C. Cell pellets were resuspended in 100 mL Ni-NTA equilibration buffer containing 1 mL of Protease Inhibitor Mix HP and

processed by a cell disruptor at 1.8 kbar. The lysate was centrifuged at 18,000 rpm and 4 °C for 25 min in a JA 25.50 rotor. The supernatant was loaded onto a pre-equilibrated 5 mL HisTrap FastFlow Ni-affinity chromatography column. The column was run with 3 mL/min and washed with 20 column volumes of equilibration buffer after loading of the protein followed by a second washing step with another 20 volumes containing 6 % of elution buffer. Elution was induced by applying 100 % elution buffer. Fractions containing the regarding protein were pooled and diluted with low-salt-buffer to a final imidazole concentration of 40 mM and a final volume of 150 mL. The protein was applied onto a Resource Q column, pre-equilibrated with low-salt-buffer. The loaded column was washed with a flow rate of 3 mL/min and 100 mL of low-salt-buffer, before a gradient over 150 mL up to 50 % of high-salt-buffer was applied. The purest fractions analysed by SDS-PAGE were pooled, concentrated in Centricon microconcentrators up to a final volume of 5 mL (3700 rpm, 4 °C) and injected onto a Superdex 75 or Superdex 200 column, equilibrated with one column volume of SEC buffer. The protein was dialysed against the final dialysis buffer, concentrated up to 30-1400 µM in AMICON devices with appropriate MWCO (3700 rpm, 4 °C), freezed in liquid nitrogen in aliquots of 100 µL and stored at -80 °C. Some proteins expressed in inclusion bodies after standard expression at 20 °C overnight. Inclusion bodies of TTC12(99-125) and Y22D7AL.9 (1-165) were solved in 40 mM HEPES/KOH, pH 8.2, 300 mM KCl, 5.5 M urea, 1 mM DTT and refolded by dialysis in 40 mM HEPES/KOH, pH 8.2, 300 mM KCl, 300 mM L-arginine, 1 mM DTT. Refolded protein was applied to size exclusion chromatography on Superdex 75 or 200. Protein purity was assessed by SDS-PAGE and the molecular mass was determined by a MALDI-TOF/TOF mass spectrometer (Bruker, Bremen, Germany). Proteins were frozen in liquid nitrogen in 40 mM HEPES/KOH, pH 7.5, 20 mM KCl, 1 mM DTT and stored at -80 °C. The purified human phosphatases PP1, PP2A and PP2B/PP3 were purified as described (Baumgrass et al, 2001; Mondragon et al, 1997; Tung et al, 1985) and a kind gift from Matthias Weiwad (Martin-Luther-Universität Halle-Wittenberg, Halle (Saale))

2.2.3.4 Absorption Spectroscopy

Proteins and peptides contain two important functional groups that absorb UV light. Amid groups like those forming the peptide bond absorb at 180 to 240 nm and the

aromatic amino acids mainly phenylalanine, tyrosine and tryptophane at 250 to 300 nm (see table 2.2.4).

Table 2.2.4: *Absorbance properties of proteins.*

	λ_{max} (nm)	ε_{max} (M^{-1} cm^{-1})
Trp	280	5700
Tyr	274	1400
Phe	257	200
disulfide bond	250	300

UV spectroscopy was used to determine the concentration of purified protein by using the law of Lambert-Beer

$$A = \varepsilon \cdot c \cdot d$$

with A Absorbance, ε molar extinction coefficient (M^{-1} cm^{-1}), c protein concentration (M) and d cell length (cm), that correlates the measured absorbance with the protein concentration. Absorbance was measured at 280 nm.

The *protparam* tool provided by www.expasy.org calculates in a first approximation the extinction coefficient of proteins according to the absorbance of the sum of each aromatic residue. These sequence-based values ignore the influence of the folding of a protein and the resulting interactions with the solvent on its absorption characteristics, but serve as heuristic extinction coefficients and were used for concentration determination in this work.

2.2.3.5 Thermal unfolding of proteins

Thermal unfolding of proteins can be followed by circular dichroism (CD) which is the relative absorption of left- and right-handed circularly polarised light and is recorded as a function of wavelength and/or temperature. This spectroscopic method detects optically active molecules such as proteins and uses the chirality of the c_α-atoms of the protein backbone and the absorbance of proteins at 170-250 nm caused by the $n \rightarrow \pi^*$ and the $\pi \rightarrow \pi^*$ transition of electrons of the peptide bond. The different absorbance of the incident left and right polarised light produces elliptically polarised light after passing a chiral sample. The ellipticity of the sample is a calculated value regarding the difference in the left and right absorption coefficient as well as the concentration of the sample and the thickness of the optical cell

$$\Theta(\lambda) = const. \cdot (\varepsilon_R - \varepsilon_L) \cdot c \cdot d$$

with Θ obtained ellipticity (deg), ε_L molar absorbance of left polarised light (cm^{-1} M^{-1}), ε_R molar absorbance of right polarised light (cm^{-1} M^{-1}), c concentration (M) and d cell length (cm) which was 0.1 cm in the cuvettes used in this work. The mean residue elipticity can be obtained from the measured data by using the equation

$$\Theta_{MRW} = \frac{\Theta \cdot 100}{d \cdot c \cdot N_{aa}}$$

with Θ obtained ellipticity (mdeg), d cell length (cm), c concentration (mM) and N_{aa} number of amino acids. Temperature-induced unfolding of TPR proteins was performed in a Jasco J-720 spectropolarimeter (Jasco, Essex, United Kingdom). Measurements were carried out with 5 µM of C34B2.5 and its variants, F52H3.5, TTC9(20-220) and huSmad4 and 2 µM ZK370.8-ΔN33 in 40 mM HEPES/KOH, pH 7.5, 20 mM KCl, 1 mM DTT by recording the change in ellipticity at 222 nm in a temperature range from 10 to 90 °C. Heating rates were 20 °C/h and the path length of the cuvette was 0.1 cm.

2.2.3.6 Phosphatase assays

A synthetic substrate was used for the phosphatase assays, the p-nitrophenyl phosphate (pNPP). The phosphate group of p-nitrophenyl phosphate is cleaved off by phosphatases and the release of the yellow product p-nitrophenol can be followed in a Varian Cary 100 spectrophotometer (Agilent Technologies, Boeblingen, Germany) at 410 nm with an extinction coefficient of 15100 M^{-1} cm^{-1} that reflects the enzyme activity. The reaction was measured in 40 mM HEPES/KOH, 20 mM KCl, 5 mM $MnCl_2$, 1 mM DTT, pH 7.5 and 60 mM pNPP at 20 °C if not indicated otherwise. Phosphatase concentration ranged from 25 to 2000 nM in the assay. If indicated, Hsp90 (3 µM), Hsp90-CTD (3 µM) or the C-terminal peptide of nematode Hsp90 (60 µM) was supplemented in the assay.

2.2.3.7 Thrombin digestion for crystallisation

After the second purification step by Resource Q column 10 mg of protein were digested with bovine thrombin at 4 °C over night. To separate undigested species, the protein was subsequently loaded onto a HisTrap column and the flow-through subjected to a Superdex

size exclusion chromatography preequilibrated with 40 mM HEPES, 300 mM KCl, 1 mM DTT, pH 7.5.

2.2.3.8 Fluorescence-labeling of protein

0.1 mg of lysine reactive Alexa 488 (Invitrogen) or 5(6)FAM, respectively, was dissolved in DMSO and added to around 1 mg of protein with a final DMSO concentration of 1 %, and incubated at RT for 1 h. Free label was separated using a HPLC-Superdex 75, preequilibrated with 40 mM HEPES, 150 mM KCl, 1 mM DTT, pH 7.5, and elution detected via UV absorption and a fluorescence detector with an excitation wavelength of 488 nm. The column was run with 0.5 ml/min. Protein eluted after approx. 20 min was aliquoted and stored at -80 °C. Labeling efficiency was 0.2 for FAM-Hsc70 and 0.7 for Alexa488-labeled human Hsp90β.

2.2.3.9 ATPase assay

The activity of the ATPases Hsc70 and Hsp90 were assessed in a coupled regenerative ATPase assay as described before (Gaiser et al, 2009). Reactions were measured in a Varian Cary 100 spectrophotometer (Agilent Technologies, Boeblingen, Germany) at 30 °C and the depletion of NADH was followed at 340 nm. Chaperone concentration was 3 µM and cochaperones were added, when indicated, at a concentration of 5 µM.

2.2.3.10 NMR measurements

The NMR experiments were performed in collaboration with Grzegorz Popowicz (Lehrstuhl für Biomolekulare NMR-Spektroskopie, Technische Universität München, Germany) on an 800 MHz spectrometer (Bruker) with cryoprobe. The measurements were done in D_2O with phosphate buffer (4 mM KH_2PO_4, 16 mM Na_2HPO_4, 120 mM NaCl, pH 7.4) and 1-5 % of d6-DMSO. The P5SA-2 without protein was recorded in high sensitivity experiments with a high number of scans. The CPMG sequence with an additional Watergate to suppress residual water was used (Hajduk et al, 1997; Sklenar et al, 1993). The T_2 filtering time was set to 400 ms to suppress signals from slowly tumbling molecules. Peak intensities were normalized by comparing residual DMSO peaks.

2.2.3.11 Crystallization and structure determination

Crystallization and data analysis was performed in collaboration with Michael Groll and Ferdinand Alte (Lehrstuhl für Biochemie, Technische Universität München, Germany). PP5 protein was concentrated to 15 mg/mL in the following buffer: 10 mM Tris, pH 7.8, 3 mM DTT. Optionally, the ligand was added with a final concentration of 1 mM. Crystals were grown at 20 °C within 4 weeks by using the hanging drop vapour diffusion method. Drops contained equal volumes of protein and reservoir solutions (0.2 M $Mg(NO_3)_2$, 20% PEG 3350). Crystals were soaked for 30 seconds in cryo buffer (mother liquor + 25% PEG 200) and were subsequently cooled in liquid nitrogen. Diffraction datasets were recorded using synchrotron radiation of $\lambda = 1.0$ Å at the beamline X06SA, Swiss Light Source (SLS), Villigen, Switzerland. Collected datasets were processed using the program package XDS (Kabsch, 1993). Determination of the crystal structure was performed by molecular replacement using the program PHASER (McCoy et al, 2007). Human PP5 (PDB ID: 1WAO) was applied as starting model for the ligand structure PP5:P5SA-2. The refined coordinates of PP5:P5SA-2 in turn were employed for the apo-structure of PP5. Model building was carried out with the graphic program MAIN and finalized applying REFMAC5 (Vagin et al, 2004) by conventional crystallographic rigid body, positional, and anisotropic temperature factor refinements with current crystallographic values of R_{work} = 23.8%, R_{free} = 27.1%, root mean square deviation (r.m.s.d.) bond lengths of 0.005 Å, and r.m.s.d. bond angle of 0.99° for PP5 apo and R_{work} = 21.4 %, R_{free} = 26.1 %, r.m.s.d. bond length of 0.015 Å, and r.m.s.d. bond angle of 1.68° for PP5:P5SA-2. Coordinates were confirmed to have good stereochemistry indicated by the Ramachandran plot. The atomic coordinates have been deposited at the RCSB Protein Data Bank under the accession codes 4JA9 for PP5 apo and 4JA7 for PP5:P5SA-2.

2.2.3.12 Radioactive dephosphorylation assay

Radioactive phosphorylated proteins were obtained as described before (Wandinger et al, 2006). CDC-37 was phosphorylated with [γ-32P]ATP using 0.1 mU CK2 at 30 °C for 180 min. Remaining ATP was hydrolyzed by addition of apyrase for 30 min at 30 °C. Phosphorylated CeCdc37 was then incubated with 3 µM of either Hsp90, Hsp90-MC, Hsp90-CTD or Hsp90-ΔMEEVD and 2 µM PPH-5 at 20 °C. After 10 and 60 min samples were taken and dephosphorylation was stopped by addition of Laemmli buffer and boiling

at 95 °C for 5 min. The relative degree of phosphorylation of CDC-37 was analyzed by SDS-PAGE followed by phosphoimaging on a Typhoon 9200 Phosphoimager (Amersham Biosciences, Freiburg, Germany).

2.2.3.13 Isothermal titration calorimetry

Isothermal titration calorimetry (ITC) is a common tool to study protein-protein-interactions and to obtain thermodynamic parameters. It is a quantitative technique to directly measure binding affinity (K_a), the free enthalpy of binding (ΔH) and the binding stoichiometry (n) of macromolecule and ligand in solution. Using the relationship

$$\Delta G = -RT \cdot \ln K = \Delta H - T \cdot \Delta S$$

where R is the gas constant (J mol^{-1} K^{-1}) and T is the absolute temperature (K), Gibbs energy of binding (ΔG) and the entropy (ΔS) can be determined. An isothermal titration calorimeter consists of two identical cells, a sample cell and a reference cell, surrounded by an adiabatic jacket. While the reference cell is filled with water, the sample cell is loaded with the protein solution and equal amounts of ligand are titrated via a stirring syringe into the cell. Binding of the ligand to the macromolecule leads to energy release or uptake which is plotted as the power in µcal/sec and a function of time. Integration with respect to time gives the total heat effect per injection. The heat effect as a function of the molar ratio of ligand to macromolecule is analysed by the MicroCal Software to give the thermodynamic parameters discussed above.

For measurements with Hsp90-CTD aliquots of 280 µM Hsp90-CTD were titrated into 30 µM of TPR protein in 40 mM HEPES/KOH, pH 7.5, 20 mM KCl, 1 mM DTT. ITC experiments with Hsc70 and C34B2.5 were performed with 15 µM Hsc70 in the cell and 182 µM C34B2.5 in the syringe. Binding constants of ZK370.8 were assessed with 10 µM Hsc70 in the cell and 82 µM ZK370.8-ΔN33 in the syringe. In case of peptide interaction, the sample cell was loaded with 30 µM protein solution and the syringe with a 1 mM peptide ligand. ITC runs were done at 20 °C. 20 injections were done per run with a volume of 2 µL, a spacing of 180 sec, a filter period of 5 sec and a stirring speed of 1000 rpm. An initial delay of 300 sec was set and a reference power of 5 µcal/sec. Binding curves were corrected for dilution heats and fitted to a one-site binding model

using the software provided by the manufacturer (Origin software package, GE Healthcare).

2.2.3.14 Analytical ultracentrifugation

Analytical ultracentrifugation (AUC) consists of the application of centrifugal force with the simultaneous real-time observation of the sedimentation of the macromolecules in the centrifugal field. Because proteins are studied in solution, AUC allows their hydrodynamic and thermodynamic characterization in solution without interaction with any matrix or surface. There are two basic types of ultracentrifugation experiments for the characterization of proteins: sedimentation velocity and sedimentation equilibrium scans.

In the sedimentation velocity experiment sufficiently high angular velocity is used to sediment macromolecules towards the cell bottom. The rate of movement of the macromolecule boundary is used to determine the sedimentation coefficient (*s*), and rate of spreading of the boundary is used to determine the diffusion coefficient (*D*). In turn, these data can be used to calculate apparent molecular weight (*M*) and characterize the shape of macromolecules. In this work only sedimentation velocity scans were performed. In such an experiment application of a large centrifugal force field leads to the movement of molecules towards the bottom of the centrifuge cell. The sedimentation process is determined by three factors: the gravitational force, the buoyancy and the hydrodynamic friction. Since the gravitational force is proportional to the square of the rotor speed, adjusting the rotor speed allows the study of a wide range of particle sizes ranging from kDa to GDa molecular weights. The Svedberg equation describes the relationship of these three forces

$$s = \frac{v}{\omega^2 r} = \frac{MD\left(1-\overline{V}\rho\right)}{RT}$$

where s is the sedimentation coefficient (S), v the observed radial velocity (m/s), ω the angular velocity of the rotor (m/s^2), $\omega^2 r$ the centrifugal field, M the molecular weight (g/mol), V the partial specific volume (cm^3/g), ρ the density of the solvent (g/cm^3), D the diffusion coefficient (m^2/s), R the gas constant (8.314 J mol^{-1} K^{-1}) and T the absolute temperature (K).

The sedimentation coefficient represents the sedimentation velocity v in relation to the centrifugal field $\omega^2 r$. The s-values are commonly reported in Svedberg (S) units that

correspond to 10^{-13} s. When the centrifugal force is sufficiently small, the process of diffusion significantly opposes the process of sedimentation and an equilibrium concentration distribution is obtained throughout the cell. For an ideal non-interacting single component system, the equilibrium distribution is an exponential function of the buoyant mass of the molecule, M (1-Vρ), as described by the following equation

$$c(r) = c_0 \cdot e^{\frac{M\left(1-\bar{V}\rho\right)\omega^2\left(r^2-r_0^2\right)}{2RT}}$$

with *c(r)* as the sample concentration at radial position *r* (M), c_0 as sample concentration at reference radial distance r_0 (M), *V* as partial specific volume (cm^3/g), ω as angular velocity of the rotor (m/s^2), *R* as gas constant (8.314 J mol^{-1} K^{-1}) and *T* as absolute temperature (K).

Sedimentation equilibrium experiments provide an accurate way to determine the molecular weight *M* and consequently the oligomeric state of macromolecules. In contrast to other techniques, such as size exclusion chromatography, sedimentation experiments are not subject to assumptions of globular shape or limitations by matrix interactions.

Binding of the TPR proteins to the chaperones was analyzed with fluroescence detection as described before (Gaiser et al, 2011). Experiments were performed in a Beckman ProteomeLab XL-A analytical ultracentrifuge (Beckman, Brea, USA) equipped with an Aviv AU-FDS detector (Aviv Biomedical, Lakewood, USA). Binding of the P5SAs to the Hsp90-PPH-5 interface was analyzed accordingly using N-terminally YFP-labeled Hsp90 as fluorescent probe. AUC runs were performed in 40 mM HEPES/KOH, pH 7.5, 20 mM KCl, 1 mM DTT, the concentration of labeled species was 300 nM. Concentrations of the TPR proteins were as indicated. For certain experiments, 60 µM of the C-terminal Hsp90-peptide (AEEDASRMEEVD) was added to the sample. Centrifugation was performed at 20 to 22 °C and 42.000 rpm for 12 hours. Scans were recorded every 90 seconds. Data analysis was performed using a dc/dt approach according to Stafford (Stafford, 1992). The dc/dt plots were fit to gaussian functions in order to obtain the $s_{20,w}$ values of the respective species as described previously (Gaiser et al, 2011).

2.2.3.15 Measuring Chevron Plots with a stopped flow apparatus

To determine the stability of proteins urea transitions of proteins were measured by fluoresence spectroscopy. Urea interacts with the protein backbone, breaks stabilising

hydrogen bonds and dissolves the secondary structure, while keeping the protein soluble. The tryptophane signal, that contributes to large amounts to the fluorescence signal of proteins, shifts its emission maximum from 340 to 360 nm during unfolding, when excited at 280 nm, caused by the exposition of the tryptophan residue to a hydrophilic solvent.

Chevron plots were recorded by rapidly diluting the respective protein with a final concentration of 1 µM into the indicated amount of urea in 40 mM HEPES/KOH, pH 7.5, 20 mM KCl, 1 mM DTT. Measurements were carried out in an Applied Photophysics SX18-MV stopped flow instrument (Applied Photophysics, Surrey, United Kingdom) at 10 °C for C34B2.5 and 20 °C for F52H3.5. Kinetics were detected by recording fluorescence with excitation at 280 nm and a cut-off filter at 305 nm. Voltage was adjusted to 420 V and 1000 data points were recorded for 3 sec for each kinetic. Kinetics were fitted with a mono-exponential equation and ln(k_{obs}) was plotted versus the final urea concentration. The data were fitted according to equation 1 and ΔG was calculated using equation 2.

$$\ln(k) = \ln\left(k_{folding}^{H_2O} \cdot e^{(-m_{folding} \cdot [urea])} + k_{unfolding}^{H_2O} \cdot e^{(-m_{unfolding} \cdot [urea])}\right) \quad \text{(equation 1)}$$

$$\Delta G = R \cdot T \cdot \ln\left(\frac{k_{unfolding}}{k_{folding}}\right) \quad \text{(equation 2)}$$

2.2.3.16 Crosslinking experiments

Proteins were crosslinked using isotope labeled di-sulfo-succinimidyl-glutarate (DSSG-H6/D6) (Creative Molecules Inc., Canada) in a 40-fold excess over protein. Protein concentrations were used as indicated and the crosslinking reaction was stopped by addition of Laemmli buffer. Samples were analysed on a neutral gels 4-12 % (Serva, Heidelberg, Germany) and bands representing crosslinked species were excised. Proteins were extracted according to the protocol as published earlier (Schafer et al, 2001). The final samples were analyzed by a LTQ Orbitrap XL (Thermo Scientific, Langenselbold, Germany) using ESI (Nanospray). Peptide mixtures were separated by an Acclaim PepMap RSLC C18 trap column on a HPLC Ultimate 3000 RSLCnano System (Dionex, Idstein, Germany). Peptides were eluted by applying a linear gradient from 5 to 35 % acetonitrile with 0.1 % formate. Scans were performed with a resolution of 60,000 from

300-2000 Da in six independent measurements. Data analysis was performed using the program MassMatrix version 2.4.2.

2.2.3.17 Phosphate detection by EnzChek

The EnzChek Phosphate Assay Kit (Invitrogen, La Jolla, USA) was used to detect free phosphate according to the manufacturer's protocol when the substrate peptide KRpTIRR was dephosphorylated by PPH-5. The reaction buffer provided by the kit was supplemented with 5 mM $MnCl_2$. Measurements were performed at 20 °C.

3. Results and Discussion

3.1 A proteome wide approach assigns the chaperone interacting TPRome of *C. elegans**

*This chapter is published in the *Journal of Molecular Biology* (Haslbeck et al, 2013).

3.1.1 Ranking of chaperone-interacting TPR proteins from *C. elegans*

The proteome of *Saccharomyces cerevisiae* contains about 25 proteins with TPR domains as identified by blast search. Seven of these proteins are confirmed to interact with either Hsp90 or Hsc70 (Table 3.1.1). The genome of *C. elegans*, however, encodes over 70 TPR proteins with mostly unknown binding partners, while nine proteins are identified to interact via their TPR domain with either Hsc70 (HSP-1) or Hsp90 (DAF-21) (Haslbeck et al, 2012). Up to now, 14 human TPR proteins have been confirmed to associate with one or both chaperones. Previous work by Klaus Richter (Lehrstuhl für Biotechnologie, Technische Universität München, Germany) had ranked the so-called TPRome of *C. elegans* according to their homology with a sample set of known chaperone-interacting TPR domains of *S. cerevisiae*, *C. elegans* and *H. sapiens* (Table 3.1.1). TPR domains of known cofactors were excised to include only the peptide-interacting protein stretch according to the TPR2A domain of Hop/STIP1 (HS_STIP1b), whose crystal structure in complex with the peptide had been solved (Figure 3.1.1) (Scheufler et al, 2000).

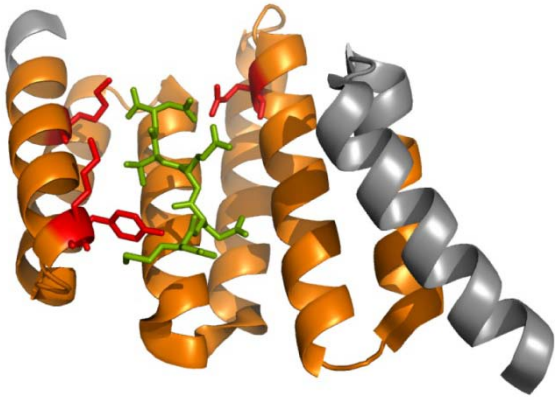

Figure 3.1.1. *Peptide-binding to the TPR2A-domain of human Hop/STIP1. The bound MEEVD-peptide (green) is surrounded by the α-helices of the TPR domain. The orange-colored protein region was used for the alignment. Electrostatic as well as hydrophobic interactions are formed between the peptide and the protein. Interacting residues Lys229, Tyr236, Lys237 and Gln298 of the TPR domain are highlighted in red and their relative position in the TPR domain was subsequently used for the alignment studies. The PDB ID of the displayed crystal structure is 1ELR (Scheufler et al, 2000).*

A sequence alignment of this sample set of protein domains was generated (Figure 3.1.2) and then applied to the software HMMER (v3.0, HHMI Janelia Farm Research Campus) to generate an ".hmm" model file to search the proteome database of *C. elegans*. The highest ranking proteins were part of the sample set (Table 3.1.2). At lower scores uncharacterized TPR containing proteins emerged. The three open reading frames C33H5.8 (76.20), C34B2.5 (71.40) and ZK370.8 (58.70) were identified from the proteome with high probabilities of being chaperone-interacting proteins. Proteins with lower scores included DNJ-28 (44.90 and 44.50), ADPR-1 (44.60), Y22D7AL.9 (44.10), F52H3.5 (43.20), DNJ-7 (41.70 and 34.90) and OGT-1 (36.60). While indications exist that the TPR domains of the human homologs of DNJ-7 and DNJ-28 might bind to the C-terminal ends of chaperones, there are no indications for OGT-1 to interact with either Hsc70 or Hsp90 via its TPR domain. Instead, its TPR-domain is used as a docking site for substrates (Iyer & Hart, 2003; Kreppel & Hart, 1999).

Table 3.1.1. *Selection of TPR domain containing proteins as sample set.*

H. sapiens	***S. cerevisiae***	***C. elegans***
HS_STIP1a	SC_Sti1a	
HS_STIP1b	SC_Sti1b	CE_STI-1a
HS_SGTA, HS_SGTB	SC_Sgt2	CE_SGT-1
HS_PPP5C	SC_Ppt1	CE_PPH-5
HS_FKBP4, HS_FKBP5		CE_FKB-6
HS_PPID	SC_Cpr6, SC_Cpr7	
HS_ST13		CE_T12D8.8
HS_STUB1		CE_CHN-1
HS_AIP		CE_C56C10.10
HS_TTC4	SC_Cns1	CE_C17G10.2
HS_UNC45B		CE_UNC-45
HS_UNC45A		

TPR domains of chaperone interacting proteins were used as a starting set for the identification of novel chaperone-interacting TPR proteins. The TPR domains within one line are excised from the corresponding proteins of the different organisms. TPR domains are numbered serially to their occurrence in the protein beginning from the N-terminus with lower case characters.

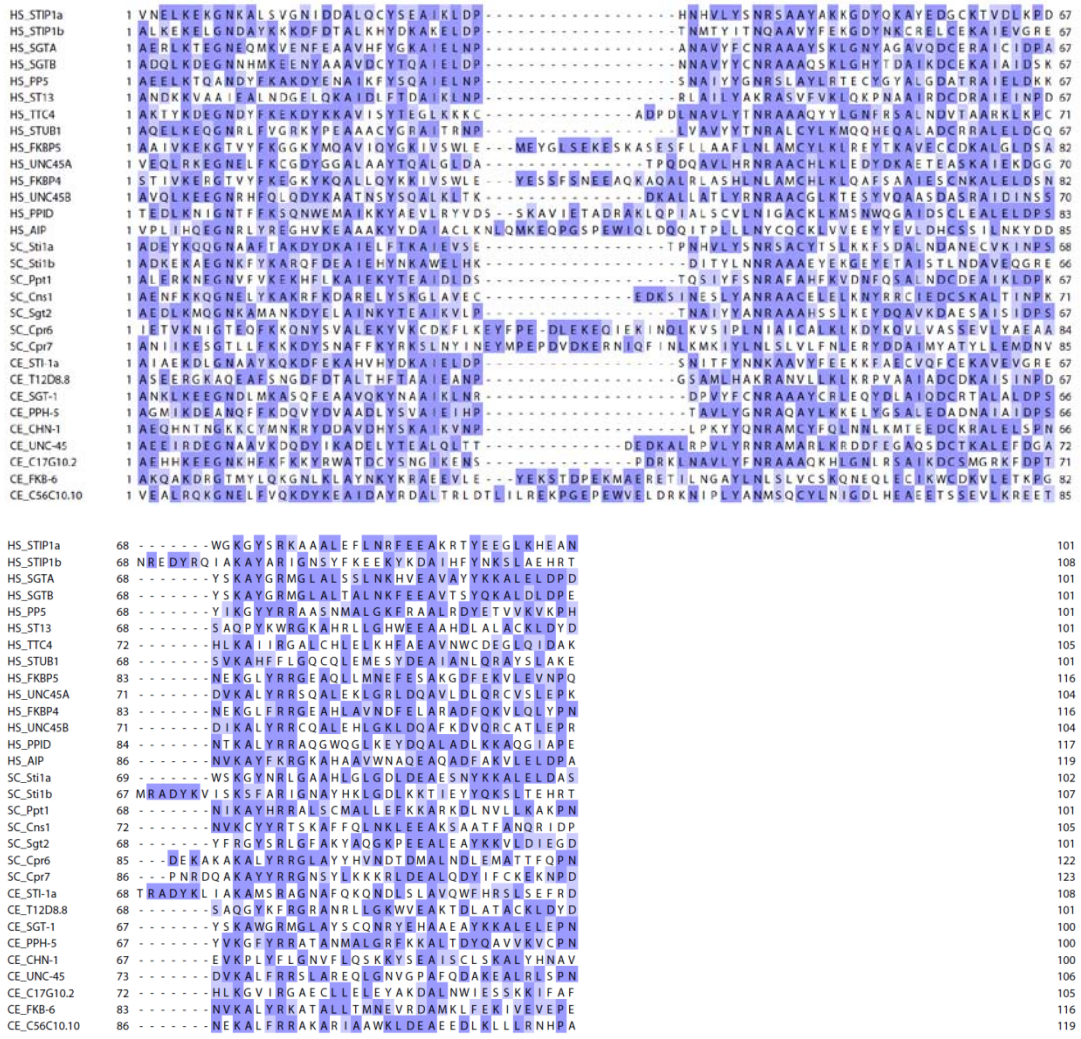

Figure 3.1.2. *Alignment of the TPR domain containing proteins of the sample set of table 3.1.1.*

Table 3.1.2. *Proteome-search using the starting set of TPR domain containing proteins to identify novel chaperone-interacting TPR proteins.*

S. cerevisiae						*C. elegans*					
TPR domain	**Score**	**5 (p)**	**12 (h)**	**13 (p)**	**74 (p)**	**TPR domain**	**Score**	**5 (p)**	**12 (h)**	**13 (p)**	**74 (p)**
STI1a	111.30	K	F	T	R	SGT-1	105.10	K	M	K	R
CNS1	107.70	K	Y	K	R	PPH-5	104.10	K	F	K	R
PPT1	105.90	K	V	K	R	STI-1b**	103.00	K	F	K	R
SGT2	104.20	K	M	A	R	CHN-1	101.50	N	Y	M	F
CPR7	89.90	K	F	K	R	UNC-45	100.80	R	V	K	R
CPR6	89.50	K	F	K	R	C17G10.2	95.40	K	F	K	R
TOM71*	84.70	K	F	T	R	C56C10.10	89.50	R	F	V	R
TOM70*	78.30	K	F	R	R	T12D8.8	87.40	R	F	S	F
STI1b	77.00	K	Y	K	V	FKB-6	86.20	K	L	Q	R
STI1c	75.90	R	F	T	R	STI-1a**	85.90	K	Y	K	L
TAH1	58.10	K	F	K	- (R)	C33H5.8	76.20	K	F	K	R
DIA2	52.10	- (I)	F	K	R	C34B2.5	71.40	K	F	A	R
SWA2	45.30	K	F	K	R	ZK370.8	58.70	K	F	K	R
CDC27*	36.60	- (C)	S	L	G	DNJ-28c	44.90	- (L)	- (I)	- (E)	Q
PEX5p	26.90	- (L)	Y	T	N	ADPR-1	44.60	R	I	R	R
CYC8/SSN6*	24.90	- (Y)	M	I	D	DNJ-28a	44.50	Y	F	V	Q
SKI3*	22.90	-	-	-	G	Y22D7AL.9	44.10	- (V)	Y	S	R
CDC16	22.50	N	F	K	S	F52H3.5	43.20	- (E)	A	E	Q
CDC23*	21.60	-	Y	N	L	DNJ-7a	41.70	- (L)	L	A	Q
TFC4*	19.20	L	F	V	R	OGT-1*	36.60	- (I)	K	E	N
CTR9/CDP1*	19.50	-	-	-	A	T20B12.1*	35.80	R	L	M	N
YDR161W	18.30	-	I	S	L	DNJ-7c	34.90	- (L)	- (V)	E	E
SRP72*	17.90	H	Y	K	-	PRX-5*	28.00	- (N)	- (N)	- (L)	N
EMW1*	16.10*	-	-	-	N	ZK328.7*	27.30	- (S)	M	K	L
SEC72	14.10	-	-	-	-	EMB-27	26.70	N	R	R	- (C)
YMR018w	17.00	-	A	N	-	DYF-1	25.60	- (I)	Y	K	- (I)
BUD7	14.70	-	-	-	L	Y37E3.1*	25.00	-	-	-	N
MSS2	13.10	K	F	E	-	B0464.2*	23.30	-	-	-	V
PFK2	12.60	-	Y	S	-	F58A4.14*	22.40	-	-	N	W
						DNJ-28b	21.70	-	-	-	E
						UTX-1*	21.40	-	-	-	R
						DNJ-7b	21.30	-	-	-	E
						KLC-1*	19.30	-	-	-	N
						BBS-8*	19.10	-	-	-	C
						MAT-1*	17.90	-	I	V	T
						AGS-3*	17.90	L	F	R	-
						Y47A7.1	17.70	-	-	-	R
						KLC-2*	17.60	-	-	-	N
						Y57G7A.10	17.50	-	E	S	Q
						CRA-1	16.90	-	-	-	L
						TAG-315*	16.30	-	-	-	Q
						K09A9.6	16.10	-	-	-	G
						MAT-3*	15.80	-	-	-	G
						RMD-6	14.50	-	-	-	Y
						RMD-4	14.60	-	-	-	Y
						FIS-1	14.60	-	-	-	L
						DYF-13	14.60	-	L	S	Y
						Y39A3CR.9	13.50	-	-	-	Q
						RMD-2	13.20	-	-	-	Y
						RMD-1	12.50	-	-	-	F
						Y59A8B.6	12.30	-	-	-	V
						F45G2.4	12.10	-	-	-	-
						F08D12.1	10.30	-	-	-	L

The HMMER3.0 score for TPR domains within the proteome of yeast and C. elegans was calculated. In cases, where proteins contain more than one TPR domain, the values are given for all of them unless indicated otherwise. (*) implies that the protein contains more than one TPR domain, but only the TPR domain with the highest score is shown in the table. Proteins that are part of the sample set are highlighted in green. (**) highlights that the nomenclature for STI-1 does not match its homologues from other species due to the absence of the first TPR domain in nematodes. Amino acid positions 5 (positive), 12 (hydrophobic), 13 (positive) and 74 (positive) are listed for each domain and colored in light grey if they match the consensus residues of chaperone-interacting TPR domains.

Part of this initial proteome search by Klaus Richter was the evaluation of the residues at positions 5/12/13/74 (Table 3.1.2). These are certain residues which are involved in the binding of the peptide and show conserved charge properties (Cortajarena et al, 2004). Residues 5 and 74 of the alignment contribute largely to the so-called carboxylate clamp which fixates the last carboxylate groups of the C-terminal aspartate of Hsp90 (Scheufler et al, 2000). In particular, the positive charge of position 5 and 74 is highly conserved with Lys and Arg, respectively. Residue 12 is always hydrophobic (Phe, Tyr or Met, Val, Leu) and contributes to van der Waals contacts to the MEEVD-peptide (Scheufler et al, 2000). In general, it is followed by a positively charged residue 13 (Lys, Arg). F52H3.5 is the first protein of the ranking which lacks conservation in all four positions suggesting that in this range the interaction with Hsc70 and Hsp90 might be lost.

Based on the ranking of the *C. elegans* TPRome, the focus of the following chapter of the thesis was the analysis of the uncharacterized ORFs C33H5.8, C34B2.5, ZK370.8, DNJ-28, ADPR-1, Y22D7AL.9 and F52H3.5 and to test their ability to interact with the chaperone system of Hsp90 and Hsc70. According to sequence alignments C33H5.8 may represent a shortened homolog of the human RNA-polymerase associated proteins RPAP3 and SPAG1, C34B2.5 is homologous to human TTC1 (homology ~58%, Figure 3.1.3) and ZK370.8 may be a very distant homolog of TOM70 (Figure 3.1.4). Furthermore, DNJ-28 is related to DNAJC3 and ADPR-1 is homologous to WDTC1 in humans. Additional proteins, which may bind to Hsc70 and Hsp90, include Y22D7AL.9, a putative homolog of human TTC28, and F52H3.5, which is related to TTC36 (Figure 3.1.5). OGT-1, which would be the next nematode candidate, shows scores in the range of 36 and no conservation in the MEEVD-interacting residues 5/12/13/74. Furthermore, its TPR is known not to bind Hsc70 and Hsp90. Therefore, proteins below this score were not considered as potential interaction partners.

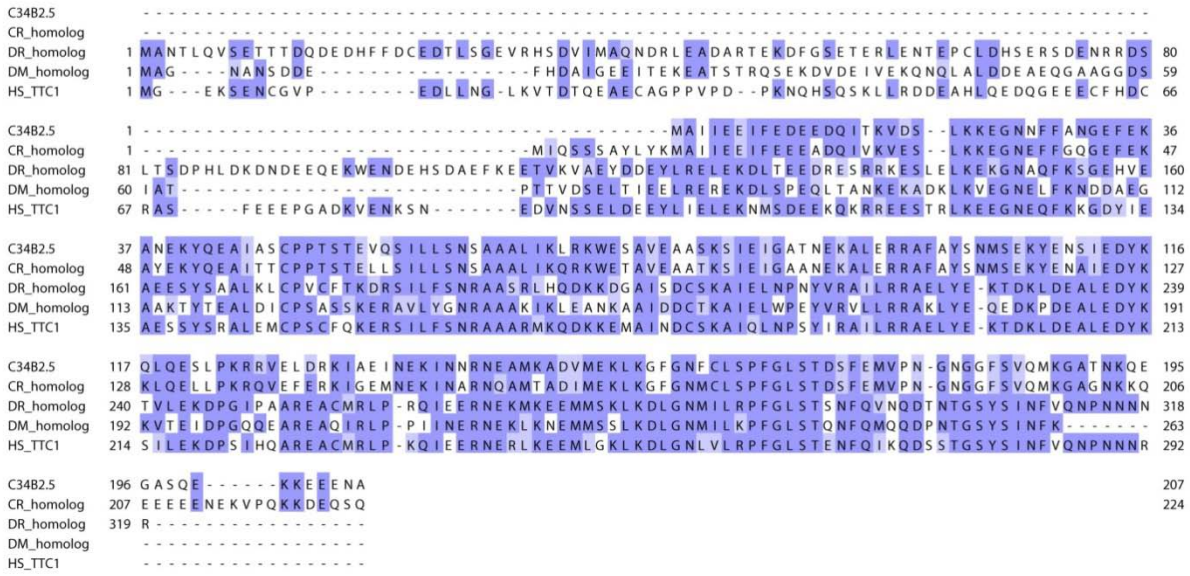

Figure 3.1.3. *Alignment of C34B2.5 with putative homologs of Caenorhabditis remanei (CR), drosophila (DM), zebrafish (DR) and humans (HS).*

Figure 3.1.4. *Alignment of ZK370.8 with putative homologs of yeast (SC), drosophila (DM), zebrafish (DR) and humans (HS).*

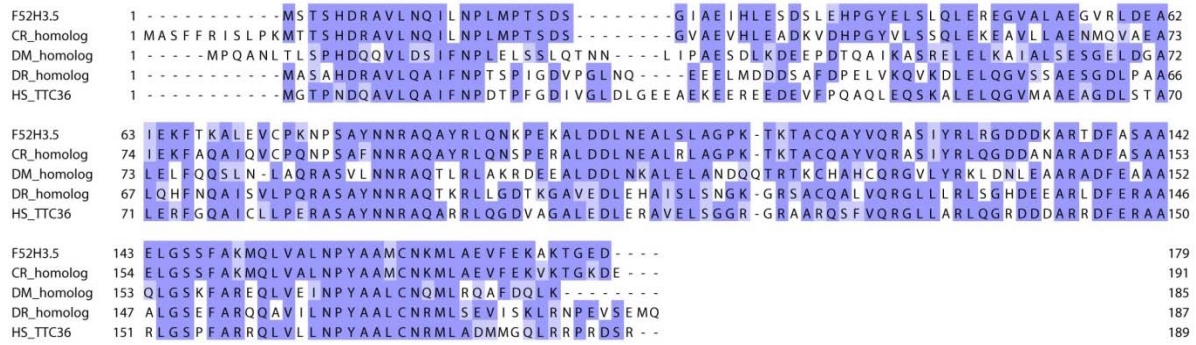

Figure 3.1.5. *Alignment of F52H3.5 with putative homologs of Caenorhabditis remanei (CR), drosophila (DM), zebrafish (DR) and humans (HS).*

3.1.2 TPR protein expression and purification for *in vitro* analysis

Earlier studies had shown that only about 15 % of the ORFs from *C. elegans* could be expressed in soluble form potentially due to the lower growth temperature of this organism (Luan et al, 2004). In order to confirm the predicted interactions however, purified protein encoded by the ORFs C33H5.8, C34B2.5, ZK370.8, DNJ-28, ADPR-1, Y22D7AL.9 and F52H3.5 would be necessary, but various proteins could neither be expressed nor purified by the established protocols stated in Materials and Methods. Recombinant C33H5.8 could only be produced in inclusion bodies and refolding attempts were unsuccessful. Analysis of the protein expression in BL21 (DE3) RIL at 37 °C for 3 h, at 30° for 3 h or overnight, at 20 °C for 3 h or overnight or at 13 °C overnight did not yield any soluble protein. Expression attempts in Arctic Express (DE3) RIL at 18 °C or 13 °C overnight did not improve solubility. The same was true for ADPR-1. As part of a protein-RNA complex like it might be the case for C33H5.8 or as member of multi-protein assemblies these proteins might lack important stabilizing contacts when expressed in *E. coli*. Expression of full-length ZK370.8 and DNJ-28 was very low even after similar attempts mentioned above and did not yield purified protein. In addition, cDNA for full-length Y22D7AL.9 is not commercially available and due to the length and distribution of introns and exons in the transcript only exon 1 (amino acid 1-165) encoding the TPR domain was tested. However, inclusion body expression (20 °C overnight) and subsequent refolding provided only around 1 mg of protein per 2 g of crude inclusion body pellet. Purification of the human homolog of ADPR-1, WDTC1, did not result in soluble protein. Expression of the TPR domain alone of WDTC1,

WDTC1aa346-490, in inclusion bodies at 20 °C overnight and refolding was as difficult as Y22D7AL.9aa1-165 purification. *In vitro* analysis of both proteins is described below.

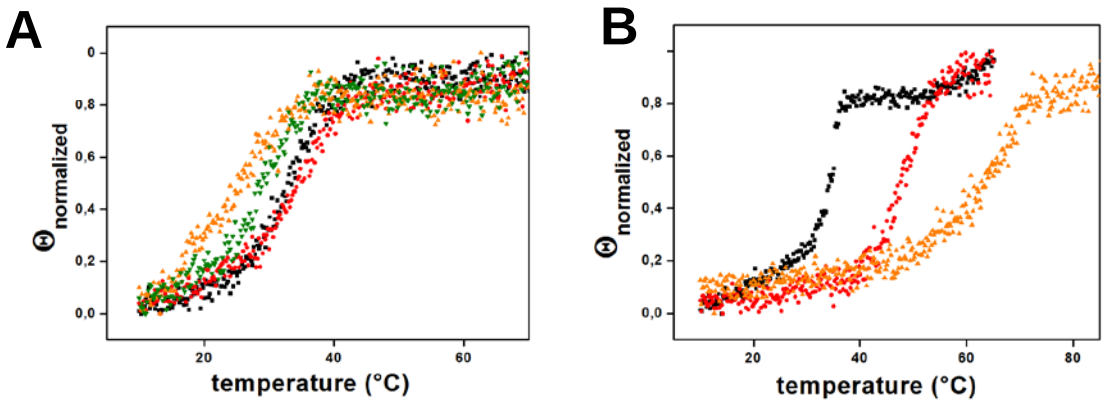

Figure 3.1.6. *Thermal unfolding of C34B2.5 and variants, ZK370.8-ΔN33, F52H3.5 and human TTC9. Thermal denaturation curves were recorded in a CD and the change in signal detected at 222 nm from 10 to 90 °C.* ***A****, C34B2.5 and variants start to unfold below 35 °C. Depicted is C34B2.5 in black, C34B2.5-K22S in red, C34B2.5-F29A in orange and C34B2.5-E85G in green.* ***B****, ZK370.8-ΔN33 is depicted in black, F52H3.5 in red and human TTC9 in orange. Curves were normalized for better comparison.*

The gene product of the second uncharacterized *C. elegans* ORF of the ranking, C34B2.5, could be expressed and purified to high amounts (~20 mg per liter LB medium). It encodes a 23 kDa protein composed of 207 amino acids. The protein is likely a homolog of TTC1 which had been shown to interact with the Hsp90 system during vesicle transport processes (Lotz et al, 2008). The protein is limited in temperature stability and starting to unfold above 25 °C, but stable under the physiological growth conditions of 20 °C of *C. elegans* (Figure 3.1.6 A). Due to the overall stability and high solubility of the protein several variants of C34B2.5 containing point mutations were expressed with similar stability (Figure 3.1.6 A) and their analysis is described below. ZK370.8 encodes a potential membrane anchored 63 kDa protein with 554 amino acids which may be the reason for the low expression yields of the full-length protein. After deletion of the N-terminal 33 amino acids of the protein, which comprise a transmembrane helix according to blast predictions, soluble protein could be expressed in bacteria up to 5 mg per liter LB medium. The purified protein is stable and denatures at temperatures higher than 25 °C (Figure 3.1.6 B).

3.1.3 C34B2.5 binds to Hsc70 and the C-terminus of Hsp90

Fluorescence based analytical ultracentrifugation was used in order to test the binding of C34B2.5 to nematode Hsc70 and Hsp90. Therefore, Hsc70 was labeled with 5(6)-FAM and sedimentation was followed by fluorescence of the dye. Labeled Hsc70 sediments at 4.6 S, whereas in presence of C34B2.5 the sedimentation peak is shifted to 4.9 S indicating a complex formation between C34B2.5 and Hsc70 (Figure 3.1.7 A). Similar experiments were performed with Hsp90, which was labeled by an N-terminal fusion of YFP. The YFP-Hsp90 dimer sediments at 7.1 S and again, the addition of C34B2.5 shifted the peak to higher $s_{20,w}$ values (Figure 3.1.7 B). Supplementation of the C-terminal MEEVD-motif of nematode Hsp90 could compete this interaction implying that complex formation is based on the TPR domain.

As the shifts are small due to the size of this TPR protein, the interaction between C34B2.5 and the two chaperones was confirmed by an independent method. ITC measurements were employed to determine the affinities of C34B2.5 to the C-terminal domain (CTD) of Hsp90 and full-length Hsc70, respectively. C34B2.5 bound to Hsp90-CTD with a K_D around 0.7 µM and a stoichiometry of 0.8 which indicates the binding of one TPR protein per Hsp90 monomer (Figure 3.1.7 C). The titration of Hsc70 with C34B2.5 resulted in a binding constant of 4.7 µM (Figure 3.1.7 D, Table 3.1.3), confirming that the putative homolog of human TTC1 indeed can interact with both chaperones. The characterization of the human protein TTC1 had so far only provided evidence for an interaction of the TPR cofactor with Hsp90 (Lotz et al, 2008).

Table 3.1.3. *Binding parameters of TPR-chaperone interactions.*

TPR protein	***ligand***	***K_D (µM)***	***N***	***$k_{folding}$ (s^{-1})***	***$k_{unfolding}$ (s^{-1})***	***ΔG (kJ/mol)***
C34B2.5	Hsp90-CTD	0.73 ± 0.17	0.84 ± 0.02			
	Hsc70	4.69 ± 1.82	0.71 ± 0.07			
	w/o peptide			100.94 ± 7.89	2.67 ± 0.39	-8.55
	Hsp90-peptide			100.02 ± 8.32	0.42 ± 0.12	-12.88
	Hsc70-peptide			104.06 ± 7.90	0.29 ± 0.10	-13.85
C34B2.5-K22S	w/o peptide			111.26 ± 7.89	0.53 ± 0.25	
	Hsc70-peptide			120.26 ± 12.48	0.93 ± 0.34	
C34B2.5-F29A	w/o peptide				19.03 ± 5.89	
	Hsc70-peptide				14.76 ± 3.07	
C34B2.5-E85G	w/o peptide			64.21 ± 4.41	3.59 ± 0.62	
	Hsp90-peptide			67.24 ± 4.81	0.54 ± 0.11	
	Hsc70-peptide			78.19 ± 6.29	0.67 ± 0.14	
ZK370.8	Hsp90-CTD	1.06 ± 0.22	0.90 ± 0.02			
	Hsc70	1.03 ± 0.39	0.61 ± 0.05			

Binding constants and stoichiometry values were determined for C34B2.5 and ZK370.8 and each chaperone at 20 °C. Folding and unfolding rates in H_2O of C34B2.5 with and without peptides were derived from fitting the chevron plots. ΔG values were calculated as described in materials and methods.

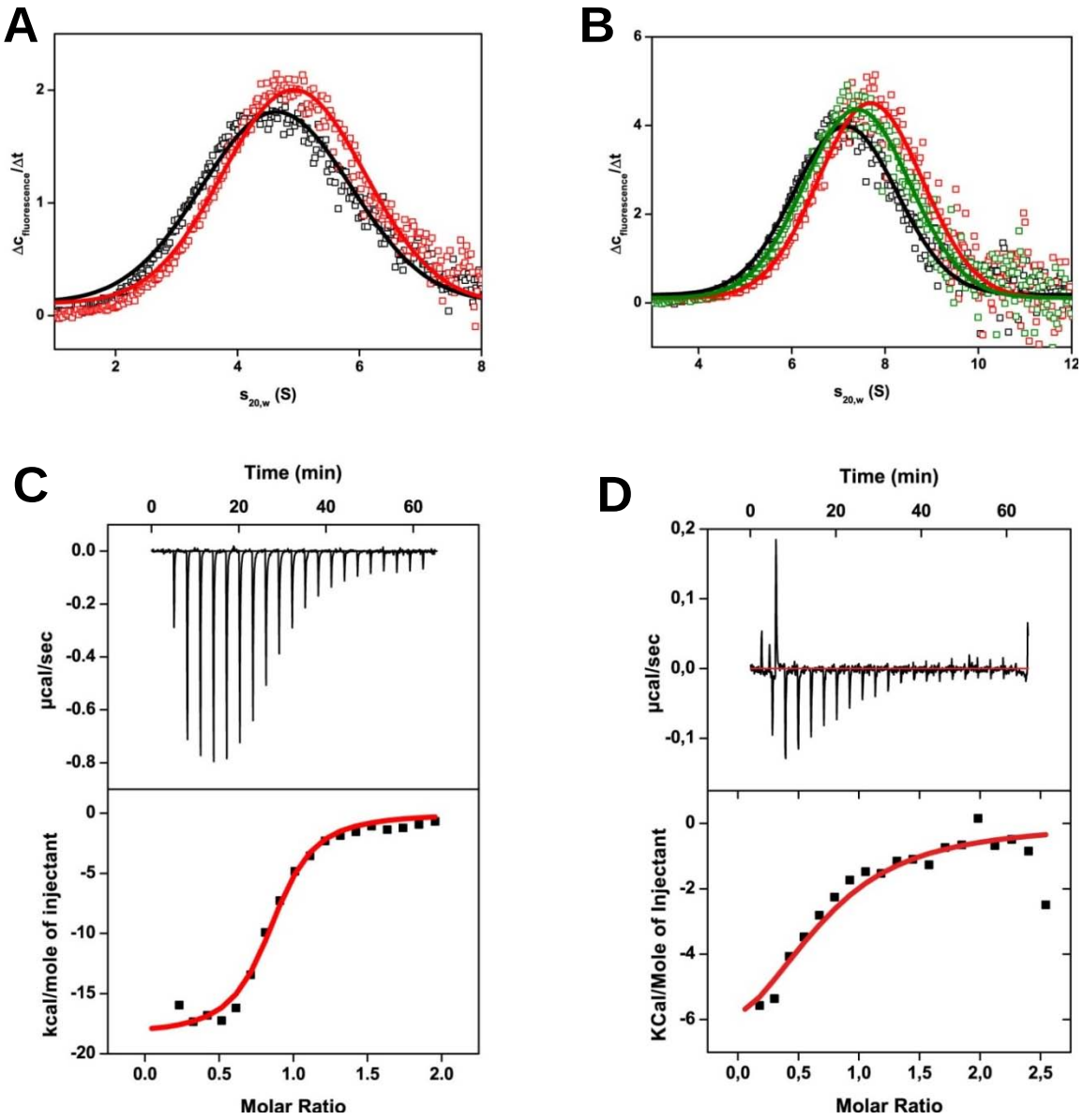

Figure 3.1.7. *C34B2.5 binds to Hsc70 and Hsp90.* ***A****, Hsc70 binding to C34B2.5 was analysed by fluorescence based analytical ultracentrifugation with 300 nM 5(6)-FAM labeled Hsc70 in absence (black) and presence (red) of 10 µM C34B2.5.* ***B****, Binding of C34B2.5 to Hsp90 was analyzed with a YFP-labeled Hsp90. Sedimentation velocity experiments were performed with 300 nM YFP-Hsp90 in absence (black) and presence of 6 µM C34B2.5 (red) and in presence of 6 µM C34B2.5 and 60 µM of the C-terminal Hsp90-peptide AEEDASRMEEVD (green).* ***C****, Affinity of Hsp90-CTD (280 µM in the syringe) for C34B2.5 (15 µM in the cell) was determined via ITC.* ***D****, Affinity of Hsc70 (15 µM in the cell) for C34B2.5 (180 µM in the syringe) was determined via ITC.*

3.1.4 Specific residues of the TPR domain of C34B2.5 mediate recognition of and stabilization via the C-terminal peptides of Hsc70 and Hsp90

Since C34B2.5 is a small protein of about 20 kDa and shows reversible folding transitions with urea, a new binding assay was established to analyze the C-terminl peptides of Hsc70 and Hsp90 whether they can bind to C34B2.5 and in this way influence the protein's stability. Unfolding and folding kinetics were measured in the absence and presence of peptides in a stopped flow fluroescence spectrophotometer. Addition of the C-terminal peptides of Hsc70 or Hsp90 clearly decreased the unfolding rate of C34B2.5 (Figure 3.1.8 A). Chevron plots were derived for both proteins in presence and absence of the C-terminal peptides of Hsc70 and Hsp90 to assess the impact of the peptides on the unfolding and refolding of the TPR domain (Figure 3.1.8 B). The resulting V-shaped plots for each setup represent the left refolding arm and the right unfolding arm separated by the denaturation midpoint. C34B2.5 clearly showed a shift of the denaturation midpoint to higher urea concentrations in presence of the peptide ligands. The overall stability of the TPR protein increases by ~4 kJ/mol and ~5 kJ/mol under our assay conditions when C-terminal peptide of Hsp90 and Hsc70 is bound, respectively (Table 3.1.3). These results demonstrate the stabilization of the TPR domain of C34B2.5 by binding to the EEVD-motifs with a more pronounced effect observable for the Hsc70 peptide. Like in other studies before (Cortajarena & Regan, 2006), these data imply that the TPR domain does not fold upon binding, but rather is stabilized by the bound peptide ligand. Further, two variants with point mutations in residue 5 and residue 12 of the alignment were tested. The exchange of Lys22 which corresponds to position 5 and contributes to the carboxylate clamp abrogated completely binding of the C34B2.5-K22S variant to Hsp90- and Hsp70-peptide (Figure 3.1.8 C), whereas the overall stability of the protein increased. Mutation of Phe29 (position 12 of the alignment) to a non-hydrophobic residue was again sufficient to abolish the interaction with the Hsc70-peptide (Figure 3.1.8 D). The exchange of this amino acid caused a pronounced loss in stability of C34B2.5-F29A. Therefore, it was important to check whether destabilization of C34B2.5 in general influences the binding capacity of the TPR domain. The less stable variant C34B2.5-E85G was cloned and purified. However, presence of both peptides strongly increased stability which demonstrates conserved binding properties of this variant despite its relaxed folding state (Figure 3.1.8 E).

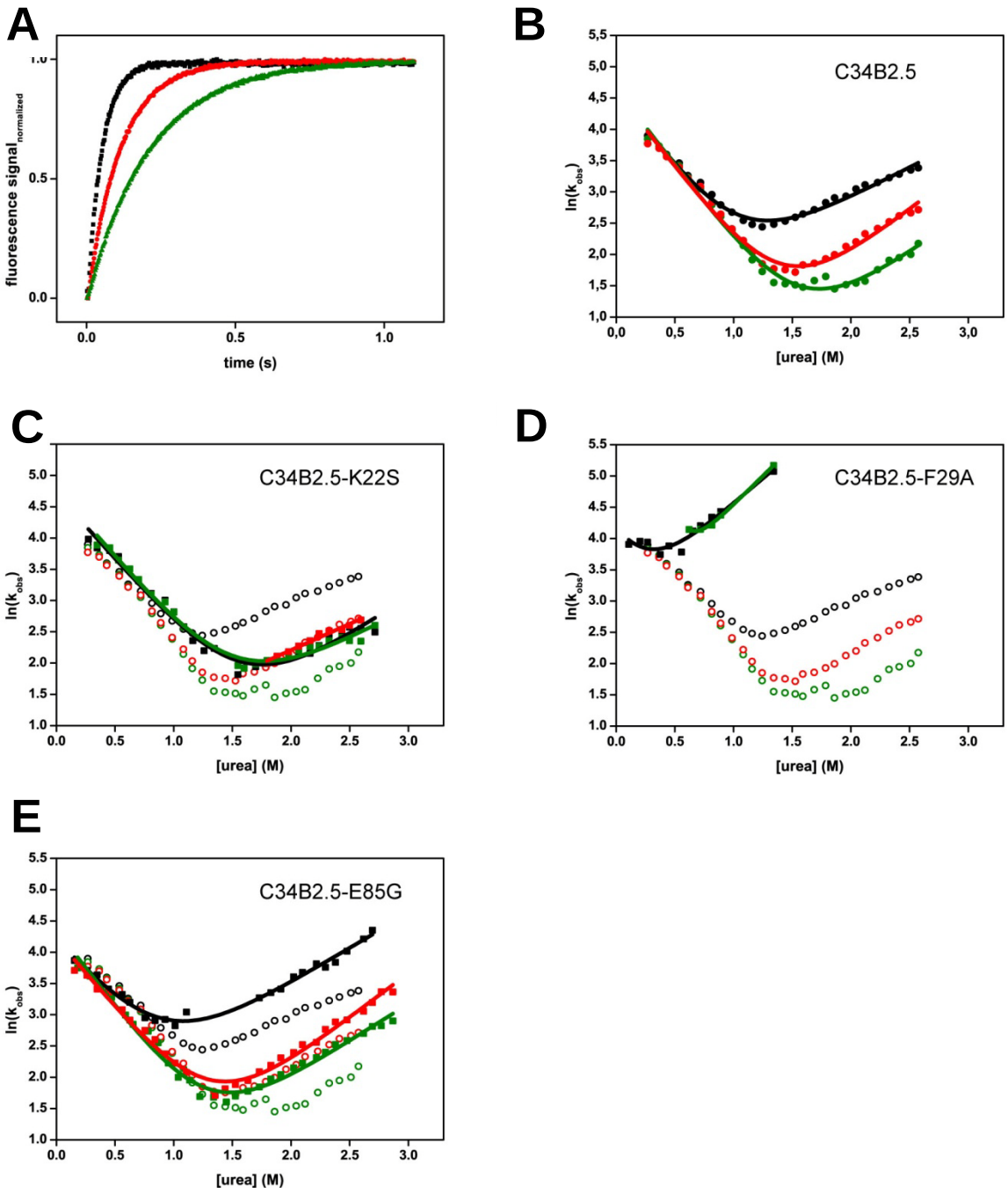

Figure 3.1.8. *Mutations in the TPR binding groove of C34B2.5 prevent peptide binding.* ***A****, The unfolding rate of 1 µM C34B2.5 in 2.0 M urea (black) was assessed using a stopped flow apparatus and is slowed down in presence of 45 µM of the peptide AEEDASRMEEVD (Hsp90, red) and of the peptide GGAGGPTIEEVD (Hsc70, green).* ***B-E****, Folding and unfolding rates of C34B2.5 and variants in increasing urea concentrations were recorded in a stopped flow apparatus and chevron plots were generated. Each data point represents the natural logarithm of the observed refolding or unfolding kinetic of 1 µM of the respective protein in urea buffer with circles for C34B2.5 and squares for the different variants (black). Settings containing 45 µM EEVD-peptides are depicted in red for the C-terminal peptides of Hsp90 and in green for the peptide of Hsc70.*

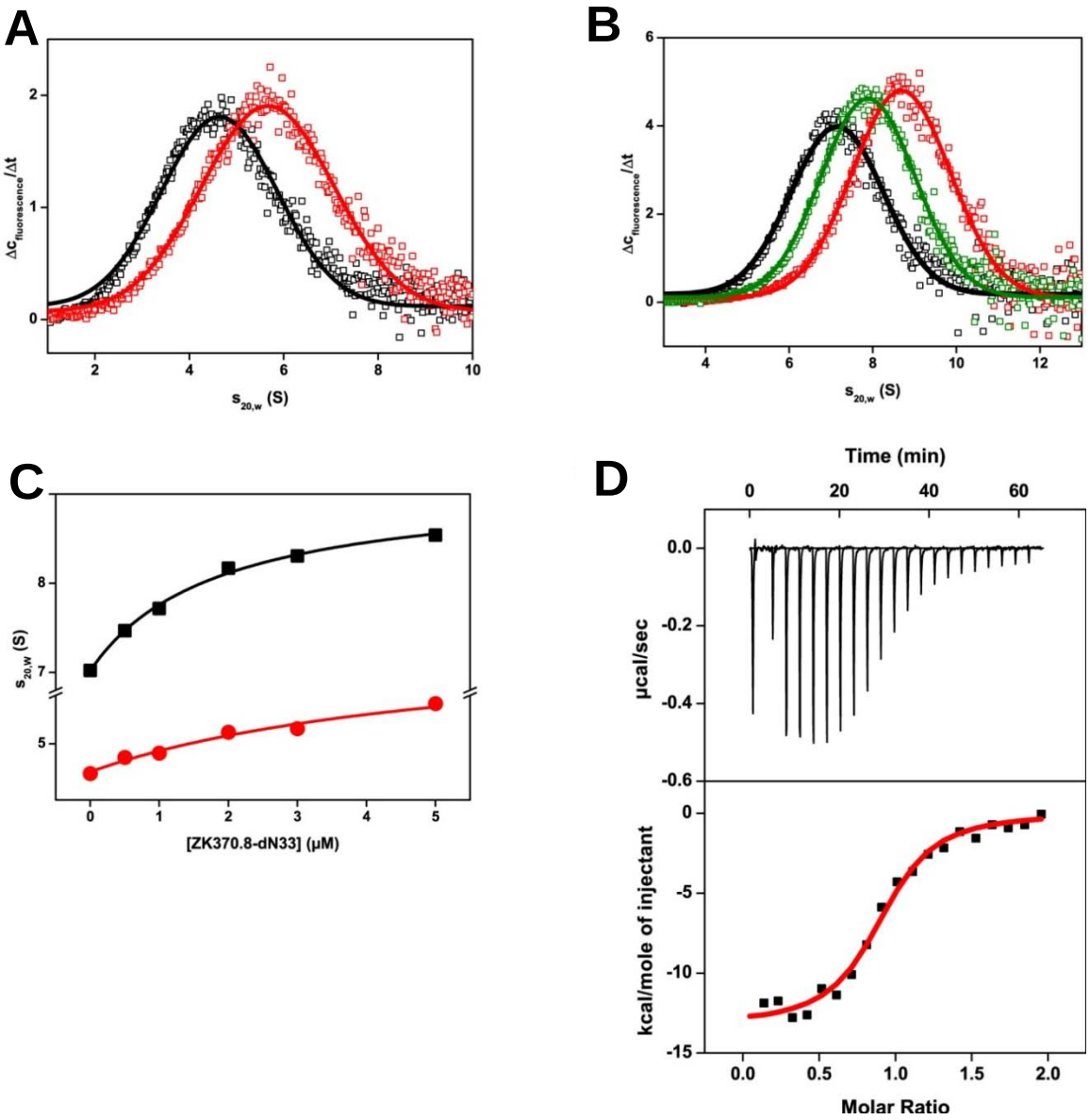

Figure 3.1.9. *ZK370.8 binds to Hsc70 and Hsp90. Binding of ZK370.8-ΔN33 to Hsp90 and Hsc70 was analyzed analogous to C34B2.5.* ***A****, Hsc70 binding to ZK370.8-ΔN33 was analyzed by AUC with 300 nM 5(6)-FAM labeled Hsc70 in absence (black) and presence (red) of 10 µM ZK370.8-ΔN33.* ***B****, 300 nM YFP-Hsp90 in absence (black) and presence of 6 µM ZK370.8-ΔN33 (red) and in presence of 6 µM ZK370.8-ΔN33 and 60 µM of the C-terminal Hsp90-peptide AEEDASRMEEVD (green) was analyzed.* ***C****, Increasing amounts of ZK370.8-ΔN33 shift the sedimentation coefficient to higher $s_{20,w}$ values. Dependence of the sedimentation coefficient of YFP-Hsp90 on cochaperone concentration is depicted in black, of labeled Hsc70 in red.* ***D,*** *Binding constants of Hsp90-CTD binding to ZK370.8-ΔN33 were determined via ITC.*

3.1.5 ZK370.8 binds to Hsc70 and the C-terminal of Hsp90

Searching the human genome for a homologous protein revealed that ZK370.8 could be related to the mitochondrial import receptor TOM70, but the similarity is very weak (Figure 3.1.3). AUC analyses were performed as described before for C34B2.5. Presence of ZK370.8-ΔN33 shifted labeled Hsc70 to 5.7 S (Figure 3.1.9 A) and YFP-Hsp90 to 8.7 S (Figure 3.1.9 B). The shift of the $s_{20,w}$ value of ZK370.8-ΔN33 allows an estimation of the dissociation constant of the chaperone interaction which seems to be in the low micromolar range for both Hsp90 and Hsc70 (Figure 3.1.9 C). This contact was confirmed by an independent method. ITC titration of ZK370.8-ΔN33 with Hsp90-CTD proved the interaction and resulted in a dissociation constant of 1.1 µM during binding of one TPR-protein per Hsp90 monomer (Figure 3.1.9 D). Titration of Hsc70 with ZK370.8-ΔN33 resulted in an apparent K_D of 1.0 µM (Table 3.1.3). Hence, ZK370.8, like C34B2.5, can interact with Hsc70 and Hsp90 *in vitro*.

3.1.6 F52H3.5/TTC-36 does not show binding to Hsc70 or Hsp90 *in vitro*

Due to the lack of sufficient purified protein to analyze the candidates DNJ-28, ADPR-1 and Y22D7AL.9, the subsequent ORF of the ranking, F52H3.5, was tested. F52H3.5 is a TPR protein with high similarity to the human protein TTC36 (Figure 3.1.5) which has not been characterized before. The protein contains 179 amino acids and is expressed in soluble and stable form (Figure 3.1.6). Using the ultracentrifugation assays described before, the binding affinities to Hsc70 and Hsp90 were assessed, but it was not possible to record any interaction. In addition, excess of F52H3.5 could not compete with the binding between ZK370.8-ΔN33 and labeled Hsc70 or YFP-Hsp90 (Figure 3.1.10 A, B). However, excess of C34B2.5 was able to weaken the interaction of ZK370.8-ΔN33 with the chaperones (Figure 3.1.10 C, B). In contrast to C34B2.5, the unfolding of F52H3.5 was unaffected by the Hsc70 peptide and by the Hsp90 peptide (Figure 3.1.10 E, F). Thus, it can be assumed that the TPR domain of this protein does not interact with the EEVD-motifs of the chaperone proteins. These finding are supported by the absence of the highly conserved residues and the comparably low HMMER3.0 score.

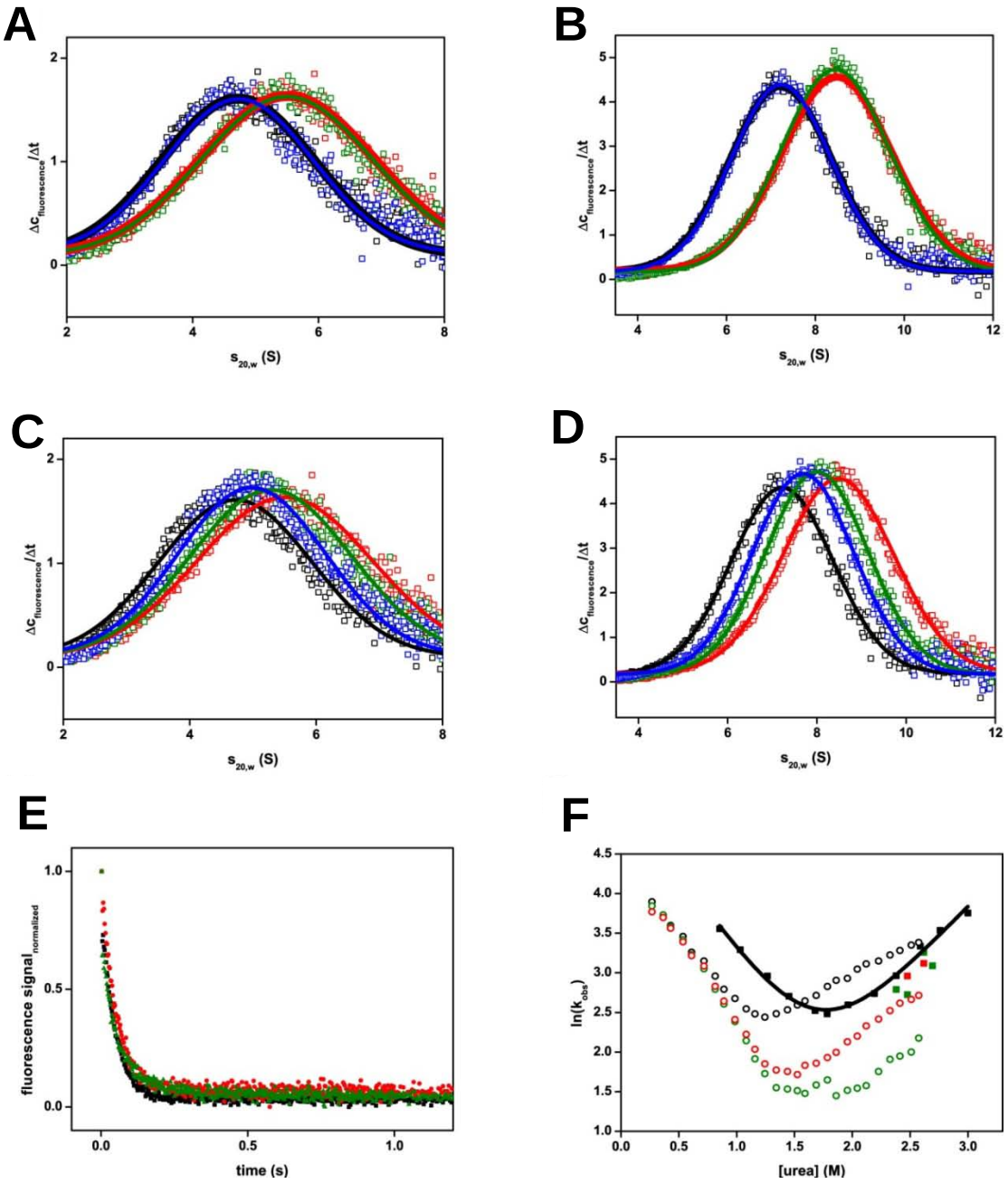

Figure 3.1.10. *F52H3.5 does not interact with Hsc70 or Hsp90.* ***A****, Sedimentation of 300 nM 5(6)-FAM-Hsc70 in absence (black) and presence of 10 µM F52H3.5 (blue) and* ***B****, 300 nM YFP-Hsp90 in absence (black) and presence of 10 µM F52H3.5 (blue) did not shift to higher $s_{20,w}$ values and therefore imply no binding to the TPR protein. Addition of 5 µM ZK370.8-ΔN33 to labeled Hsc70 (****A****) and 3 µM ZK370.8-ΔN33 to YFP-Hsp90 (****B****) led to a pronounced shift in the sedimentation coefficient (red curves). Supplementation of the chaperone-ZK370.8-ΔN33 setting with 10 µM F52H3.5 could not decrease the $s_{20,w}$ values of either chaperone (green).* ***C****,* ***D****, Same AUC runs were perfomed as in* ***A*** *and* ***B*** *with C34B2.5 instead of F52H3.5 using identical settings and concentrations. Presence of C34B2.5 led to a shift of the sedimentation coefficient of 5(6)-FAM-Hsc70 (****C****) and YFP-Hsp90 (****D****) to higher $s_{20,w}$ values (compare black and blue curves). The small protein C34B2.5 could compete with the larger protein ZK370.8-ΔN33 for chaperone binding leading to a decrease of the sedimentation coefficient (compare red and green curves).* ***E****, The unfolding rate of 1 µM F52H3.5 in 2.5 M urea is not influenced by 45 µM of the Hsp90-peptide AEEDASRMEEVD (red) and the Hsc70-*

peptide GGAGGPTIEEVD (green). ***F,*** *Folding and unfolding rates of F52H3.5 and C34B2.5 in increasing urea concentrations were recorded and chevron plots were generated with filled squares for F52H3.5 and open circles for C34B2.5 (black). Settings containing 45 µM EEVD-peptides are depicted in red for the C-terminal peptide of Hsp90 and in green for the peptide of Hsc70.*

3.1.7 C34B2.5 and ZK370.8 are spatially regulated

Finally, it is interesting to know whether the two TPR-proteins are expressed at detectable levels and whether certain tissues can be defined, where the interaction with chaperones is relevant in the multicellular nematode. The tissue specific expression for Hsp90 has been analyzed before and the protein was found in muscle cells, but also in pharynx and some other tissues.(Gaiser et al, 2011) *daf-21*-RNAi treatment of the integrated *hsp-70::GFP* heat shock reporter strain led to reduced motility and sterility as well as expression of GFP in muscle cells, highlighting the importance of functional Hsp90 in muscles (Figure 3.1.11 A and (Gaiser et al, 2011)). In contrast, genome wide promoter studies (www.wormbase.org) suggest that Hsc70 expresses predominantly in intestinal cells (Guisbert et al, 2013). Gene knock-down was used to localize functional Hsc70 protein in the *hsp-70::GFP* containing heat-shock reporter strain. RNAi against Hsc70 leads to larval arrest and sterility(Gaiser et al, 2009), but also led to a dramatic induction of the heat-shock response in cells of the gut as reported before (Guisbert et al, 2013) (Figure 3.1.11 B), suggesting that Hsc70 is involved in processes which prevent stress in intestinal cells.

To estimate the tissue-specific expression of the cofactors, full-length fusions of the two TPR proteins C34B2.5 and ZK370.8 were generated with C-terminal YFP under control of their endogenous promoter sequences. The constructs were injected and stable nematode strains were generated. ZK370.8-YFP is observable in muscle cells and several other tissues like the pharynx and structures in the tail (Figure 3.1.11 C). Clearly the protein was not present freely in the cytosol, but attached to cellular substructures. In order to test, whether ZK370.8, like its potential homolog TOM70 (Gava et al, 2011), localizes to the mitochondria, co-staining with the dye Mitotracker Red was performed. Comparing the appearance of MitoTracker and of ZK370.8 the TPR protein could be localized to the mitochondria (Figure 3.1.11 E), where ZK370.8 is presumably anchored in the mitochondrial membrane and can interact there with the cytosolic Hsp90 pool in muscles and other tissues. C34B2.5, instead, was predominantly expressed in intestinal cells as well as in selected neurons (Figure 3.1.11 D). This expression pattern is supported

by genome-wide studies employing transcriptional fusions of fluorescent proteins to promoter sequences.(Dupuy et al, 2007) To test, whether subcellular localization of C34B2.5 and Hsc70 overlaps in intestinal cells, another strain was generated that coexpresses C34B2.5-YFP and Hsc70-CFP under the C34B2.5 promoter. Both proteins colocalized to spot-like structures in intestinal cells (Figure 3.1.11 F) which highlights the potential of Hsc70 to interact with C34B2.5 also *in vivo* and suggest that this interaction likely is relevant in intestinal cells in *C. elegans*.

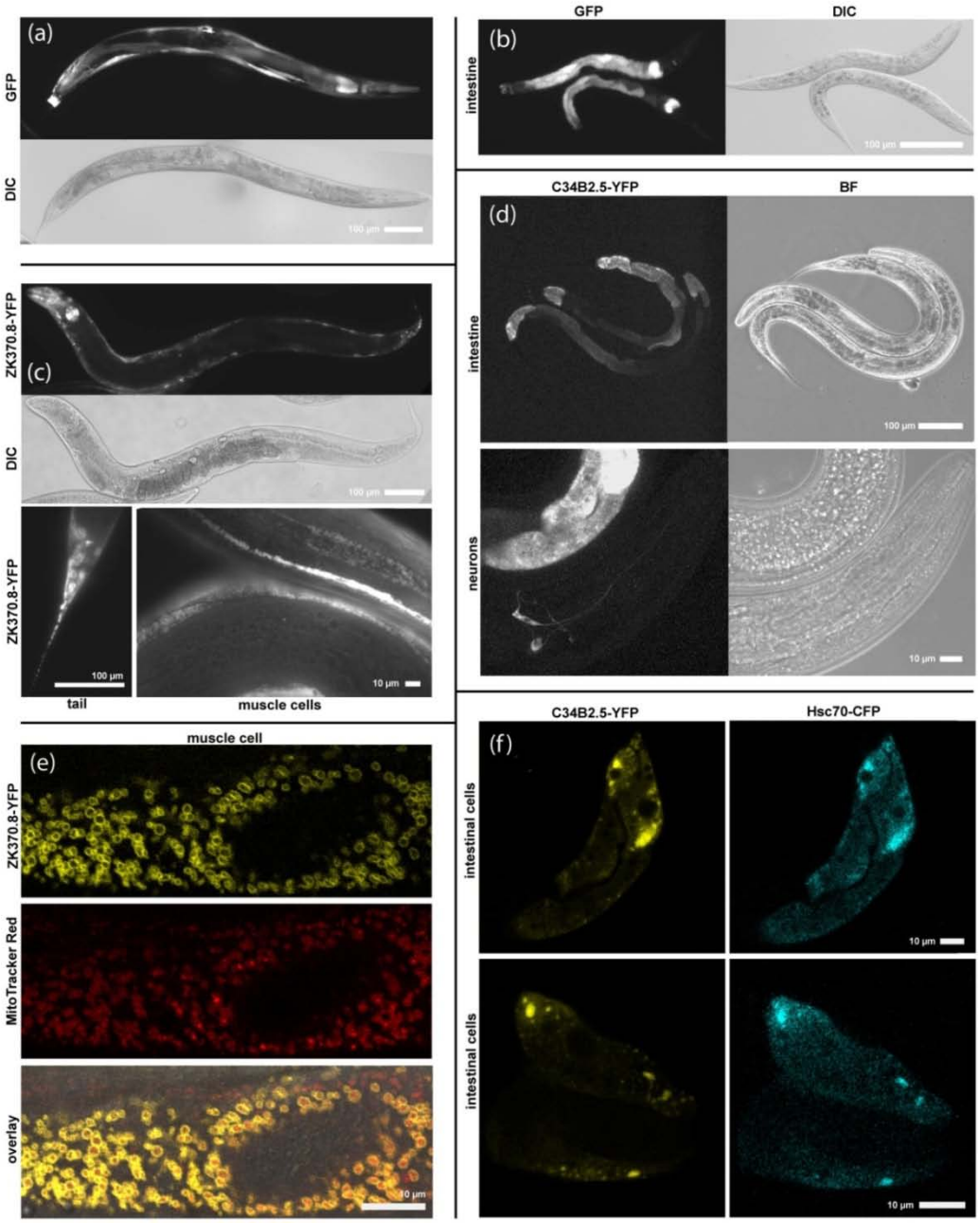

Figure 3.1.11. *ZK370.8 and C34B2.5 coexpress with the chaperones Hsp90 and Hsc70, respectively.* ***A****, Feeding of daf-21 RNAi constructs to the reporter strain hsp-70::GFP causes a heat shock response in muscle cells. (Gaiser et al, 2011)* ***B****, A strong heat shock response is switched on in the reporter strain hsp-70::GFP in response to hsp-1 knock-down in the intestine.* ***C-F****, Transgenic C. elegans strains were generated by injection of constructs carrying YFP-fusions of the TPR cochaperones under the endogenous promoter into wildtype N2 nematodes.* ***C****, Like Hsp90, ZK370.8 is largely expressed in body wall muscle cells, but also in the pharynx and structures in the tail.* ***D****, C34B2.5 is mainly expressed in the intestine where also Hsc70 is present, but also in some neurons projecting to the head.* ***E****, Staining transgenic C. elegans carrying the ZK370.8-YFP fusion protein with MitoTracker Red localizes the TPR protein to the membrane of mitochondrias.* ***F****, Intestinal cells that coexpress C34B2.5-YFP and Hsc70-CFP under the C34B2.5 promoter show colocalization of both proteins at certain spots and structures in one cell.*

3.1.8 Uncharacterized human and nematode TPR proteins show binding to Hsp90

Finally, the same HMMER analysis was performed on the human TPRome using the sample set descriebed before (Table 3.1.4). The TPR domains of potential interactors of the chaperone systems of Hsp90 and Hsc70 were purified. TTC9(20-222) was obtained in high purity, whereas WDTC1(346-490), TTC12(99-225) and Y22D7AL.9(1-165) could only be enriched up to approximately 50% of the total protein (estimated by SDS-PAGE). Y22.D7AL.9 was analyzed as putative *C. elegans* homolog of human TTC28. The low purity of the proteins can cause artifacts, but as *E. coli* does not contain TPR domain containing proteins and, in addition, no bacterial interactors of HtpG/Hsp90 are known to date, an AUC analysis using YFP-Hsp90 allows an initial characterization of their ability to act as cochaperone. For all three proteins an interaction with YFP-Hsp90 could be observed, if high concentrations (6 µM) of the different TPR proteins were added (Figure 3.1.12 A). A slight shift for labeled Hsc70 could only be observed for TTC9(22-220) (data not shown).

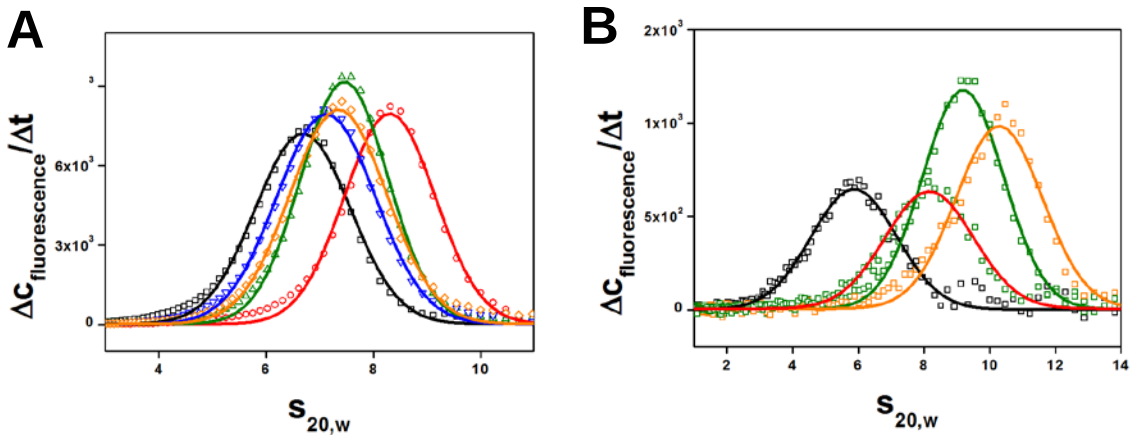

Figure 3.1.12. *New putative cochaperones bind to Hsp90 in AUC experiments.* ***A,*** *Several putative interactors of Hsp90 shift the sedimentation coefficient of nematode YFP-Hsp90 (control in black) to higher $s_{20,w}$ values. Presence of TTC9(20-222) is depicted in red, WDTC1(346-490) in orange, TTC12(99-225) in green and Y22D7AL.9(1-165) in blue.* ***B,*** *Binding of TTC9(22-220) was confirmed using labeled human Hsp90. Presence of 6 µM TTC9(22-220) (red) could shifted fluorescent Hsp90 (control in black). Addition of rat PP5 could further shifted the complex of Hsp90 and the TT9 fragment to higher $s_{20,w}$ values (orange). Addition of PP5 alone is depicted in green.*

A positive interaction, however, could also indicate unspecific chaperone-substrate interaction and would not allow substantial interpretation of the AUC data. Based on these data the interaction of these TPR proteins with Hsp90 can be assumed, but the affinity may be weak compared to that of C34B2.5 and ZK370.8. The interaction of the

TTC9 fragment was confirmed using labeled human Hsp90-alpha which was kindly provided by Oliver Lorenz (Lehrstuhl für Biotechnologie, Technische Universität München, Germany). Presence of TTC9(22-220) was able to shift human Hsp90 (Figure 3.1.12 B). Addition of rat PP5 further shifted the Hsp90-TTC9 complex to higher $s_{20,w}$ values indicating the formation of mixed Hsp90-cochaperone complexes that contain two different cochaperones. TTC9 likely represents a new, so far undescribed cochaperone of the human Hsp90 system which was identified by the algorithm described in this thesis.

Table 3.1.4. *Cross-comparison of the TPRomes of C. elegans and H. sapiens.*

C. elegans		*H. sapiens*	
TPR domain	**Score**	**TPR domain**	**Score**
SGT-1	105.1	SGTB	121.4
		SGTA	112.6
PPH-5	104.1	PPP5C	108.1
STI-1b**	103.0	STIP1c	99.7
CHN-1	101.5	STUB1	104.1
UNC-45	100.8	UNC45A	112.4
		UNC45B	106.7
C17G10.2	95.4	TTC4	98.2
C56C10.10	89.5	AIP	93.4
T12D8.8	87.4	SP13	90.4
FKB-6	86.2	FKBP4	107.4
		FKBP5	105.3
STI-1a**	85.9	STIP1b	81.6
C33H5.8	76.2	RPAP3a	103.4
C34B2.5	71.4	TTC1	89.8
ZK370.8	58.7	TOMM70A	92.6
DNJ-28c	44.9	DNAJC3c	57.9
ADPR-1	44.6	WDTC1	74.4
DNJ-28a	44.5	DNAJC3a	40.7
Y22D7AL.9	44.1	TTC28	64.8
F52H3.5	43.2	TTC36	33.7
DNJ-7a	41.7	DNAJC3a	40.7
OGT-1	36.6	OGT	44.0
T20B12.1	35.8	TTC27	32.2
DNJ-7c	34.9	DNAJC3c	57.9
PRX-5	28.0	PEX5b	23.4
ZK328.7	27.3	TTC21B TTC21A	30.2
			30.1
EMB-27	26.7	CDC16	31.4
DYF-1	25.6	TTC30B	19.3
		TTC30A	19.8
Y37E3.1	25.0	TTC5	19.6
B0464.2	23.3	CTR9	25.7
F58A4.14	22.4	BBS4	39.7
DNJ-28b	21.7	DNAJC3b	40.6
UTX-1	21.4	KDM6A	16.4
DNJ-7b	21.3	DNAJC3b	40.6
KLC-1	19.3	KLC4	17.5
BBS-8	19.1	TTC8	22.9
MAT-1	17.9	CDC27	37.5
AGS-3	17.9	GPSM2	24.2
		GPSM1	21.0
Y47A7.1	17.7	TTC37	36.3
KLC-2	17.6	KLC4	17.5
Y57G7A.10	17.5	TTC35	14.3
CRA-1	16.9	NAA16	31.1
TAG-315	16.3	GTF3C3	22.8
K09A9.6	16.1	444ASPH/ASPH	<10
MAT-3	15.8	CDC23	20.2
RMD-6	14.5	RMD2/FAM82A1	<10
RMD-4	14.6	RMD2/FAM82A1	<10
FIS-1	14.6	FIS1	<10
DYF-13	14.6	TTC26	18.9
F33H2.6	13.5	RMD1/FAM82B	11.0
RMD-2	13.2	RMD1/FAM82B	11.0
RMD-1	12.5	RMD1/FAM82B	11.0
Y59A8B.6	12.3	PRPF6	<10
F45G2.4	12.1	TRAF4	<10
F08D12.1	10.3	SRP72	18.1
		TTC12	90.3
		TTC9	57.6

All TPR domain containing proteins of C. elegans are listed with the putative homolog and the respective score of the TPR proteins of humans. Regions outside the TPR domain were used to assess homology of the orthologs. Asterisks labeling is applied as in Table 3.1.2. Proteins whose TPR domains were analyzed in vitro are marked in green.

3.2 Selective activation of protein phosphatase 5 by small molecules*

*This chapter is currently submitted for publication (Haslbeck et al, *Submitted manuscript*).

3.2.1 Identification of novel small molecule activators of PPH-5

The protein phosphatase 5 is a highly regulated enzyme. The autoinhibition of the phosphatase is controlled by the N-terminal TPR domain and the C-terminal αJ helix, implying a complex mechanism to control the turnover rate. The aim of the compound screen described in the following chapter was to identify small molecules which can alter the activity of the phosphatase. Due to the 5-fold higher activity of nematode PPH-5 (~0.62 sec^{-1}) compared to mammalian PP5 (~0.12 sec^{-1}) at a screening temperature of 20 °C, the *C. elegans* homolog was used for the initial screen. The homology between nematode PPH-5 and human PP5 is pronounced with a sequence conservation of almost 80 % (Figure 3.2.1).

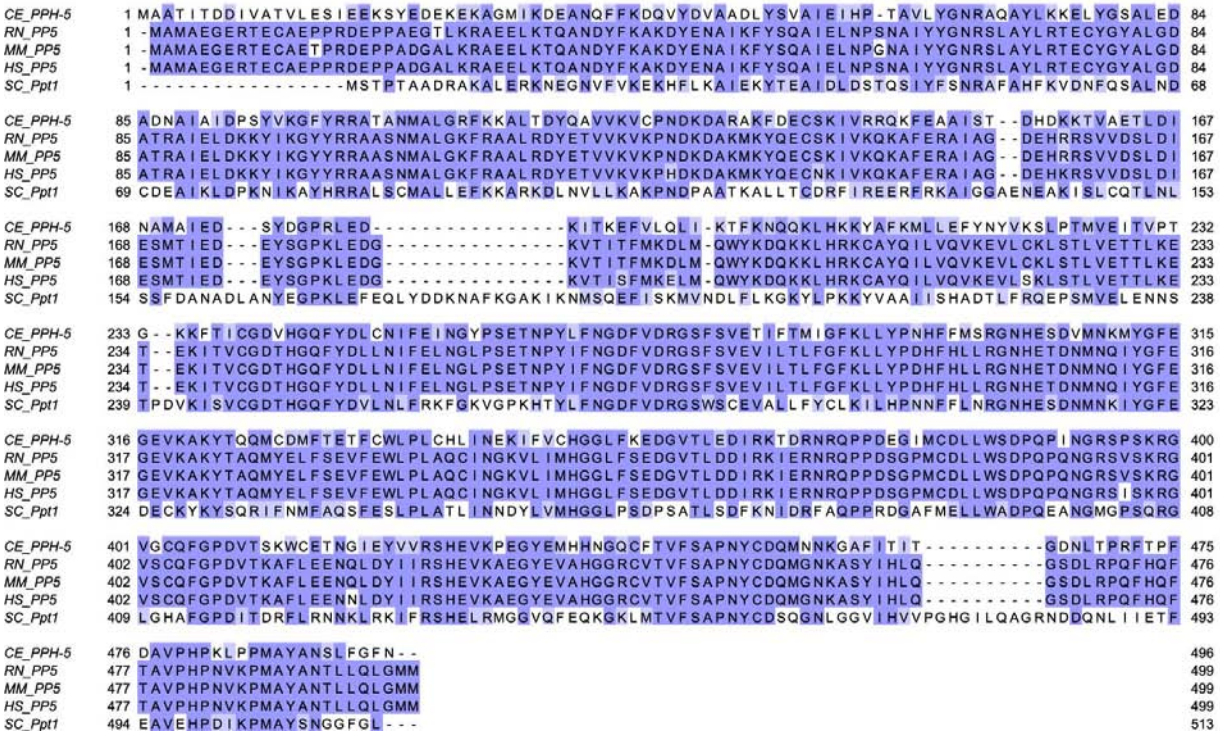

Figure 3.2.1. *Alignment of protein phosphatase 5 of different species. The protein sequence of PPH-5 of C. elegans (CE), PP5 of Rattus norvegicus (RN), of Mus musculus (MM) and of Homo sapiens (HS) and Ppt1 of S. cerevisiae (SC) were aligned using ClustalW. The alignment was processed by Jalview and therein the Blosum62 matrix used for visualization of the sequence homology.*

Using the substrate para-nitrophenyl phosphate (pNPP), a library of 15,000 compounds was screened and five substances could be identified which strongly accelerate the enzymatic activity of PPH-5 (Figure 3.2.2 A). All molecules are smaller than 500 Da (Figure 3.2.2 B), are stable at room temperature and follow the Lipinsky's rule of five. In the following text the acronyms ***P***rotein phosphatase ***5*** ***S***mall molecule ***A***ctivator 1 to 5 (P5SA-1 to P5SA-5) are used for the substances. The P5SAs were utilized at different concentrations to determine the apparent K_D-value in the pNPP-based assy yielding dissociation constants in the range of 6 µM to 26 µM causing a 4 to 10-fold activation under these conditions (Table 3.2.1).

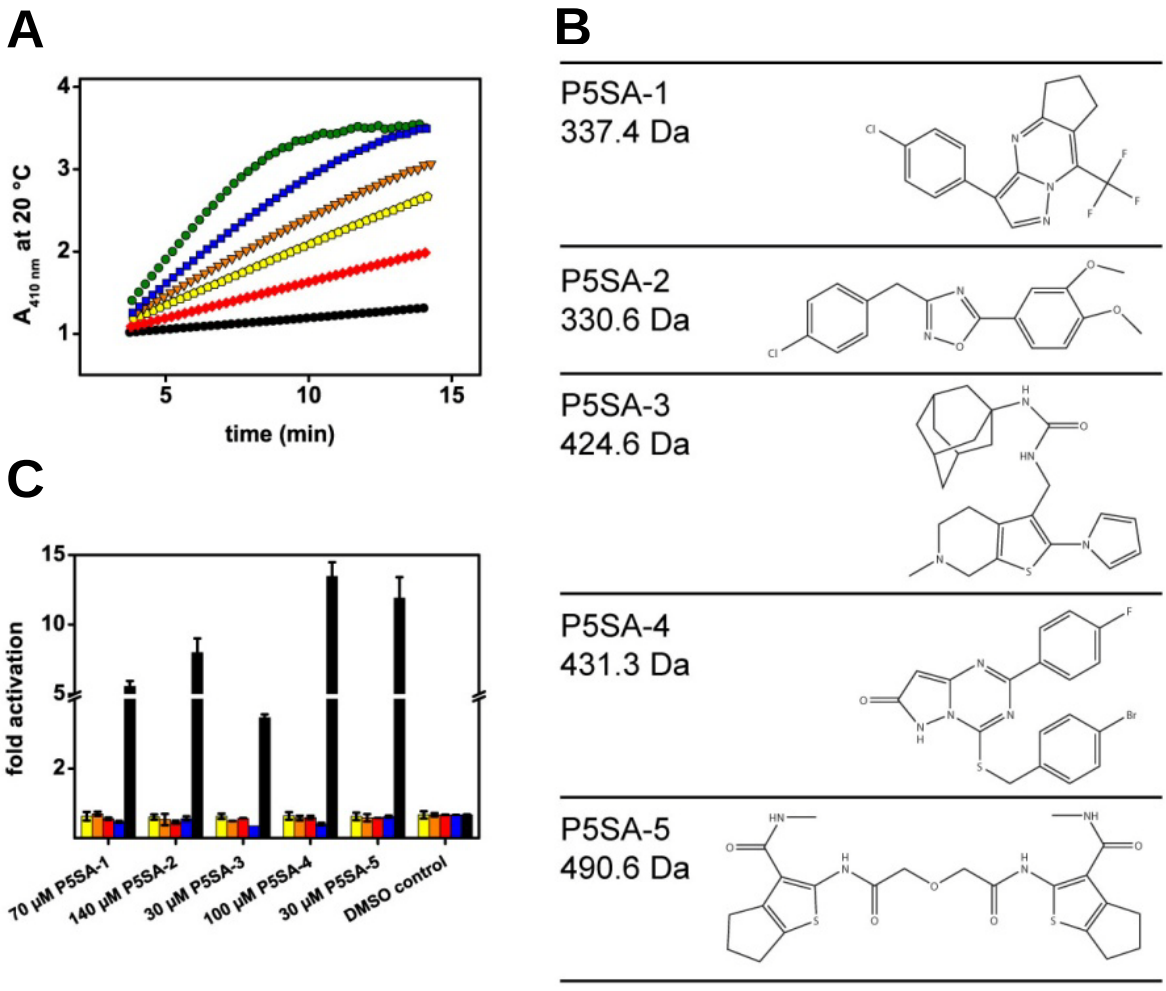

Figure 3.2.2. *Small molecules selectively activate nematode PPH-5.* ***A,*** *The substances (50 ng/mL) P5SA-1 (yellow), P5SA-2, (orange), P5SA-3, (red), P5SA-4 (blue) and P5SA-5 (green) activate PPH-5 (DMSO control in black).* ***B****, Chemical structures of the five activators.* ***C****, Human paralogs of PP5, PP1 (yellow), PP2A (orange) and PP2B/PP3 (red), as well as the bovine intestinal alkaline phosphatase (BIAP, blue) are not affected by the small molecules in contrast to PPH-5 (black). Each bar represents at least three independent experiments.*

Table 3.2.1. *Enzymatic parameters in presence of the P5SAs.*

	PPH-5 (*C. elegans*)				**PP5 (*R. norvegicus*)**
	K_D (µM)	**K_M (mM)**	**k_{cat} (sec^{-1})**	**fold activation**	**fold activation**
DMSO	-	7.0 ± 0.4	0.62 ± 0.02	-	-
P5SA-1	13.3 ± 4.2	3.0 ± 0.2	2.28 ± 0.03	3.7 (sat.)	2.7 at 143 µM
P5SA-2	7.8 ± 1.4	2.5 ± 0.1	5.98 ± 0.06	9.6 (sat.)	13.7 at 714 µM
P5SA-3	N/D	N/D	N/D	4.0 at 714 µM	7.0 at 714 µM
P5SA-4	25.7 ± 5.5	5.0 ± 0.3	4.85 ± 0.08	7.8 (sat.)	16.4 at 143 µM
P5SA-5	6.4 ± 1.8	4.3 ± 0.3	5.22 ± 0.09	8.4 (sat.)	22.1 at 45 µM

3.2.2 Small molecule activation is highly specific to PP5-like proteins

The first question to address was whether the hits of the compound screen act due to unspecific hydrophobic interactions. It is important to check, if other enzyme classes are influenced by the presence of the small molecules. To rule out that the P5SAs have any unspecific effect on other proteins, the ATPase active Hsc70 and Hsp90 were employed. As these chaperones potentially bind via hydrophobic patches to a broad set of proteins and nonpolar structures, it seemed to be a well-suited control for unspecific binding of the screened molecules. The P5SAs neither impacted the ATPase activity of both chaperones, nor abrogated the binding of cofactors to Hsc70 or Hsp90 (Figure 3.2.3).

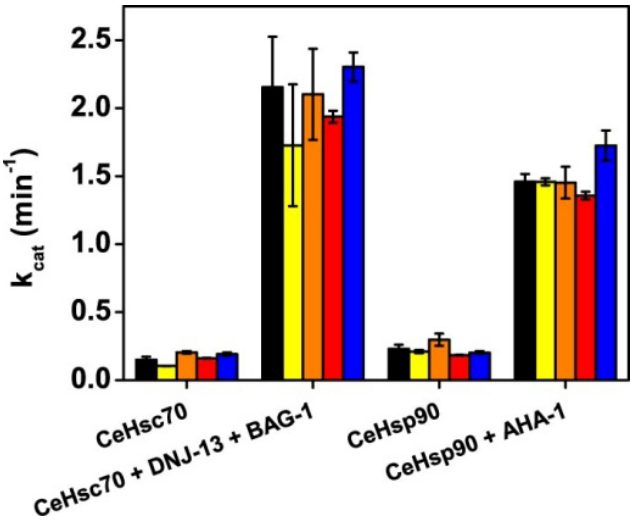

Figure 3.2.3. *The P5SAs neither influence the ATPase activity of C. elegans Hsc70 and C. elegans Hsp90 nor interfere with the interaction sites between the chaperones and their cochaperones. Concentrations well above the K_D of P5SA-1 (yellow), P5SA-2 (orange), P5SA-4 (red) and P5SA-5 (blue) were tested for their ability to interfere with the ATPase rates of the nematode chaperone systems of Hsc70 and Hsp90. DMSO controls are shown in black. Addition of the nucleotide exchange factor BAG-1 and the the J protein DNJ-13 increases the activity of Hsc70/HSP-1, but the P5SAs have no additional effect. The activator of Hsp90 AHA-1 acts as predicted by increasing the ATPase rate. P5SAs have again no effect on this chaperone system. Each bar represents three independent experiments.*

In addition to specificity, a high selectivity for a certain member of a protein family is very important for a potential drug candidate. Since the phosphatase domain of members of the PPP family is highly homologous, the human PP1, PP2A and PP2B/PP3 were analyzed. Neither activation nor inhibition of the respective phosphatase activity was detected, implying that the identified molecules are specific activators of the Hsp90-associated PP5/PPH-5 (Figure 3.2.2 C). Unspecific pNPP hydrolysis could be excluded as well, as bovine intestinal alkaline phosphatase (BIAP) was not affected. The next step was to challenge homologs of PPH-5 from other species. Activation of the yeast homolog Ppt1 could not be detected which shows reduced similarity of around 60% and more sequence deviations to human PP5 (Figure 3.2.1, Figure 3.2.4).

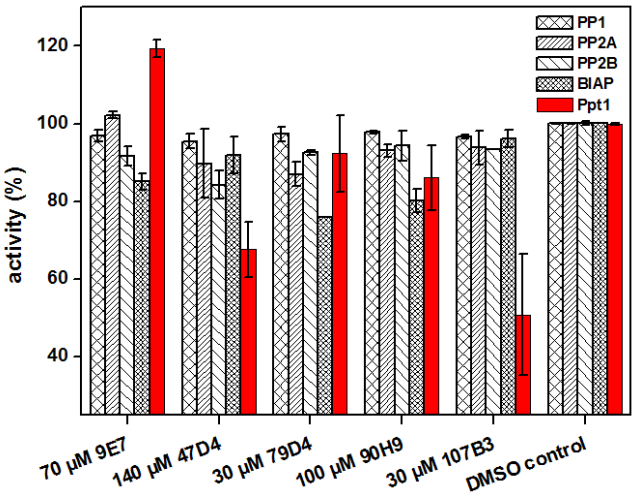

Figure 3.2.4. *The activity of the yeast homolog Ppt1 is only weakly influenced by the presence of the P5SAs. Applied concentrations are indicated. For better comparison, activities of PP1, PP2A, PP2B and BIAP are shown in the figure.*

However, PP5 from *Rattus norvegicus* with 98% sequence identity to human PP5 exhibited vast activation when treated with P5SAs and showed an even more pronounced response than nematode PPH-5 used in the initial screen (Table 3.2.1). Therefore, the affinity of theses activators towards the mammalian protein was assessed resulting in a binding constant of 10 ± 5 µM for P5SA-5, while the other P5SAs showed decreased affinities towards rat PP5 in comparison to PPH-5 from *C. elegans* (Table 3.2.1, Figure 3.2.5). The conserved activation potential of the P5SAs for higher eukaryotes and their selectivity for PP5 suggest that the activation depends on the specific architecture of PP5 and its complex reaction pathway.

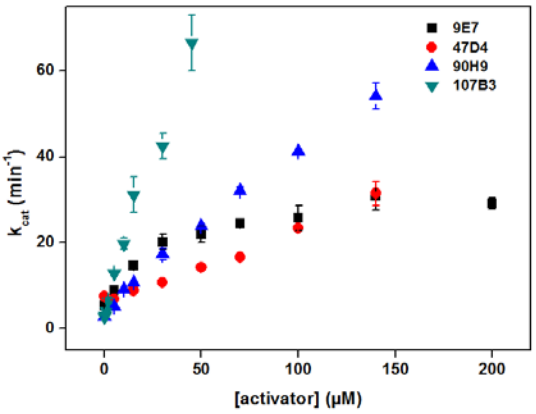

Figure 3.2.5. *P5SA affinity is reduced for the rat homolog PP5. Phosphatase activity was measured in presence of increasing amounts of activator using pNPP as substrate.*

3.2.3 The P5SAs are allosteric regulators of PPH-5

In order to gain insight into the activation mechanism, the question was addressed whether the substrate pNPP interacts with the P5SAs during the dephosphorylation reaction. Direct involvement of the small molecules in the hydrolysis of pNPP should be reflected in a change of the apparent K_M value under saturating concentrations of the activators. All P5SAs reflect a strong alteration of the k_{cat} value, but only weakly influence the observed K_M-value for pNPP (Figure 3.2.6, Table 3.2.1). Hence, there is no specific interaction between the substrate pNPP and the P5SAs demonstrating allosteric activation of PPH-5.

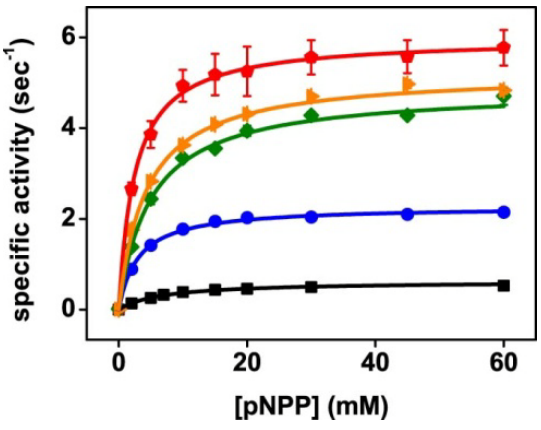

Figure 3.2.6. *The P5SAs only weakly influence the apparent K_M of pNPP. Substrate titrations of pNPP were done with 100 nM of PPH-5. The substrate binding curve in absence of activators is depicted in black. P5SA-1 (blue) was added to 70 µM, P5SA-2 (red) to 140 µM, P5SA-4 (green) to 100 µM and P5SA-5 (orange) to 30 µM. Each data point represents three to six independent experiments.*

To further test the binding of P5SA-2 to PPH-5, relaxation-edited NMR spectra of the substance with and without 10 µM PPH-5 were recorded in collaboration with Grzegorz Popowicz (Lehrstuhl für Biomolekulare NMR-Spektroskopie, Technische Universität München, Germany). Relaxation-editing strongly attenuates signals from big, slowly tumbling molecules but retains signals from small, fast tumbling moieties (Hajduk et al, 1997). Most of the peaks of P5SA-2 disappeared after addition of PPH-5 (Figure 3.2.7). This is caused by a much slower tumbling rate of the protein-ligand complex in comparison to the free molecule. Some substance peaks remained visible indicating that certain moieties of the P5SA-2 molecule are still able to rotate freely. Due to a low signal the other P5SAs could not be analyzed by NMR. One reason may be that these substances have reduced solubility and, in addition, form micelles or oligomers causing a low signal-to-noise ratio.

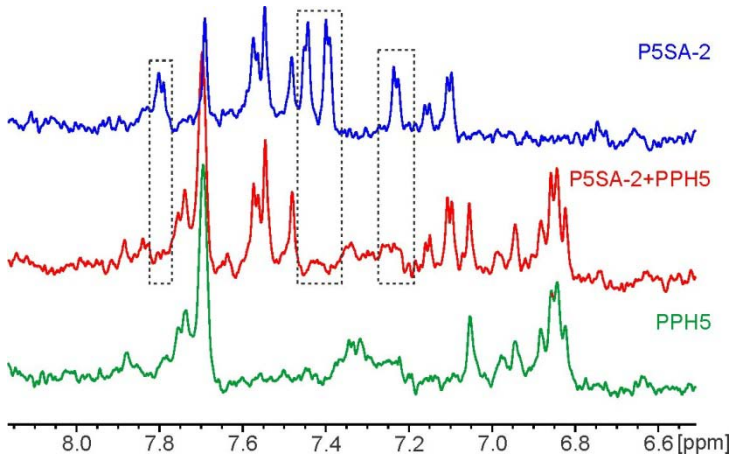

Figure 3.2.7. *NMR analysis of P5SA-2 confirms binding of P5SA-2 to PPH-5. P5SA-2 specific peaks (blue) disappear upon addition of 10 µM of PPH-5 (red). The PPH-5 spectrum is shown below for comparison (green). Missing peaks indicate decrease of the P5SA-2 tumbling rate caused by binding to PPH-5. Peaks that do not disappear after protein addition indicate that certain moieties of P5SA-2 is not directly immobilized by PPH-5. Peaks around 7.7 ppm originate from buffer impurities.*

Given that all five P5SAs are activators of PPH-5, the question arose whether they stimulate in an additive manner. To address this, the combinatorial effects of the P5SAs on the stimulation of pNPP hydrolysis were measured. Substance concentrations of 3 times higher than the apparent K_D value were used by combining the different activators. The observed activities showed no additional stimulation and complied with the

estimations of individual but competitive interaction (Figure 3.2.8). These results suggest that the P5SAs accelerate the same rate-limiting step during the enzymatic cycle.

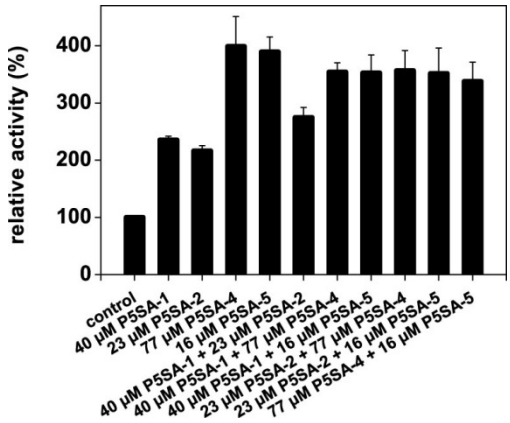

Figure 3.2.8. *The P5SAs act on the same enzymatic step and are not able to activate in an additive manner. Concentrations of three times the K_D were used for each substance and added in different combinations as indicated. Each bar represents three independent experiments.*

3.2.4 The P5SAs lead to a faster hydrolysis of the substrate pNPP

Steady state kinetic measurements are sufficient to analyze the influence on the maximal turnover rate when the rate limiting step (RLS) of an enzymatic reaction is enhanced by a certain compound. To dissect, however, which step of the catalytic cycle of the dephosphorylation is enhanced by the P5SAs, pre-steady state methods have to be applied. One way to study enzyme kinetics is the analysis of the reaction in a stopped flow apparatus. Here, the reaction is started by rapid mixing of enzyme and substrate and detection of the product after a certain dead time of the instrument. In case of the substrate pNPP, the formation of the product can be monitored after hydrolysis of pNPP to para-nitrophenole (pNP) which can be detected when it is still bound to the active site (depicted in blue in the formulas below). Applying stopped flow-based kinetic measurements allows to analyze whether the RLS of a reaction is before (formula I) or after (formula II) the formation of detectable product. The former case would give a slow linear increase in signal according to steady state kinetics, whereas the latter case would result in an initial burst phase of product formation followed by the same slow linear rate.

$$E + S \overset{\text{RLS}}{\leftrightarrow} [ES] \overset{\text{RLS}}{\rightarrow} [EP_1P_2] \leftrightarrow E + P_1 + P_2 \quad \text{(I)}$$

$$E + S \leftrightarrow [ES] \rightarrow [EP_1P_2] \overset{\text{RLS}}{\leftrightarrow} E + P_1 + P_2 \quad \text{(II)}$$

The amplitude of the burst phase depends on the enzyme concentration used and on the rates following the RLS. If the latter are not negligible, the amplitude is reduced. By performing measurements with and without activator, it can be deduced whether pNPP hydrolysis or product release is enhanced by the activators.

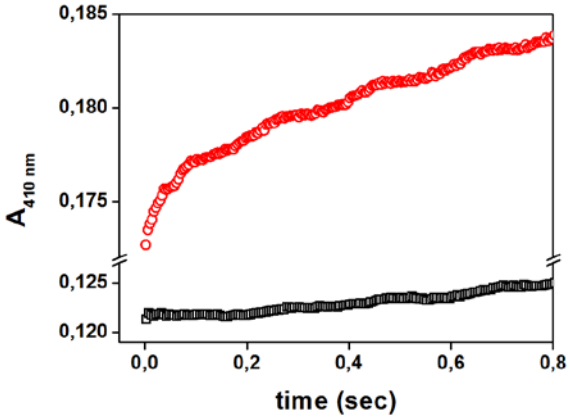

Figure 3.2.9. *The P5SAs increase the dephosphorylation reaction of PP5. 13 µM of rat PP5 in absence (black) or presence (red) of 10 µM P5SA-5 was mixed with 66 mM pNPP in a 1:11 ratio in stopped flow instrument. Each data set is the average of two measurements.*

In absence of P5SA-5, pNP formation by rat PP5 does not show an initial burst phase. The linear rate is 0.03 sec^{-1} and accounts to 25% of the rate determined in steady state kinetic measurements (Figure 3.2.9). Due to the very different techniques it is unlikely that this change in rate displays a significant change in product formation. Addition of the most potent P5SA-5, however, introduced an initial burst phase. The amplitude is caused by the production of approximately 3.6 µM pNP which corresponds to around 30% of the final enzyme concentration. The following linear phase gives a rate of 0.05 sec^{-1} indicating the enhanced dephsophorylation of pNPP in the presence of activator P5SA-5 and contributes to a decrease of the amplitude. These results point out two facts. First, the RLS of pNPP hydrolysis in absence of activator is before the formation of the product

and second, P5SA-5 activates either the formation of the enzyme-substrate complex or the hydrolysis of pNPP in the active site. The first, however, is rather unlikely considering the negligible effect on the K_M of pNPP in presence of the P5SAs.

3.2.5 Hsp90 binding is not compromised by the small molecules

Human PP5 is well-known to be activated upon binding to the molecular chaperone Hsp90 or its C-terminal fragments. The addition of the Hsp90-derived C-terminal MEEVD peptide resulted in activation of the nematode PPH-5 (Figure 3.2.10 A). The mechanism involves an autoinhibitory interaction between the TPR domain and the C-terminal αJ helix of the phosphatase domain, which is maintained until the TPR domain is occupied by the MEEVD-motif. Interestingly, the Hsp90 peptide has no additional effect when supplemented in the presence of the P5SAs (Figure 3.2.10 A). These findings suggest that the same regulatory mechanism is targeted by both, the small molecules and the MEEVD-peptide of Hsp90, which would be the breakup of the autoinhibition. Full-length Hsp90, in contrast, is able to regulate PP5 in a more complex way. Under saturating substrate concentrations used in this assay Hsp90 is able to reduce the turnover rate of the phosphatase (see also section 3.3.1). After addition of the different P5SAs to the PP5-Hsp90 complex this regulation is still observable. The compounds cannot fully reverse the Hsp90 effect as shown by the clearly reduced activation levels. Apparently, the activators cannot compete with those Hsp90 interaction sites that are distinct from the MEEVD-peptide contacts. The C-terminal domain of Hsp90 (Hsp90-CTD, amino acid 524-702) confers a similar but less pronounced effect as full-length Hsp90. The additional contacts that compete with the activators can therefore be assigned to this domain. Another observation is that all activators although distinct in their chemistry act all in competition with this specific interaction site between full-length Hsp90 and PP5.

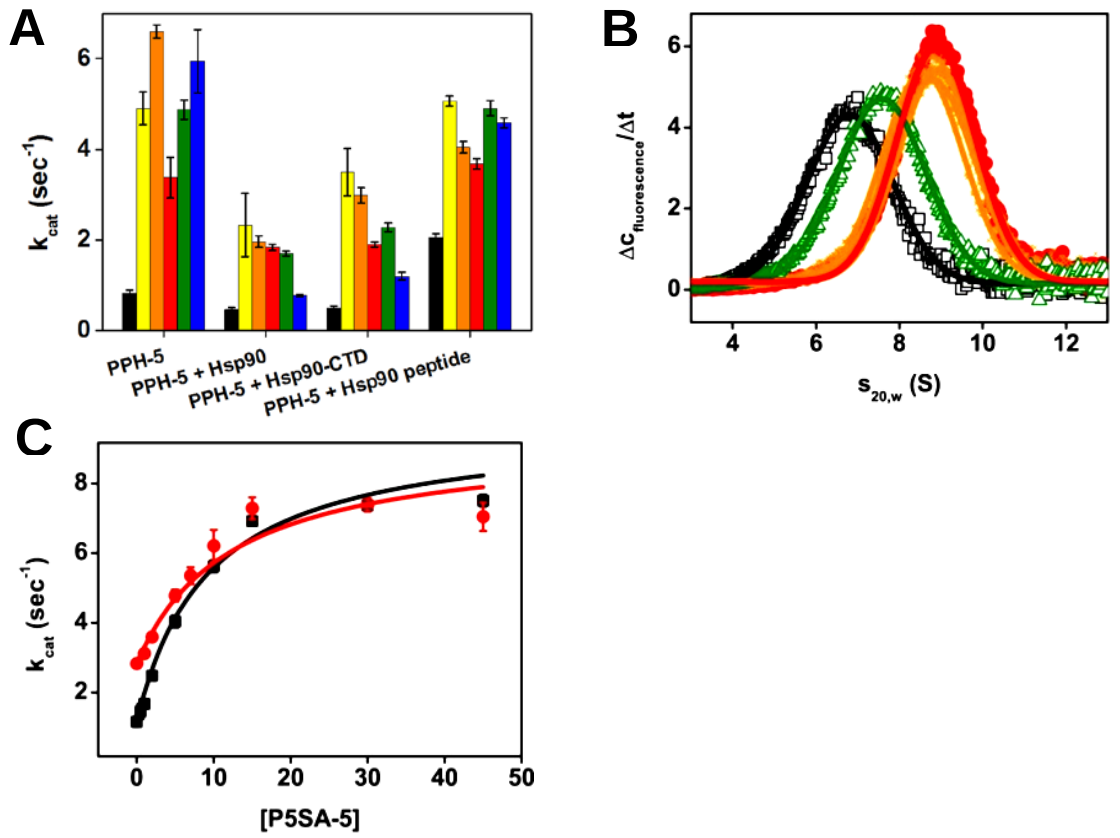

Figure 3.2.10. *PPH-5-Hsp90 complex formation is unaffected by the P5SAs.* ***A****, Different parts of Hsp90 regulate PPH-5 activity (compare black bars). 3 µM Hsp90 or Hsp90-CTD or 60 µM C-terminal MEEVD peptide were used. Presence of 70 µM of P5SA-1 (yellow), 140 µM of P5SA-2 (orange), 50 µM of P5SA-3 (red), 100 µM of P5SA-4 (green) or 45 µM of P5SA-5 (blue) has diverse effects on the different protein complexes. Each bar represents three to six independent experiments.* ***B****, Complex formation between PPH-5 and Hsp90 is not influenced by the presence of the P5SA in fluorescence-based AUC experimentss. The sedimentation coefficient of YFP-Hsp90 is shifted from a $s_{20,w}$ value of 6.8 S (black) to 8.9 S in presence of 1.7 µM PPH-5 (red). Supplementation of different P5SAs (orange) does not alter the sedimentation coefficient of the phosphatase-chaperone complex. Presence of the Hsp90 derived MEEVD peptide shifts the $s_{20,w}$ value from 8.9 S to 7.6 S (green). P5SA-1 and P5SA-2 were added to 70 µM, P5SA-3 to 50 µM, P5SA-4 to 100 µM and 107B3 P5SA-5 to 30 µM.* ***C****, Titration of PPH-5 activity with P5SA-5 in absence of MEEVD peptide is depicted in black whereas activation in presence of 60 µM peptide is shown in red. Each data point represents three independent experiments.*

To rule out the possibility that the activators lead to the expulsion of the MEEVD-peptide out of the TPR domain and thereby cause the above results, complex formation between full-length Hsp90 and PPH-5 was analyzed in presence of the P5SAs. N-terminal YFP-tagged Hsp90 was used as a probe in sedimentation velocity ultracentrifugation experiments. Complexes with PPH-5 induce a shift of YFP-Hsp90's sedimentation coefficient from 6.8 S to 8.9 S (Figure 3.2.10 B). Binding of chaperone to the phosphatase

was then analyzed in the presence of the P5SAs. None of the P5SAs abrogated the complex formation, while the isolated MEEVD peptide clearly reduced complex formation between Hsp90 and PPH-5. The next test was whether P5SA affinity is affected in the presence of large excess of MEEVD peptide. If the activators bind independently of the MEEVD-peptide binding residues as indicated by the previous experiments, the affinity for either the activators or the MEEVD-peptide would not change in presence of the respective other ligand. Therefore, 60 µM of the peptide were supplemented and the binding characteristic of P5SA-5 was evaluated using the pNPP assay. Only a minor influence on its affinity was observed despite the high concentration of MEEVD peptide (Figure 3.2.10 C). Thus, the P5SAs appear to bind to a site distinct from the peptide binding groove of the TPR domain while releasing autoinhibition similar to the Hsp90 derived peptide.

3.2.6 The P5SAs bind at the intersection of the phosphatase and the TPR domain

To characterize of the binding site of the P5SAs, deletion constructs of rat PP5 were generated. Using the mammalian homolog of the protein phosphatase 5 enabled studying the impact of certain domains of the phosphatase, as shortened variants of *C. elegans* PPH-5 resulted in insoluble protein. The full-length PP5 and its deletion variants were purified and the activity was determined in the absence and presence of 10 µM and 100 µM (45 µM in case of P5SA-5) of the substances, respectively (3.2.10 A-C).

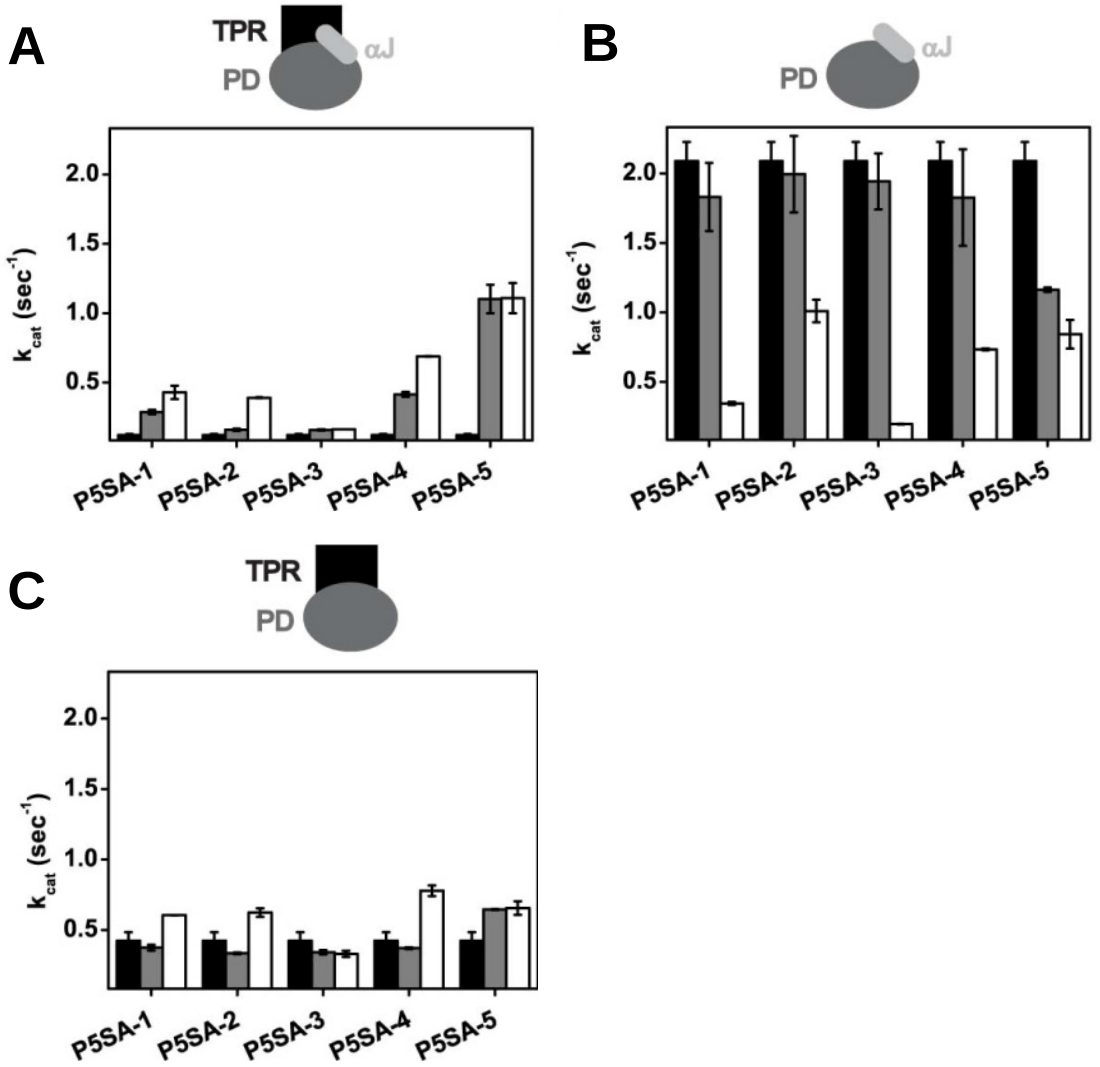

Figure 3.2.11. *The P5SAs interfere with the autoregulatory mechanisms of mammalian PP5.* ***A-C****, Activity in absence of activators is depicted in black, in presence of 10 µM substance in grey and of 100 µM (45 µM in case of P5SA-5) in white.* ***A****, Activation of full-length PP5 by the P5SAs.* ***B****, Inhibition of PP5-ΔN165 in the presence of activators.* ***C****, Moderate stimulation of PP5-ΔC8 under activator influence. Each bar represents at least three independent experiments.*

The activity of the phosphatase domain variant PP5-ΔN165 which lacks the complete TPR domain and is therefore not autoinhibited, was increased almost 20-fold from 0.12 sec^{-1} to 2.22 sec^{-1} compared to wild type protein (Figure 3.2.11 A, B). Remarkably, while wt-PP5 is strongly activated by the P5SAs, the P5SAs are able to inhibit the phosphatase activity of the TPR domain free protein. These results point out that the P5SAs do not bind to the TPR domain of PP5, but interact with the phosphatase domain. The second functional region of the autoinhibitory mechanism is composed by the αJ helix. The last 8 amino acids of the protein were deleted including Gln495 which is

known to be essential for maintaining the tight regulation of PP5 (Kang et al, 2001). Furthermore, the autoinhibitory mechanism of PP5-ΔC8 was disturbed causing an increased turnover of 0.49 sec^{-1} compared to full-length PP5. Interestingly, addition of the P5SAs still influenced the activity of PP5-ΔC8, but only with a minor effect (Figure 3.2.11 C, see crystallographic results below, Figure 3.2.13). Based on these findings, the P5SAs do not appear to interact directly with the autoregulatory domains. Instead, the modulators bind to the phosphatase core domain which appears sufficient to control the turnover rate independent of the PP5 variant used in this study (Figure 3.2.12).

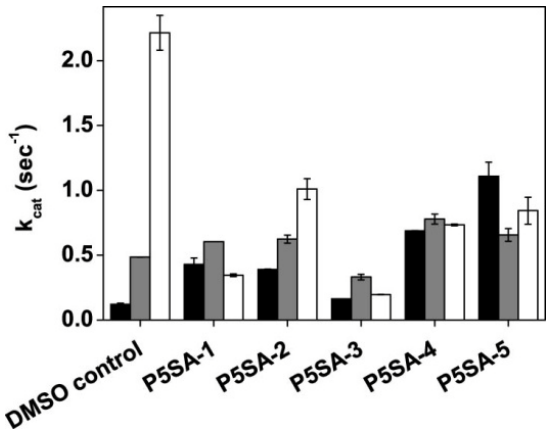

Figure 3.2.12. *Activity levels of the different deletion constructs of PP5 converge in presence of the P5SAs. Addition of 100 µM of the P5SAs (45 µM in case of P5SA-5) leads to an approximation of the enzymatic activity to similar k_{cat} values of the otherwise different PP5 variants. Full-length PP5 is shown in black, PP5-ΔC8 in grey and PP5-ΔN165 in white where each bar represents three independent experiments.*

To get structural insights into the binding site and the mode of action of the activators the crystal structures of rat PP5 in its apo-state as well as in presence of the ligand P5SA-2 were determined. The structures were solved in collaboration with Michael Groll and Ferdinand Alte (Lehrstuhl für Biochemie, Technische Universität München, Germany) by molecular replacement (McCoy et al, 2007) using the atomic coordinates of human PP5 (PDB ID: 1WAO) as a search model. The PP5:P5SA-2 dataset was refined to 2.0 Å (PDB ID: 4JA7) and used as a model to determine the apo-structure with a final resolution of 2.3 Å (PDB ID: 4JA9, Table 3.2.2). In both structures the first defined amino acid is Gly23. The loop connecting the TPR domain with the phosphatase domain (Arg150 - Arg158) is flexible and therefore not defined in the electron density map. Additionally, Met499 of the apo-structure and Met498 as well as Met499 of the active ligand structure were not resolved. The electron density of P5SA-2 was only partially defined, however,

comparison of both structures PP5 apo and the PP5:P5SA-2 complex, clearly assigned the binding site of the ligand at the interface between the TPR and the phosphatase domain. The flexible character of the P5SA-2 interaction is in agreement with NMR data obtained from P5SA-2 measurements with PP5. Here, some ligand peaks remained unaffected by binding to the protein which indicates that P5SA-2 is not fully restricted upon interaction with PP5 (Figure 3.2.7).

Only limited structural rearrangements could be observed within the phosphatase domain in the presence of the activator P5SA-2, whereas certain helices in the TPR domain displayed a tilting up to 10 ° under these conditions (Figure 3.2.13 A). Regarding the αJ helices from Asn491 to Gly497 or to Met498, respectively, a considerable displacement of the Cα atom of Gly497 occured (Figure 3.2.13 B, C). The conformational rearrangements of both the TPR domain and the αJ helix indicate opening of the active site channel and can be visualized in particular when the surface area is displayed (Figure 3.2.14). In summary, the observed structural rearrangements induced by ligand binding support the functional characterization of the P5SAs that act on the release of the autoinhibiton of PP5.

Table 3.2.2 *Data collection and refinement statistics (Molecular replacement)*

	PP5 apo	PP5 + P5SA-2
Data collection		
Space group	$P4_12_12$	$P4_12_12$
Cell dimensions		
a, *b*, *c* (Å)	50.1, 50.1, 379.2	51.1, 51.1, 365.7
α, β, γ (°)	90.0, 90.0, 90.0	90.0, 90.0, 90.0
Resolution (Å)	40 - 2.3	30 - 2.0
R_{merge} (%)	4.1 (53.7)*	3.8 (43.5)
$I/\sigma I$	22.3 (4.4)	28.8 (5.6)
Completeness (%)	99.5 (99.9)	98.5 (93.1)
No. observed reflections	140950	286970
No. unique reflections	22932	34075
Redundancy	6.1 (6.0)	8.4 (8.8)
Refinement		
Resolution (Å)	15 - 2.3	15 - 2.0
No. reflections	21718	32308
R_{work}/R_{free} (%)	23.8 / 27.1	21.4 / 26.1
No. atoms		
Protein	3757	3749
Water	63	106
Average B-factor (Å^2)	74.1	51.0
R.m.s deviations		
Bond lengths (Å)	0.005	0.015
Bond angles (°)	0.99	1.68

**Highest resolution shell is shown in parenthesis.*

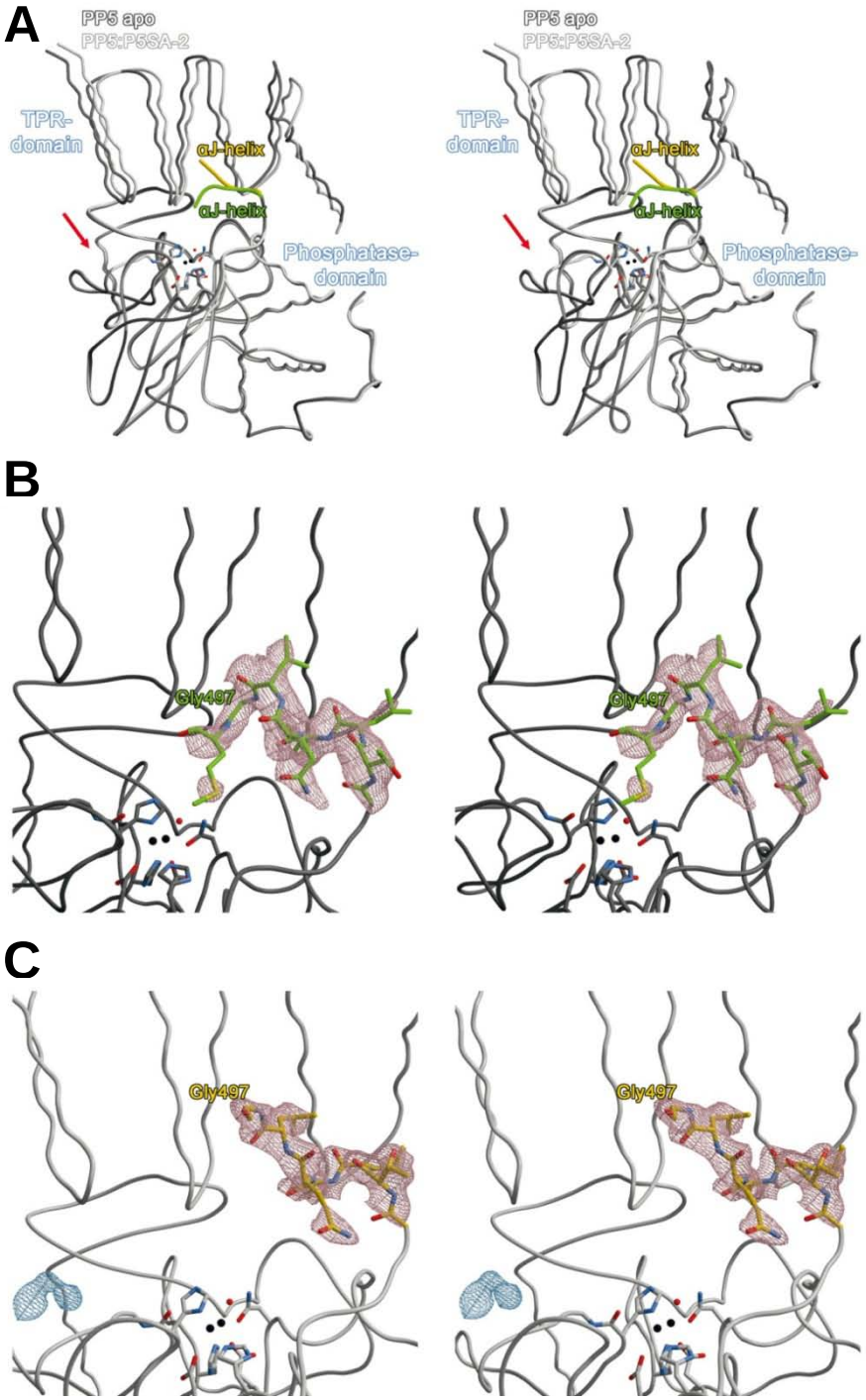

Figure 3.2.13. *P5SA-2 leads to break-up of regulatory domain contacts.* ***A****, Stereo view of the backbone superposition of both molecules shown as ribbon plots: PP5 apo with αJ-helix in dark grey and green, PP5:P5SA-2 with αJ-helix in light grey and yellow. The position of the additional electron density which is only visible in the PP5:P5SA-2 structure is indicated with a red arrow. Active site residues are depicted as sticks and the two magnesium ions (black) and one water molecule (red) are shown as balls (also in* ***B*** *and* ***C****).* ***B****, Stereo view of the $2F_o$-F_c omit electron density map (countered at 1σ) for the αJ-helix (Thr492 - Met498) of PP5 apo, in which the αJ-helix has been removed for phase calculations. The position of Gly497 is indicated.* ***C****, Stereo view of the $2F_o$-F_c omit electron density map (at 1σ) for the αJ-helix (Thr492 - Gly497) of PP5 in complex with P5SA-2. The electron density depicted in blue at 1σ indicates the binding site of the ligand P5SA-2.*

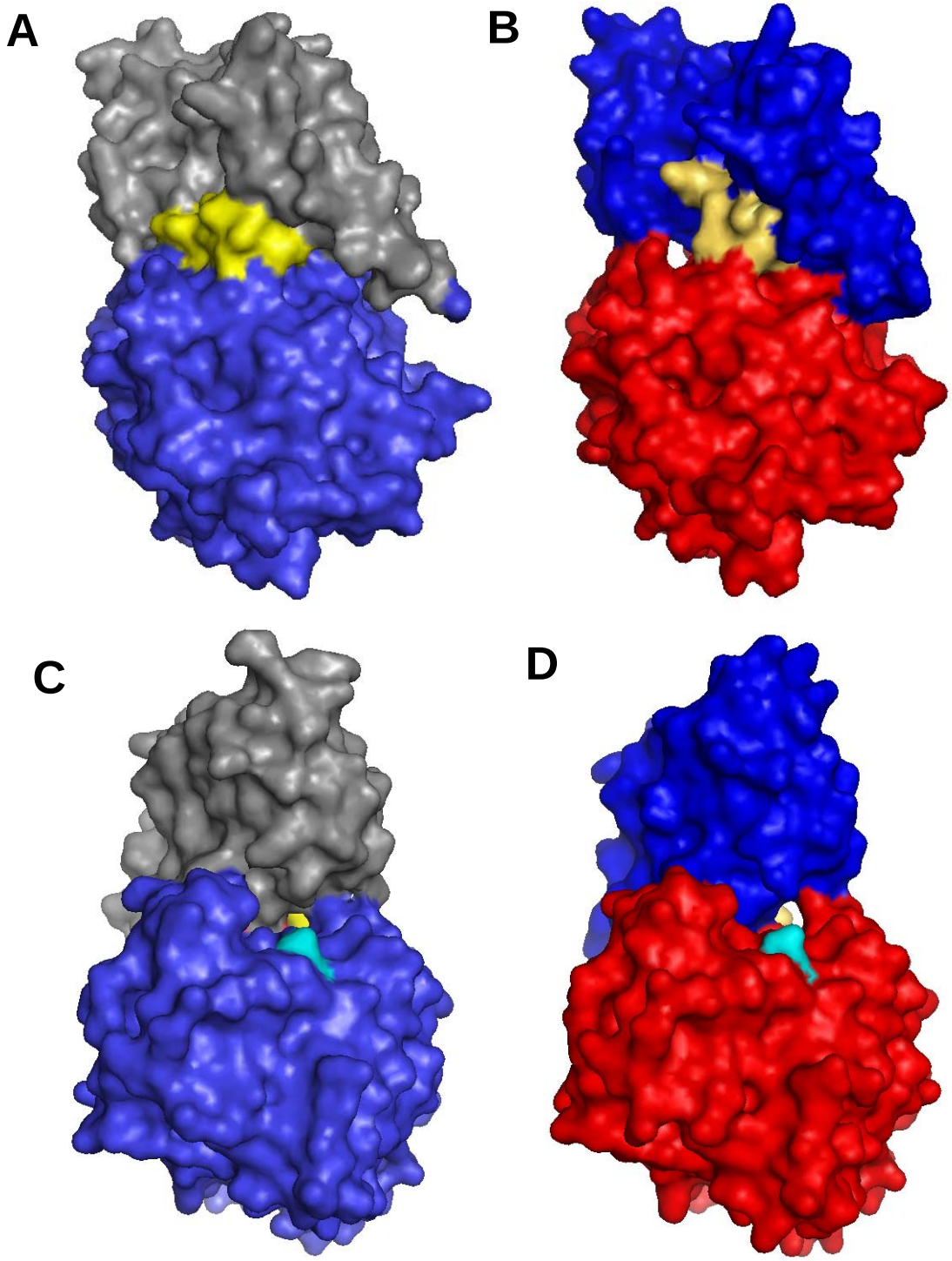

Figure 3.2.14. *Presence of P5SA-2 favors the opening of the substrate channel.* ***A,*** *Human PP5 (PDB ID: 1WAO) exerts a completely closed substrate channel regarding its surface. The TPR domain is shown in grey, the phosphatase domain in dark blue, the αJ domain in yellow.* ***B,*** *Opening of the substrate channel is clearly visible in presence of P5SA-2 (PDB ID: 4JA7). The TPR domain is displayed in dark blue, the phosphates domain in red and the αJ domain in gold. Both structures were rotated to the same degree.* ***C-D****, View from the backside of the actie site shows a closed (apo-state of 1WAO,* ***C****) and open (4JA7,* ***D****) substrate channel. E435 is depicted in cyan and should indicate the region where the residual electron densitiy is located in the PP5::P5SA-2 crystal. Representation of structures is according to* ***A*** *and* ***B****, respectively.*

3.2.7 Testing PP5 activators in an Alzheimer mouse model to evaluate *in vivo* efficacy

It is of high clinical interest whether a specific and potent *in vitro*-compound is applicable in the living organism. To test this, an experimental model was chosen, in which treatment with the PP5 activators may have a beneficial effect in case of a certain disease. The human tau variant tau-P301L and its hyperphosphorylated form is a key player in familial frontotemporal dementia and Alzheimer's disease. PP5, however, was shown to specifically dephosphorylate various serine and threonine residues of human tau and its activity was found to be reduced in neurons of Alzheimer brains (Liu et al, 2005a). Hence, the influence of P5SA-2, P5SA-3, P5SA-4 and P5SA-5 on tau phosphorylation and tau-induced pathogenesis in human tau-P301L-transfected mice was analyzed in collaboration with Martin Helmuth and Frank Stiggow (DZNE, Magdeburg, Germany). As a result, PP5 activation decreased tau phosphorylation and prevented tauP301L-induced neuronal degeneration in the hippocampus. The corresponding images of brain slices are not shown in this thesis all animal experiments and confocal images were performed and recorded by the Striggow group and are currently submitted for publication together with other results of this chapter.

3.3 Activity and specificity of PPH-5 are tightly regulated by Hsp90 via interactions outside the TPR domain*

*Parts of this chapter will be submitted for publication (Haslbeck et al, *Manuscript in preparation (a)*).

3.3.1 The phosphatase domain of PPH-5 is involved in a secondary binding site with Hsp90

The protein phosphatase 5 conveys phosphatase activity to the Hsp90 chaperone system. In this chapter of the thesis, the interaction and regulation mechanism was studied using the nematode homologs of both, phosphatase and Hsp90. To analyze the contribution of the MEEVD-peptide interaction to complex formation between Hsp90 and PPH-5, fluorescence-based AUC experiments were performed using YFP-Hsp90. In presence of PPH-5 the fluorescent labeled chaperone shifted to high $s_{20,w}$ values as was reported in chapter 3.1 (Figure 3.3.1 and Figure 3.2.10 B). Large excess of the C-terminal peptide of Hsp90 was able to compete with the chaperone-cochaperone complex. However, using 60 µM Hsp90-peptide could not fully disassociate the protein assembly. Binding of PPH-5 to Hsp90 apparently depends to a large extent on the recognition of the MEEVD-peptide, but additional interactions might contribute to the complex formation.

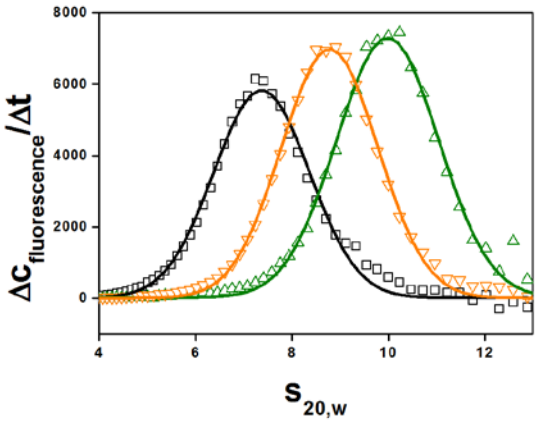

Figure 3.3.1. *PPH-5 binding to Hsp90 predominantly depends on the recognition of the MEEVD-peptide.* ***A****, The sedimentation coefficient of YFP-Hsp90 (black) shifts in presence of 6 µM of PPH-5 (green), whereas presence of 60 µM C-terminal MEEVD-peptide induced a shift of the probe to lower* $s_{20,w}$ *values (orange).*

To quantify the affinity of additional Hsp90 contacts, binding constants of PPH-5 to Hsp90-CTD or the MEEVD-peptide were measured by ITC. Here, the affinity for Hsp90-CTD was higher with 1.2 µM compared to the binding constant of 2.0 µM for the peptide

(Figure 3.3.2) which indicates that residues outside the last 12 C-terminal residues of Hsp90 interact with sites at the PPH-5 molecule.

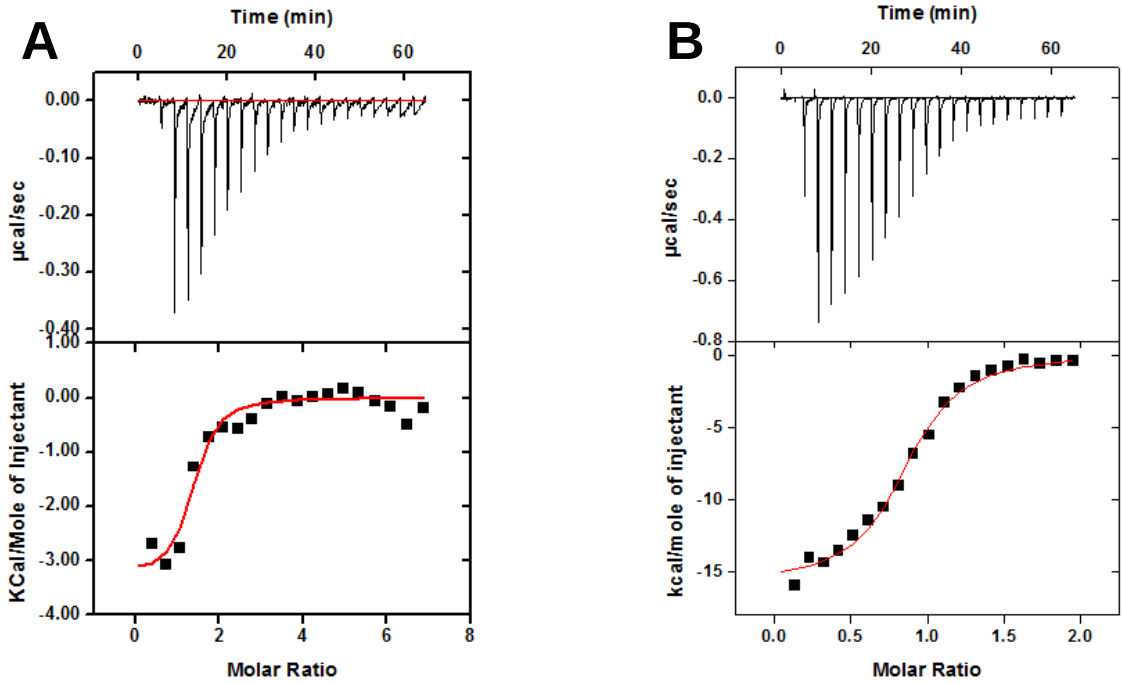

Figure 3.3.2. *Binding constants of PPH-5 for Hsp90-CTD and MEEVD-peptide are different according to ITC measurements.* ***A,*** *30 µM PPH-5 was titrated with 1 mM MEEVD-peptide in the syringe.* ***B,*** *30 µM PPH-5 was titrated with 280 µM Hsp90-CTD in the syringe.*

Therefore, crosslinking experiments were performed using the lysine reactive isotope labeled crosslinker DSSG-H6/D6 (Creative Molecules Inc., Canada) to detect close proximity of lysines in the Hsp90-PPH-5 complex and to gain insights into the contact surface between both proteins. The crosslinking reaction was stopped after 15 min and different species of crosslinked proteins were separated by SDS-PAGE (Figure 3.3.3 A).

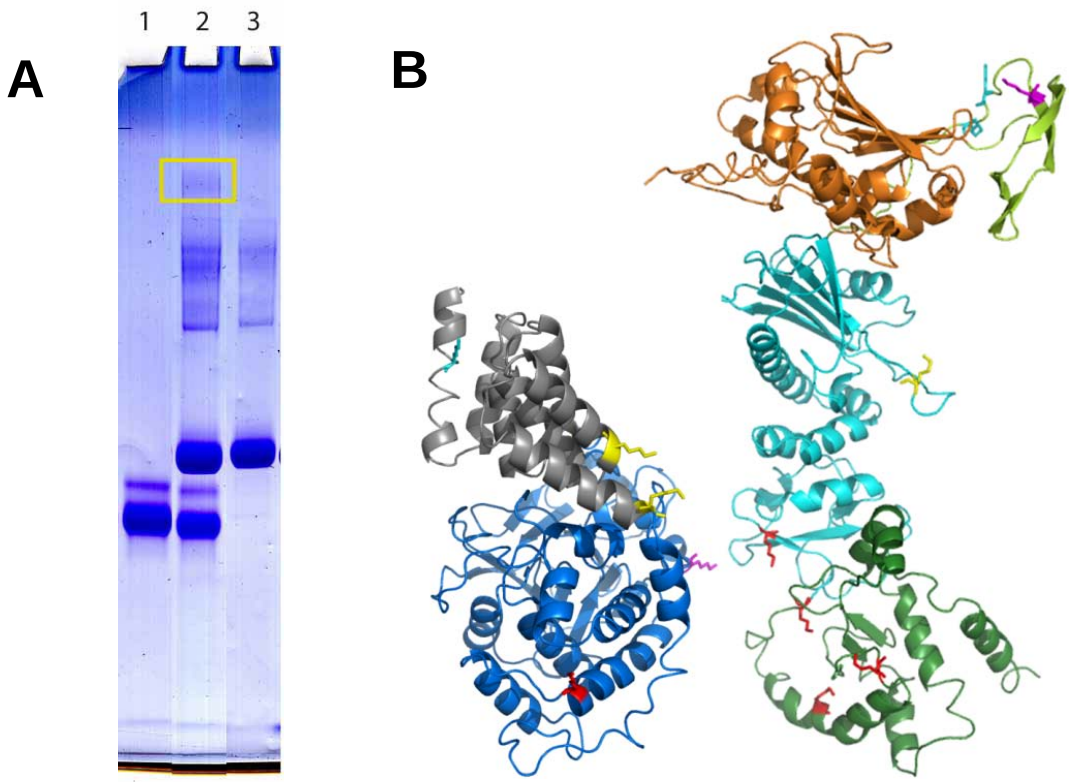

Figure 3.3.3. *The phosphatase domain of PPH-5 is in close proximity to Hsp90-CTD in the protein complex.* ***A****, 3 µM of PPH-5 was crosslinked alone (lane 1) or in presence of 6 µM Hsp90 (lane 2). Lane 3 represent the crosslinking reaction containing 6 µM Hsp90 alone. The crosslinker DSSG-H6/D6 was added in 40-fold excess. The band analyzed by OrbiTrap is highlighted by a yellow box.* ***B****, A SWISS-MODELL representation is shown of PPH-5 (left) and nematode Hsp90 (right). The TPR domain of PPH-5 is depicted in grey, the phosphatase domain in blue. The N-terminal domain of Hsp90 is shown in orange, the linker in light green, the middle domain in cyan and the C-terminal domain in dark green. Lysines which were found in crosslinked peptides from both proteins are colored correspondingly.*

Table 3.3.1. *Crosslinks detected by Orbitrap using DSSG-H6/D6*

X-link	PPH-5	Hsp90	color code
1	K33	K252, K254	cyan
2	K113, K147	K326, K585	yellow
3	K205	K510, K516, K535, K551	red
4	K367	K246	magenta

Additional bands in the complex mixture compared to reactions containing only PPH-5 or Hsp90 were excised (Figure 3.3.3 A, lane 2), digested with trypsin and subjected to Orbitrap analysis by Thomas Kriehuber (Lehrstuhl für Biotechnologie, Technische Universität München, Germany). The mass of possible crosslinks comprising peptides of

both PPH-5 and Hsp90 was calculated using the program MassMatrix. Working with a 50:50 ratio of D6 labeled versus H6 labeled crosslinker allows to verify each proposed crosslink by the occurrence of the respective isotope pattern in 6 Da distance. Four intermolecular crosslinks listed in table 3.3.1 could be verified by this method. To place and localize crosslinked lysines in the 3D structure of PPH-5 and Hsp90, respectively, model structures of the two nematode proteins were generated by the SWISS-MODEL tool (swissmodel.expasy.org) according to homolog crystal structures. For PPH-5 the human homolog PP5 was applied (1WAO), whereas yeast Hsp90 (2CG9) was the basis for nematode Hsp90 modeling (Figure 3.3.3 B). According to the Orbitrap analysis of crosslinked lysines, the phosphatase domain of PPH-5 is in contact with the C-terminal domain of Hsp90. In the protein complex Lys226 of the phosphatase domain is in close proximity with several lysines of Hsp90-CTD. These crosslinks were found in three different experiments and were highly reproducible. All other crosslinks were found at least in two different experiments. Regarding the complex pattern and the distance some interactions would have to span across the protein assembly, it cannot be excluded that some hits correspond to secondary crosslinks that occur after the protein complex is covalently linked by a first successful crosslinking event which drastically enhances the chance of additional artificial linkage of lysines. However, various non-trivial contacts would be possible in a Hsp90-PPH-5 complex where the two domains of PPH-5 can twist around the Hsp90 dimer and interact with the different monomers of the chaperone.

Therefore, subunit exchange experiments were performed to elucidate whether the additional contacts act within the same monomer of Hsp90 where PPH-5 is bound to the MEEVD-motif. The Hsp90 dimer is able to exchange its monomer subunits with a certain rate. This subunit exchange can be detected using a FRET pair as published earlier (Hessling et al, 2009). The labeled Hsp90 monomers were provided by Klaus Richter (Lehrstuhl für Biotechnologie, Technische Universität München, Germany). Presence of both donor (ATTO-488) and acceptor (ATTO-550) labeled yeast Hsp90 monomers exhibits a strong signal in the acceptor channel due to FRET between the different fluorophores attached to the N-domains of each Hsp90 monomer. This can be monitored in a fluorescence spectrophotometer. Excessive addition of unlabeled yeast Hsp90 leads to a decrease in the acceptor channel causing an increase in the donor channel. The rate of this reaction corresponds to the monomer exchange of Hsp90 (Figure 3.3.4, black and grey curves). The presence of PPH-5 caused a pronounced decrease in the subunit

exchange rate of the Hsp90 dimer (Figure 3.3.4, red and orange curves). PPH-5 is apparently able to crosslink the yeast chaperone dimer with intermolecular contacts to each monomer. It might also be that PPH-5 leads to a closing of the N-terminal domains or other compaction of the Hsp90 dimer causing the increased intermolecular affinity of the yeast monomers. Such an effect would probably lead to a modification of the ATPase rate which could not be detected for nematode Hsp90 in presence of PPH-5 (data not shown). In summary, these results confirm the involvement of a second binding site in the Hsp90-PPH-5 complex and shed light on the intertwining of the phosphatase around the Hsp90 monomers. Mere binding of the MEEVD-motif into the TPR domain of PPH-5 would not be sufficient to crosslink the different monomers of Hsp90. As shown by crosslinking experiments these interactions occur between phosphatase domain of PPH-5 and the C-terminal domain of Hsp90.

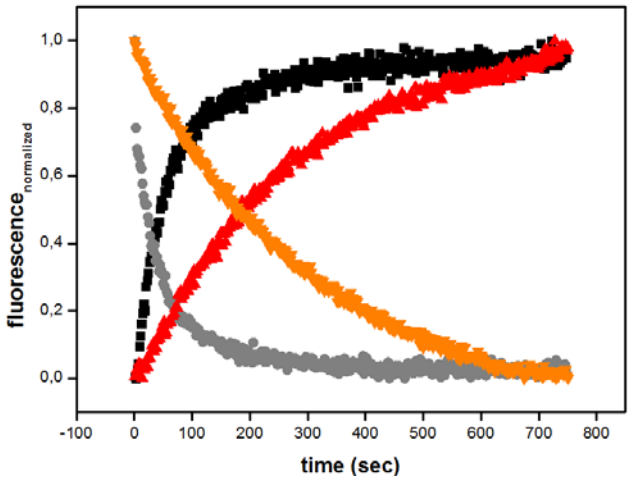

Figure 3.3.4. *PPH-5 is able to crosslink the Hsp90 dimer. To an equal mixture of N-terminally ATTO488-labeled yeast Hsp90 and N-terminally ATTO550-labeled yeast Hsp90 ten-fold excess of unlabeled yeast Hsp90 was added in absence and presence of nematode PPH-5. Donor channel signal is coloured in black in absence of PPH-5 and in red in presence of the phosphatase. The acceptor in absence of cochaperone is depicted in grey, and in presence of PPH-5 in orange.*

The group of TPR cochaperones is defined by the TPR domain dependent interaction with the Hsp90. In the proposed Hsp90 chaperone cycle this variety of TPR proteins acts at different stages during processing of the client (Li et al, 2013; Wegele et al, 2006). For instance, the protein phosphatase 5 is supposed to bind to Hsp90-Hop/STIP1-GR complexes, before it is displaced by FKBP proteins, but evidence for such an event is still

lacking. The directionality of the chaperone cycle requires the preference of a certain TPR cofactor for a specific Hsp90-client conformation. This would include additional binding sites apart from the TPR domain considering that the affinities of many TPR domains to the MEEVD-peptide are in the same range. Therefore, the identification and characterization of additional binding sites between Hsp90 and its TPR cochaperones is essential to fully understand how the binding of the different cofactors is regulated in the cell. Interestingly, analyzing the interaction of the TPR cofactor FKB-6 with Hsp90 indicates that this protein predominantly binds to the chaperone with contacts outside the MEEVD-peptide binding groove, as the MEEVD-peptide could not compete complex formation (Figure 3.3.5 A). If both TPR cofactors were present, YFP-Hsp90 shifted to an $s_{20,w}$ value similar to presence of PPH-5 alone (Figure 3.3.5 B). To scrutinize a possible heterocomplex formation of Hsp90 with two different TPR cochaperones, AUC analyses were performed using N-terminally YFP-labeled PPH-5. Hsp90 bound complexes can be formed with this probe (Figure 3.3.5 C). Addition of 1 µM STI-1 did not influence this complex, whereas 1 µM FKB-6 was able to increase free YFP-PPH-5 indicating that it competes with the phosphatase for Hsp90 binding. When 6 µM of either cofactor were used, STI-1 shifted the labeled species to higher $s_{20,w}$ values due to the formation of a ternary complex with two different TPR cofactors bound to the Hsp90 dimer Figure 3.3.5 D). However, the excess FKB-6 did not lead to a heterocomplex with mixed cochaperones, but to the full displacement of YFP-PPH-5 from Hsp90. Taking together all AUC results, it can be assumed that PPH-5 and STI-1 predominantly bind via the TPR domain and can occupy a MEEVD-binding site independent of the other Hsp90 monomer. In contrast, FKB-6 prefers PPH-5 free Hsp90 dimers. Apparently, the binding sites of both, FKB-6 and PPH-5, compete with each other. They may have identical binding sites or induce chaperone conformations that exclude binding of the respective other cofactor. Interestingly, FKB-6 did not reduce subunit exchange rates of the yeast Hsp90 FRET pair (data not shown) implying that FKB-6 is not able to crosslink the different monomers in contrast to PPH-5. It cannot be excluded, however, that crucial binding interfaces are not conserved in the yeast Hsp90 molecule.

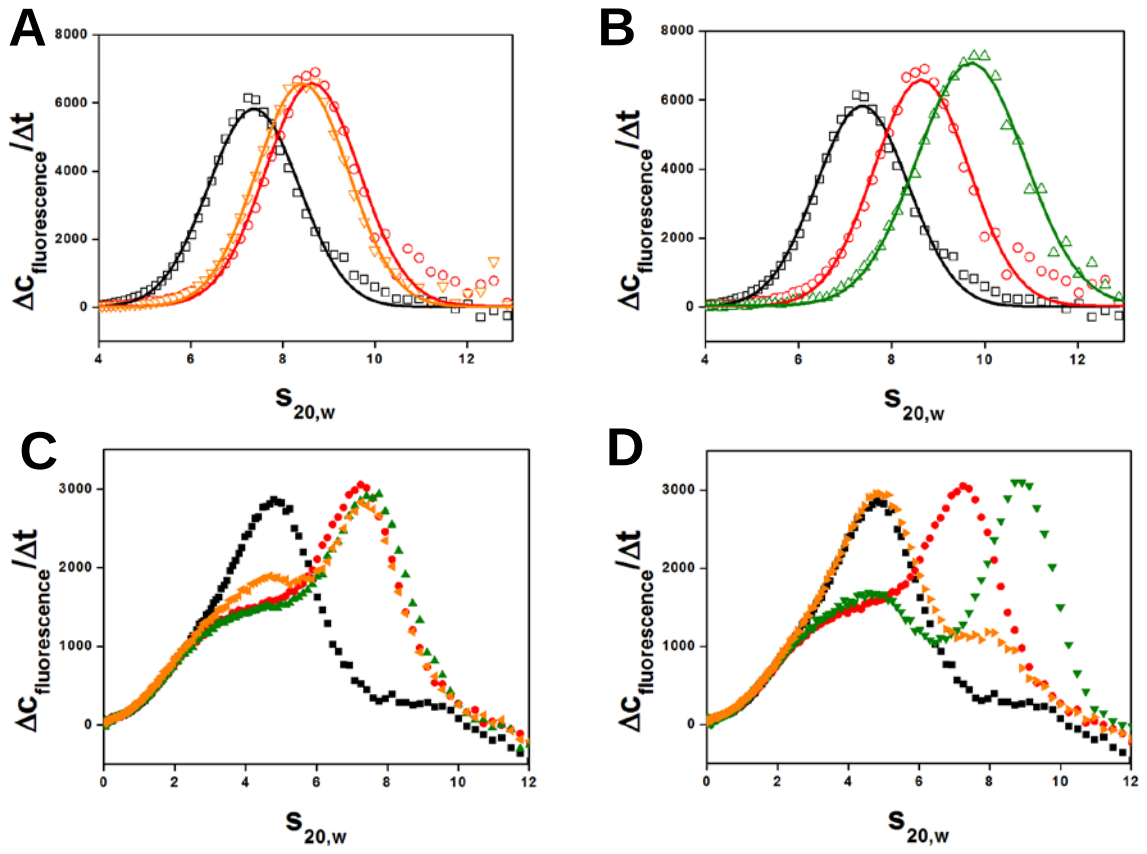

Figure 3.3.5. *PPH-5 binding to Hsp90 predominantly depends on the recognition of the MEEVD-peptide.* ***A****, The sedimentation coefficient of YFP-Hsp90 (black) shifts in presence of 6 µM FKB-6 (red). Presence of 60 µM C-terminal MEEVD-peptide does not disassemble the complex (orange).* ***B****, YFP-Hsp90 (black) is shifted to a higher sedimentation coefficient in presence of 6 µM FKB-6 (red). Presence of 6 µM PPH-5 (green) leads to an additional shift of the sedimentation coefficient of the Hsp90 probe.* ***C,*** *Presence of 2 µM Hsp90 (red) leads to a $s_{20,w}$ shift of N-terminal YFP-labeled PPH-5 (black). Supplementation of 1 µM STI-1 (green) of 1 µM FKB-6 (orange) does not further shift the PPH-5-Hsp90 complex. In presence of FKB-6 the amount of free YFP-PPH-5 at 4.6 S is slightly increased.* ***D,*** *Black and red curve are as in (****C****). Addition of 6 µM STI-1 (green) leads to a shift of the labeled PPH-5 to higher $s_{20,w}$ values indicating the formation of a ternary complex of PPH-5, Hsp90 and STI-1. Addition of 6 µM FKB-6 (orange) decreases the amount of Hsp90 bound YFP-PPH-5 and increases the concentration of free labeled PPH-5 without forming a ternary complex at higher $s_{20,w}$ values.*

3.3.2 Nematode Hsp90 regulates PPH-5 activity via two binding sites

The activatory effects of Hsp90 on PP5 had been discovered years ago and had shown that the enzyme reaches its full activity only upon binding to Hsp90 (Kang et al, 2001; Yang et al, 2005). Therefore, the activation of the nematode phosphatase-chaperone system was tested in a pNPP-based spectrophotometric assay (Figure 3.3.6 A).

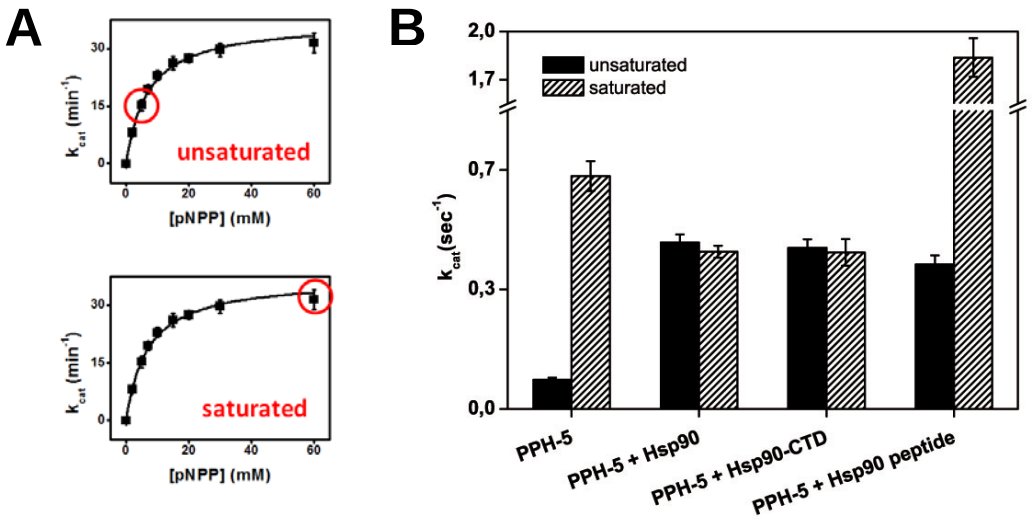

Figure 3.3.6. *The regulation of PPH-5 by Hsp90 underlies a complex mechanism in the nematode system.* ***A****, Two different substrate concentrations, below and above the K_M of pNPP were tested for PPH-5 activation by Hsp90.* ***B****, For unsaturated measurements 5 mM pNPP and 6 µM Hsp90, 6 µM Hsp90-CTD and 60 µM MEEVD-peptide (AEEDASRMEEVD) were used. For saturated conditions 60 mM pNPP and 3 µM Hsp90, 3 µM Hsp90-CTD and 60 µM MEEVD-peptide were applied.*

When using substrate concentrations around the K_M of pNPP, the enzymatic activity of PPH-5 was enhanced from 0.08 sec^{-1} to 0.46 sec^{-1} in presence of Hsp90 (Figure 3.3.6 A). Acceleration by a factor of ~ 6 resembles the activation of human PP5 in the Hsp90 complex (Yang et al, 2005). Presence of the C-terminal domain of Hsp90 as well as the MEEVD-peptide showed comparable effects. Interestingly, under saturating substrate conditions the Hsp90 regulation exhibited reverse effects (Figure 3.3.6 B) that have not been reported before. Again Hsp90 and Hsp90-CTD had similar influence, but inhibited the phosphatase by one third. The peptide, however, did not impede PPH-5 and still activated the enzyme around three-fold. The dependence of the turnover rate of PPH-5 in complex with Hsp90 on the substrate concentration suggests that the newly identified interaction site between phosphatase domain and Hsp90-CTD is able to modulate the enzyme's activity. Such effects could not be observed using rat PP5 (data not shown).

Therefore, the nematode proteins in combination with the small artificial substrate pNPP can be exploited to investigate the contribution of different parts of Hsp90 to the phosphatase regulation which might not be observable when other homologs or protein substrates are used.

The results above propose that the MEEVD-peptide is able to release the phosphatase's TPR domain from its autoregulation by competing with the αJ helix, but does not contribute to PPH-5 regulation to the same extent as Hsp90 and Hsp90-CTD. To assess the impact of different Hsp90-binding sites on the phosphatase activity, full-length Hsp90, the MEEVD-peptide and its counterpart, Hsp90-ΔMEEVD, were titrated to PPH-5. The enzymatic activity was measured by pNPP hydrolysis under saturating substrate conditions (60 mM pNPP). As a result, full-length Hsp90 showed again a complex regulation and inhibition in the low µM range with a maximum effect around 1µM (Figure 3.3.7 A). The concentration of 1 µM Hsp90 correlates with the binding constant of Hsp90-CTD measured by ITC. Beyond this concentration activating binding sites of full-length Hsp90 apparently compensate substrate inhibition effects caused by the second binding site. The shape of the curve may reflect the different binding affinities of each of the two binding sites, as titration of PPH-5 with the MEEVD-peptide resulted in an apparent K_D of ~ 60 mM (Figure 3.3.7 B). The affinity is strongly decreased when compared to ITC data obtained for the peptide, but is well in the range of the K_D of 57 µM obtained by Yang and coworkers in the pNPP assay using the human proteins (Yang et al, 2005). Interesting to note is, however, that an Hsp90 construct lacking the last five C-terminal amino acids, Hsp90-ΔMEEVD, is able to influence the activity of PPH-5. Increasing amounts of this deletion variant could reduce the enzymatic activity towards pNPP by around 70% with an apparent K_D of below 0.5 µM (Figure 3.3.7 C). This curve clearly reflects the initial drop when titrating full-length Hsp90 to PPH-5 and indicates that residues apart from the MEEVD-motif are responsible for causing substrate inhibition. Current literature states that the MEEVD-motif is essential for the complex formation between Hsp90 and the phosphatase. During the enzymatic cycle, however, it is possible that PPH-5 attains a conformation with high affinity for the second binding site of Hsp90 and less affine for the MEEVD-peptide. A similar principle is known for Hsp70 where substrate affinity is largely decreased when ATP is bound during the ATPase cycle (Otero et al, 2010). In this way, interaction of the phosphatase and Hsp90-ΔMEEVD could be observable in activity assays, but would not be seen in protein-protein

interaction measurements that exclude conformational changes during catalysis. In the same respect, ITC measurements with MEEVD-peptide would yield a higher apparent affinity than respective activation experiments.

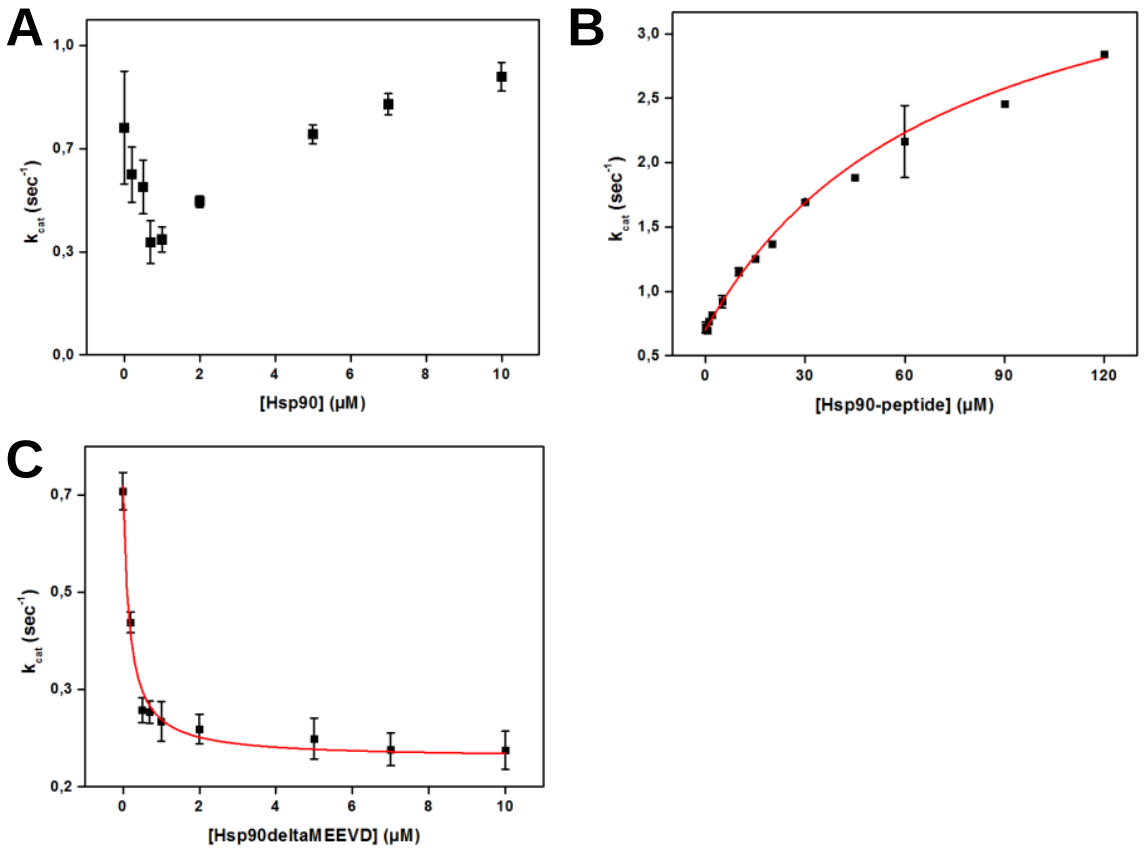

Figure 3.3.7. *Different parts of Hsp90 show distinct impact on the PPH-5 activity. A, Titration of PPH-5 with full-length Hsp90 under saturating pNPP concentrations of 60 mM. B, Titration of PPH-5 with MEEVD-peptide under saturating pNPP concentrations of 60 mM. C, Titration of PPH-5 with Hsp90-ΔMEEVD under saturating pNPP concentrations of 60 mM.*

The findings above visualize the different mechanisms that are conveyed by either full-length Hsp90 or MEEVD-peptide. In case of the peptide, the mode of action was only activation of the enzyme. As for the residual Hsp90 fragment, additional contacts confer a substrate inhibition like mechanism also in absence of the MEEVD-motif implying again that Hsp90 is interacting with the catalytic domain of the phosphatase as shown by the protein-protein interaction experiments described earlier.

Finally, the K_M of pNPP in presence of either Hsp90 or MEEVD-peptide was measured. While the full-length chaperone tightened the interaction with pNPP, the addition of the peptide apparently weakened the K_M of the small substrate pNPP to PPH-5 (Figure 3.3.8).

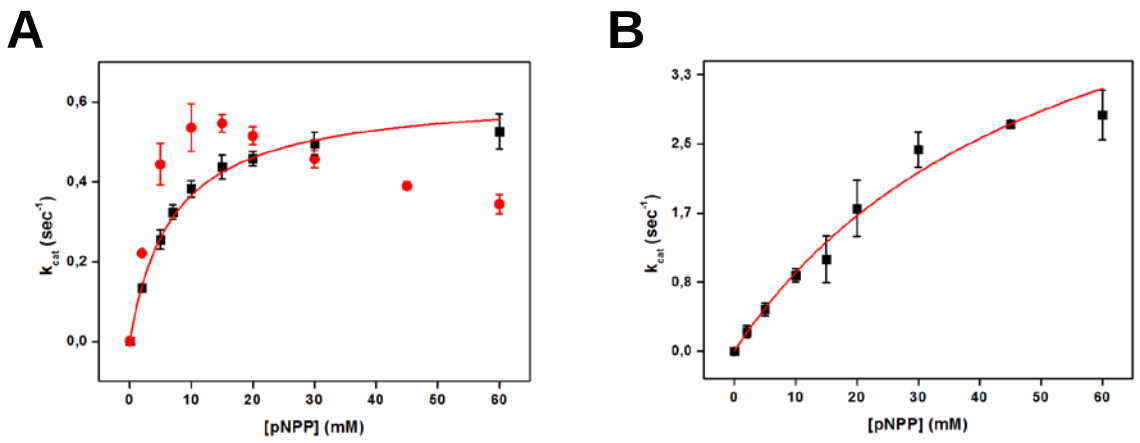

Figure 3.3.8. *Full-length Hsp90 and its C-terminal peptide influence the K_M of pNPP differently.* ***A****, Titration of PPH-5 with pNPP in presence (red) and absence (black) of Hsp90.* ***B****, Titration of PPH-5 with pNPP in presence of MEEVD-peptide.*

Hsp90 causes a decrease in pNPP turnover at higher substrate concentrations. In contrast, the MEEVD-peptide acts in effect opposite increasing the maximal turnover rate but decreasing at the same time the K_M for the substrate pNPP. These effects could be caused by processes like substrate inhibition in the PPH-5-Hsp90 protein complex. Hsp90 bound PPH-5 might be able to form unproductive [EPS]-complexes where leaving of either pNP or the organic phosphate is delayed inhibiting successful hydrolysis of pNPP. The rate to form this unproductive [EPS]-complex is presumably negligible under limited substrate concentrations. Important to note is, that the dodecapeptide of the Hsp90 C-terminal does not impede the maximal turnover rate of PPH-5 and may not be sufficient to confer the ability to form [EPS]-complexes.

Finally, a phosphorylated peptide was used as substrate to check how Hsp90 influences a more physiological phosphorylation site. Therefore, the phosphorylated peptide KRpTIRR was used and the dephosphorylation reaction followed by detecting the free phosphate using the EnzChek system. Titration of the substrate in absence of Hsp90 showed an apparent K_M of around 20 µM and again a substrate inhibition like effect at concentrations higher than 100 µM of the peptide (Figure 3.3.9 A). Addition of Hsp90 led to a shift of substrate inhibition to higher concentrations without little influence on the apparent K_M. At 150 µM peptide the activity of PPH-5 is reduced to less than 20% of the maximal turnover rate in absence of Hsp90, whereas it is still over 80% in the PPH-5-Hsp90 complex. Hence, Hsp90 can also modify the dephosphorylation of the substrate

KRpTIRR besides it activatory effect. The C-terminal domain of Hsp90 could act on the phosphatase, however with reduced efficiency (Figure 3.3.9 B, C). Interestingly, the MEEVD-peptide was not able to influence the dephosphorylation. Apparently, the RLS for this reaction is different than for pNPP dephosphorylation. As a consequence, the last 12 amino acids of Hsp90 are not sufficient to activate this new RLS, but act on another step of the catalytic cycle. Also the phosphatase activator P5SA-5 could not enhance this reaction (data not shown) indicating that both MEEVD-peptide and the activators act at steps distinct from full-length Hsp90.

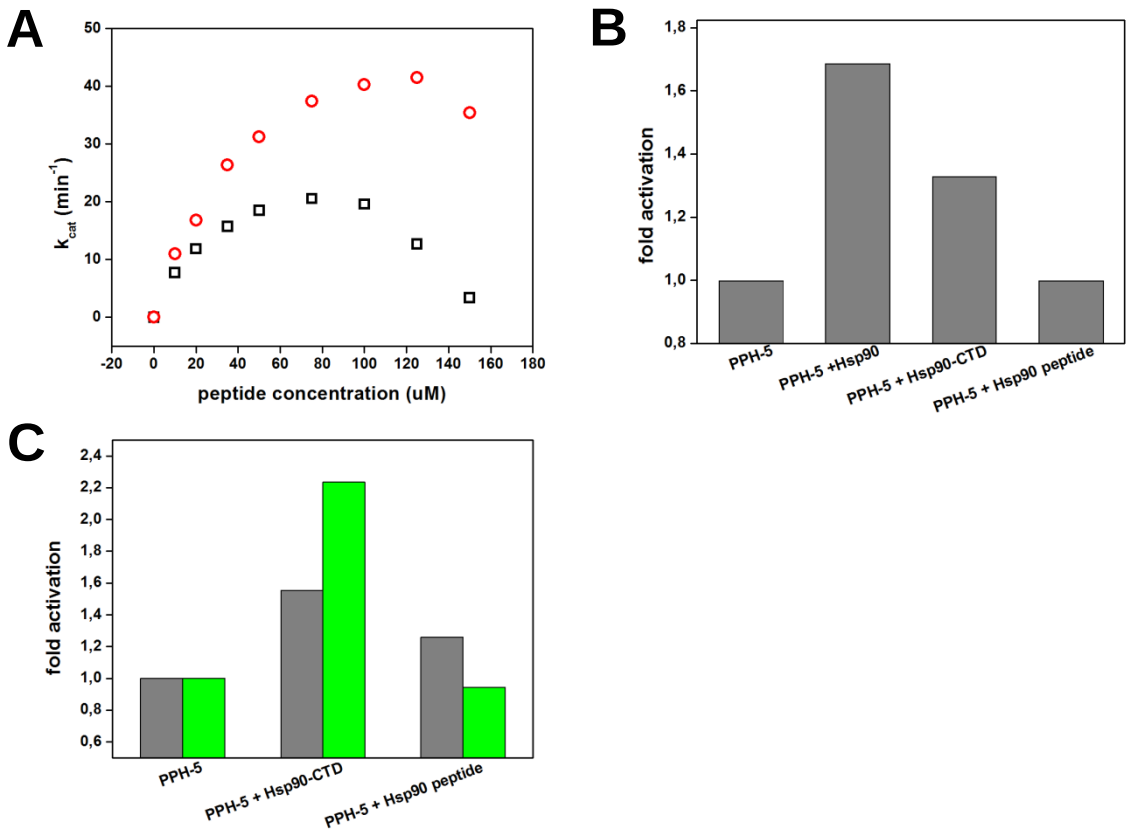

Figure 3.3.9. *Dephosphorylation of the peptide KRpTIRR by PPH-5 is activated by Hsp90.* ***A,*** *A substrate titration in absence (black) and presence (red) of Hsp90 was recorded using 25 nM PPH-5 and detected by EnzChek.* ***B,*** *Different parts of Hsp90 influence the dephosphorylation reaction. 3 µM Hsp90 or Hsp90-CTD and 60 µM Hsp90 peptide were used.* ***C,*** *Comparison of the activation by Hsp90-CTD and the Hsp90 peptide in presence of 10 µM (grey) or 75 µM (green) substrate.*

3.3.3 CDC-37 dephosphorylation by PPH-5 is dependent on the ternary complex with Hsp90*

*Parts of this chapter contributed to an article published in the *Journal of Biological Chemistry* (Eckl et al, 2013).

The nematode homolog of Cdc37, termed CDC-37, was used to investigate the differential influences of Hsp90 fragments on the dephosphorylation of this PP5 substrate. Earlier studies had showed that the kinase-dedicated cochaperone Cdc37 is dephosphorylated by the protein phosphatase 5 when both are bound to Hsp90 (Vaughan et al, 2008; Wandinger et al, 2006). However, it is still unclear whether Hsp90 needs to bring CDC-37 in a PPH-5 substrate-like state. Regarding the phsophatase, Hsp90 may be necessary to activate PPH-5 sufficiently to dephosphorylate CDC-37, to alter the enzyme specificity in a way that phosphorylated CDC-37 is recognized as a substrate or both. To study nematode CDC-37 dephosphorylation, the cofactor needs to become phosphorylated by human CKII. The phosphorylation state can be visualized by detection of radioactive phosphate, if not released by PPH-5. Application of the samples on SDS-PAGE fixates CDC-37 for detection.

PPH-5 alone was able to dephosphorylate CDC-37, but with very low efficiency (Figure 3.3.10). The presence of Hsp90 enhanced drastically this reaction. To dissect the contribution of certain parts of Hsp90 on the CDC-37 dephosphorylation different parts of the chaperone were supplemented in the assay.

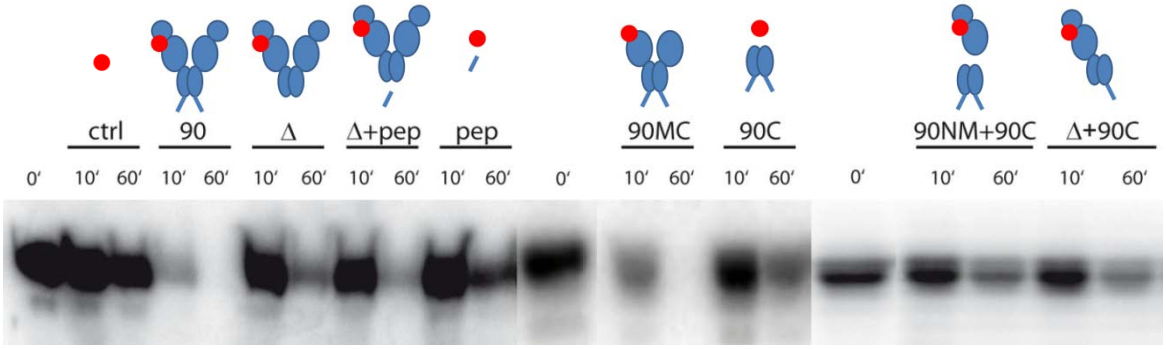

Figure 3.3.10. *CDC-37 dephosphorylation by PPH-5 is dependent on the CDC-37-Hsp90-PPH-5 complex. 10 µM CDC-37 was phosphorylated with ^{32}P-γ-ATP by human CKII for 1 h at 30 °C. After addition of 2 µM PPH-5 and 3 µM of different parts of Hsp90 samples were taken after 10 and 60 min. The setting containing PPH-5 alone is indicated by ctrl, with Hsp90 by 90, with Hsp90-ΔMEEVD by Δ, with Hsp90-ΔMEEVD and MEEVD-peptide by Δ+pep, with a deletion variant lacking the N-terminal domain of Hsp90 by 90MC, with the Hsp90-CTD by 90C and with a deletion variant lacking the C-terminal domain of Hsp90 by 90NM. The t = 0 band corresponds the time point before addition of PPH-5. Models above the radioactive bands indicate the supplemented Hsp90 fragments in blue with bound or unbound CDC-37 in red.*

Addition of the MEEVD-peptide to the reaction increased the enzymatic activity towards phosphorylated CDC-37 compared to PPH-5 alone. The addition of Hsp90-CTD could accelerated the dephosphorylation, but not to the same extent as Hsp90-MC showing a similar effect than full-length Hsp90. Hsp90 and Hsp90-MC can bind both, PPH-5 and CDC-37, and thereby lead to fast dephosphorylation of the latter. The peptide apparently caused the least effect, because it is not sufficient to generate a ternary complex of Hsp90 and both cochaperones. Same is true for Hsp90-CTD, although this domain is in principle able to substitute full-length Hsp90 in pNPP-based phosphatase assays (Figure 3.3.6 B). However, in the presence of Hsp90-MC containing a binding site for CDC-37 and the phosphatase both are in close proximity and dephosphorylation was highly efficient. Formation of a ternary complex seems to be essential, as supplementation of Hsp90-NM and Hsp90-CTD in similar amounts was not enough to yield maximal CDC-37 dephosphorylation. This experiment also suggests that a certain Hsp90 induced conformation of CDC-37 is not critical for the enzymatic efficiency of PPH-5. The presence of Hsp90-ΔMEEVD and MEEVD-peptide in the same reaction showed also little effect which indicates again that PPH-5 reactivity is mainly depending on a ternary complex with Hsp90 and CDC-37 rather than an activated phosphatase and an Hsp90-bound CDC-37. Interestingly, when this complex was assembled by adding equal amounts of Hsp90-ΔMEEVD and Hsp90-CTD to the reaction, PPH-5 efficiency towards CDC-37 was still impaired. These two different Hsp90 species are able to exchange subunits and to form heterodimers consisting of one Hsp90-ΔMEEVD monomer bound to one C-terminal domain of Hsp90 comprising the MEEVD-motif (see below, Figure 3.4.3). Although PPH-5 is able to crosslink the monomers in an Hsp90 dimer (Figure 3.3.3), the enzyme apparently acts only on the monomer it is bound to by its TPR domain. These results suggest that Hsp90 not only activates the phosphatase, but can direct dephosphorylation activity to chaperone bound proteins. As a consequence, PPH-5 and Hsp90 may share a number of client proteins assuming that free PPH-5 is not sufficiently reactive. Other cytosolic or nuclear proteins exhibiting an MEEVD-motif or motifs that resemble this sequence after posttranslational modifications could, however, act in a similar way on the phosphatase as Hsp90.

3.3.4 PPH-5 dehosphorylates different Hsp90 interactors

The next question to address was whether Hsp90 cofactors and other interactors are possibly regulated by PPH-5 dephosphorylation. Apart from CDC-37 other Hsp90 interactors like p23 and HSF-1, as well as the kinase PMK-1 are well-known phosphoproteins. Therefore, the radioactive assay reported before was used to analyze, if the nematode p23, FKB-6, AHA-1, PMK-1, HIP and HSF-1 can be dephosphorylated by PPH-5. Prerequisite for this assay is a successful phosphorylation of the respective protein by human CKII. This was not the case for nematode p23 and FKB-6. Analysis of the latter would be interesting, as it binds like PPH-5 to the C-terminal MEEVD-motif of Hsp90 and might compete formation of a ternary complex. The signal for AHA-1 was rather low, but could be detected. In summary, AHA-1, PMK-1, HIP and HSF-1 were all dephosphorylated by the phosphatase in presence of Hsp90 (Figure 3.3.11). Purified PMK-1 kinase was provided by Julia M. Eckl and is a putative client of the Hsp90 chaperone system (Julia M. Eckl, personal communication, Lehrstuhl für Biotechnologie, Technische Universität München, Germany). It is unclear, however, whether the respective phosphorylation sites are relevant *in vivo*. Likely, kinases other than CKII may be involved in the phosphorylation of the different proteins. It would be also interesting to analyze the dephosphorylation in absence of Hsp90 to elucidate the dependence of a ternary complex for these proteins.

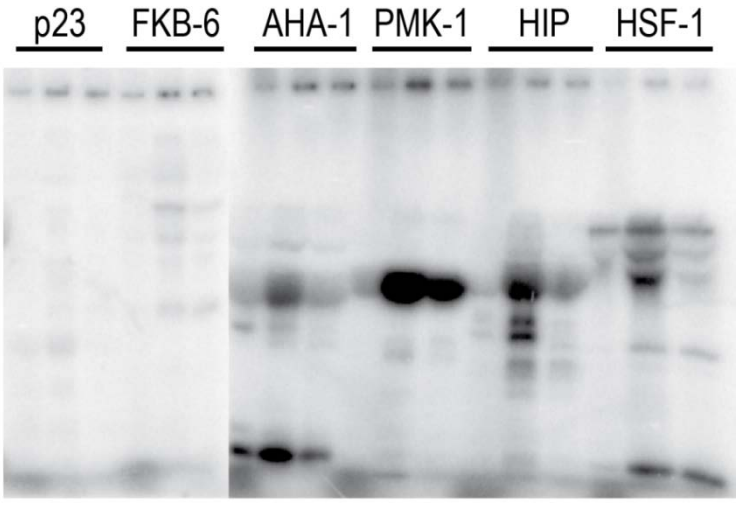

Figure 3.3.11. *Interactors of the Hsp90 chaperone system can be dephosporylated by PPH-5. Each cofactor was incubated with radioactive ATP and human CKII for 2h at 30 °C prior to addition of PPH-5. The three lanes for each cofactor represent a sample of the reaction batch before phosporylation in lane 1, before PPH-5 addition in lane 2 and after incubation with PPH-5 for 1 h at 20 °C in the respective lane 3.*

Another putative interactor of both protein phosphatase 5 and the Hsp90 chaperone system is the transcription factor Smad4. In a genome wide yeast two hybrid screen of *C. elegans* an *in vivo* interaction of the nematode homolog SMA-4 with either protein was identified (Li et al, 2004). As the nematode homolog could not be expressed in *E. coli* BL21 (DE3) cells at 20 °C overnight, the human protein Smad4 was cloned, purified and stable under room temperature (Figure 3.3.12 D). AUC analysis could confirm the interaction of the transcription factor with YFP-Hsp90 (Figure 3.3.12 A). The protein complex, however, proved to be sensitive in addition with ATP and Mg^{2+}, as Smad4 did not bind in presence of these compounds which cause the closing of YFP-Hsp90 and a respective shift to higher $s_{20,w}$ values. In further AUC experiments Smad4 also bound to human Hsp90β labeled with lysine reactive Alexa488 (Figure 3.3.12 C).

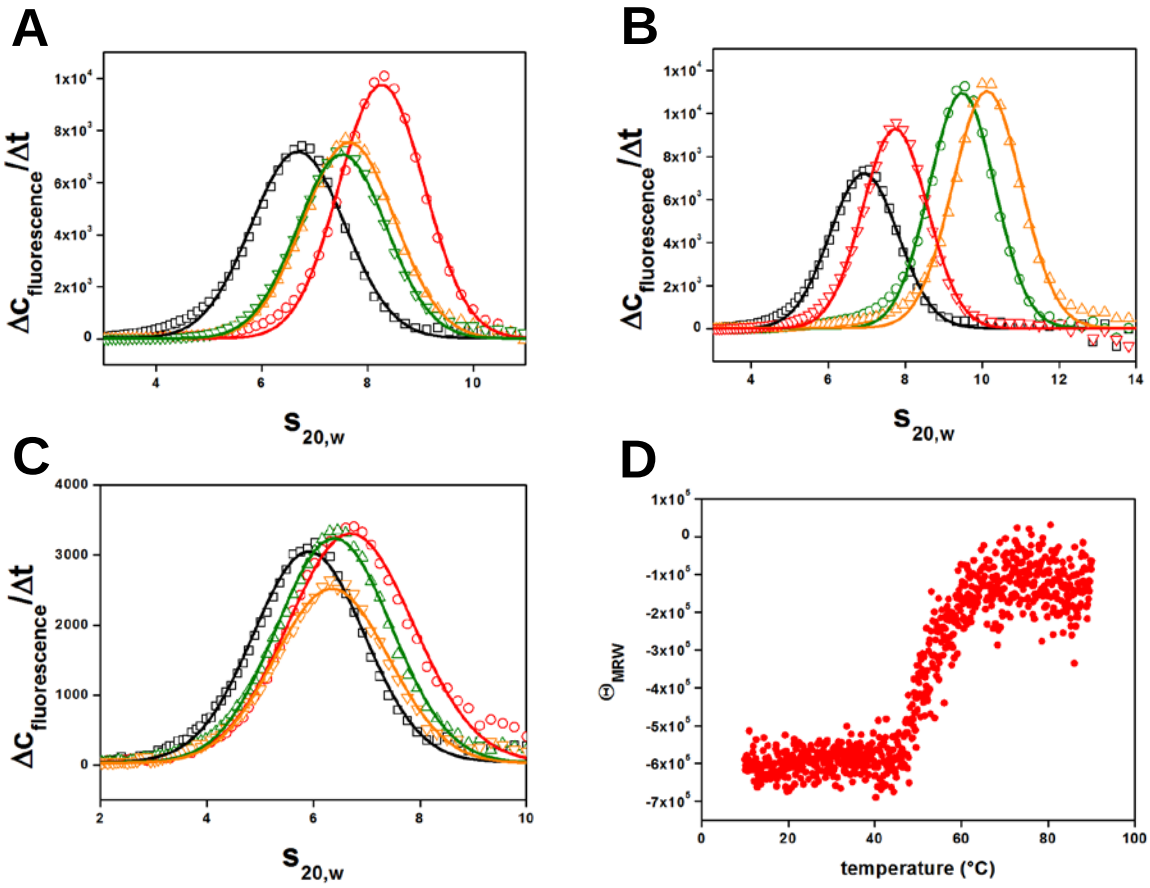

Figure 3.3.12. *The transcription factor Smad4 binds to Hsp90 and forms a ternary complex in presence of PPH-5.* ***A****, YFP-Hsp90 (black) is shifted to higher* $s_{20,w}$ *in presence of 5 µM human Smad4 (red). Addition of 2 mM ATP and 5 mM* Mg^{2+} *(green) induces closing of the Hsp90 dimer and leads a shift to higher sedimentation coefficients compared to YFP-Hsp90 alone. Supplementation with 5 µM Smad4 has no further effect (orange).* ***B,*** *Addition of 5 µM Smad4 (red) induces a shift of YFP-Hsp90 (black) to higher sedimentation coefficients. Addition of 2 µM PPH-5(green) also shifts*

YFP-Hsp90. Presence of both Smad4 and PPH-5 leads to a ternary complex with a $s_{20,w}$ value over 10 S (orange). ***C,*** *Addition of 6 µM Smad4 (red) induces a shift of random Alexa488-labeled human Hsp90β (black) to higher sedimentation coefficients. Addition of 2 mM ATP and 5 mM Mg^{2+} (green) induces closing of the Hsp90 dimer and leads a shift to higher sedimentation coefficients compared to Alexa488-Hsp90 alone. Supplementation with 5 µM Smad4 has no further effect.* ***D****, Thermal unfolding of 5 µM Smad4 in 40 mM HEPES, 20 mM KCl, 1 mM DTT, pH 7.5.*

A ternary complex of Hsp90, PPH-5 and human Smad4 could also be assembled and detected in AUC experiments (Figure 3.3.12 B). Analysis of the corresponding protein complexes in the radioactive dephosphorylation assay showed that human Smad4 can be dephosphorylated by rat PP5 in presence or absence of human Hsp90α (Figure 3.3.13). The phosphorylation efficiency towards Smad4 was very low when compared to phosphorylated CDC-37. One reason may be that human CKII is not the physiological kinase for Smad4 phosphorylation. Therefore, these results are not suitable for quantitative analysis. It may be also possible that the Hsp90-phosphatse complex predominantly interacts with the fully assembled and active Smad2-Smad3-Smad4 heterotrimer where components other than Smad4 are dephosphorylated and the signaling pathway thereby switched off by PP5.

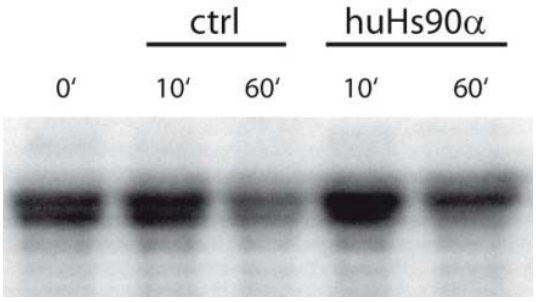

Figure 3.3.13. *Dephosphorylation of human Smad4 by rat PP5. Samples were taken 10 and 60 minutes after addition of the phosphatase. Prior to this Smad4 had been incubated with CKII and radioactive ATP. The control reaction batch contained 10 µM Smad4 and 2 µM rat PP5. Where indicated, 3 µM human Hsp90α was added to the reaction.*

3.4 The muscle-dedicated cochaperone UNC-45 binds to Hsp90 and Hsc70 via its N-terminus*

* Parts of this chapter contributed to an article published in *PLOS ONE* (Gaiser et al, 2011). Other unpublished data will be submitted for publication (Haslbeck et al, *Manuscript in preparation (b)*).

3.4.1 YFP-tagging of Hsp90 allows UNC-45 interaction studies *in vitro* and *in vivo*

During the first phenotypic screens by Sydney Brenner, the *C. elegans* mutant e286 with severe motility defects was discovered which turned out to carry a point mutation in the gene encoding the TPR domain containing protein UNC-45 (Brenner, 1974). Fully functional UNC-45 is responsible for correct patterning and maintenance of the myofibrillar lattice in body wall muscle cells of the nematode. Knockdown studies and *in vivo* imaging in zebrafish had further suggested that Hsp90 as well plays a crucial role in muscle maintenance and that both proteins act together at the site of the muscular ultrastructure (Du et al, 2008; Etard et al, 2008). In collaboration with Andreas M. Gaiser and Christoph J. O. Kaiser (Lehrstuhl für Biotechnologie, Technische Universität München, Germany) the point mutation E292K in nematode Hsp90 was analyzed in this thesis, as the respective *C. elegans* mutant strain exhibits motility defects similar to UNC-45 knockdown or the mutant e286 which suggested an involvement of nematode Hsp90 in muscle maintenance.

To be able to study the interaction of UNC-45 with the Hsp90 chaperone system either in the living nematode or *in vitro*, a fluorescent YFP label was cloned into the flexible linker region of Hsp90 between amino acid 230 and 231. The idea was not to interfere with the enzymatically important N-domain and the C-terminal domain responsible for dimerization of Hsp90. This construct termed Hsp90-YFP(li) was cloned into a T7 expression system and purified out of *E. coli*. The question arose whether this Hsp90-probe is still able to achive ATP hydrolysis and chaperoning functions. Therefore the ATPase activity of Hsp90-YFP(li) was assessed in comparison to wiltype Hsp90 (Figure 3.4.1). The fusion protein shows a reduced hydrolysis rate, but it can still be activated by nematode AHA-1 which is a well-known activator of Hsp90. This demonstrates that the interaction site for the cofactor AHA-1 is still intact despite the YFP-insertion.

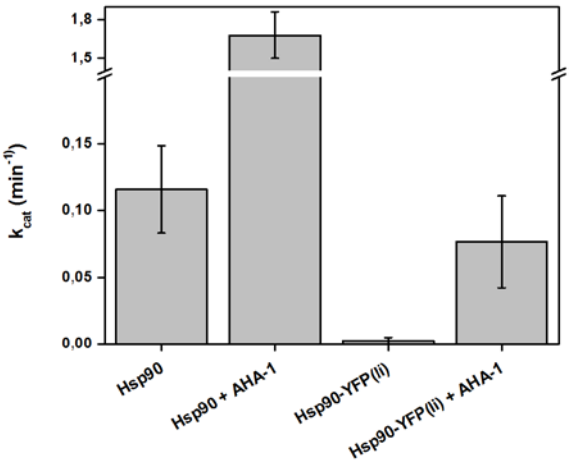

Figure 3.4.1. *The hydrolysis rate of Hsp90-YFP(li) is reduced, but can be stimulated by AHA-1. Upon the addition of 6 µM AHA-1, the ATPase of Hsp90-YFP(li) increases. The ATPase assays were performed at 25°C in low salt buffer.*

In aggregation assays Hsp90-YFP(li) could suppress the aggregation of citrate synthase and showed even increased chaperone activity compared to Hsp90 (Figure 3.4.2 A). Therefore, full functionality of Hsp90-YFP(li) is conserved in this variant.

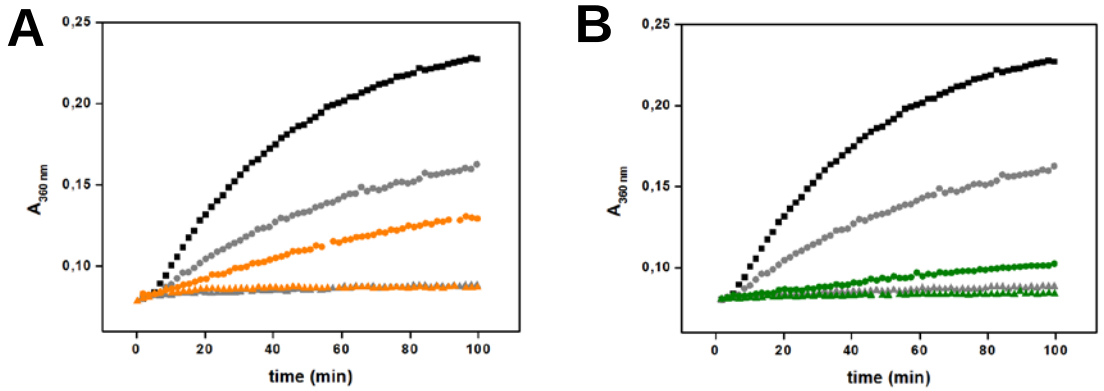

Figure 3.4.2. *Hsp90, Hsp90-YFP(li) and Hsp90-E292K are active chaperones. Thermally denatured citrate synthase aggregation (black boxes) is inhibited by the addition of 0.1 µM Hsp90 (grey circles), Hsp90-YFP(li) (yellow circles, A) and Hsp90-E292K (green circles, B). Upon the addition of 0.5 µM Hsp90 (grey triangles), Hsp90-YFP(li) (yellow triangles, A) or Hsp90-E292K (green triangles, B) aggregation of citrate synthase is fully suppressed.*

In addition, the chaperone activity of the variant Hsp90-E292K was determined and showed similar results as the wildtype protein (Figure 3.4.2, B), whereas the ATPase

activity had been shown to be drastically reduced in this mutant (Gaiser et al, 2011). Chaperone activity is apparently not proportionally linked to ATPase hydrolysis.

Subsequently, the fluorescent probe Hsp90-YFP(li) was analyzed by fluorescence based analytical ultracentrifugation. In presence of excess of unlabelled Hsp90-CTD the sedimentation coefficient of Hsp90-YFP(li) was shifted to smaller $s_{20,w}$ values indicating that subunit exchange between the Hsp90 monomers is not affected by insertion of YFP into the linker region (Figure 3.4.3 A). Furthermore, established cofactors of the Hsp90 chaperone system were used to assess the integrity of various binding sites of the fusion protein. Presence of either PPH-5, STI-1 or C34B2.5 could shift the peak of the labeled species to higher $s_{20,w}$ values (Figure 3.4.3 B). Together with the results of the ATPase assays that had confirmed binding of AHA-1 to the fusion protein, it can be assumed that Hsp90-YFP(li) is fully accessible by its cofactors.

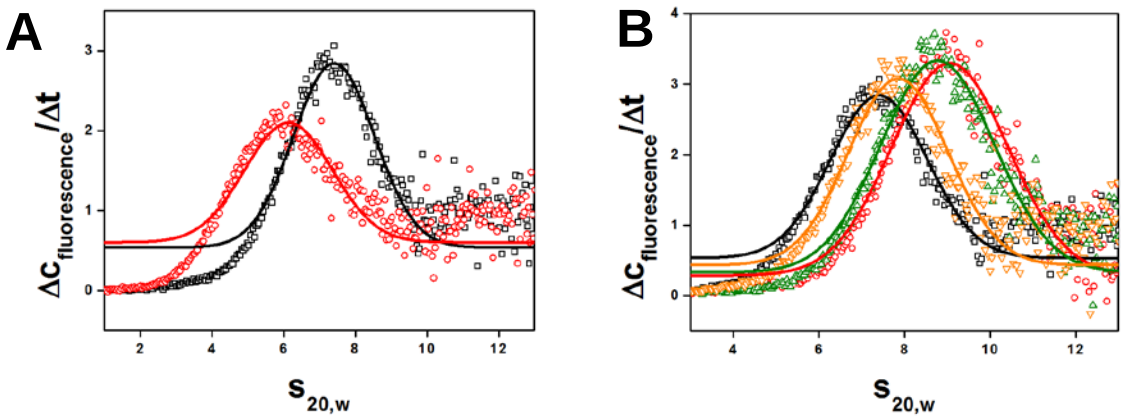

Figure 3.4.3. *Hsp90-YFP(li) shows wildtype like binding properties. A, Hsp90-YFP(li) can form heterodimers with a C-terminal fragment of Hsp90.* ***A,*** *Fluorescence based AUC analysis confirms heterodimer formation of a C-terminal fragment of Hsp90 and Hsp90-YFP(li). Hsp90-YFP(li) has a sedimentation coefficient of 7.3 S (black). By adding the C-terminal fragment Hsp90(524–702), the sedimentation coefficient shifts to 6.0 S implying heterodimer formation and a consequent loss of molecular mass (red).* ***B,*** *Hsp90-YFP(li) can bind TPR domain containing cofactors. Despite the YFP insertion, Hsp90-YFP(li) (black) binds PPH-5 (green), STI-1 (red) and the small TPR protein C34B2.5 (orange), as indicated by a shift to higher sedimentation coefficients.*

3.4.2 UNC-45 binds to Hsp90 via its N-terminal domain

It is still not completely understood where and how specific UNC-45 binds to the chaperones Hsp90 and Hsp70. Earlier results by Barral and coworkers (Barral et al, 2002) had shown that UNC-45 binds to Hsp90 via its TPR domain recognizing the C-terminal MEEVD-motif. The binding to Hsp70, however, did not depend on the presence of the TPR domain and could not be competed with excessive addition of the C-terminal peptide of Hsp70 implying a possible chaperone-client interaction. In contrast, a recent study by (Gazda et al, 2013) demonstrated that UNC-45 interacts via the TPR domain with Hsp70 with a binding constant of 120 µM between TPR domain and the C-terminal peptide of Hsp70. Mutations in the binding groove of the UNC-45 TPR domain did completely abrogate this interaction.

In this thesis data obtained from analytical ultracentrifugation should help to clearify the question, how UNC-45 binds to full-length Hsp90. Therefore, an N-terminal part of UNC-45, UNC-45(1-461), was purified. The sedimentation of unlabeled Hsp90 together with UNC-45(1-461) was analyzed. UNC-45(1-461) showed a $s_{20,w}$ value of 3.8 S and Hsp90 of 5.9 S (Figure 3.4.4 A). Adding the cofactor in a twofold molar excess to dimeric Hsp90, the UNC-45(1-461) peak at 3.8 S was decreased in intensity and the Hsp90 peak shifted to a higher sedimentation coefficient. This interaction could be confirmed using the fluorescently labeled Hsp90-YFP(li). By this setup, only the labeled species is detected and was shifted to higher $s_{20,w}$ values in presence of UNC-45(1-461) (Figure 3.4.4 B). Using an N-terminally YFP-tagged Hsp90 probe confirmed this interaction (Figure 3.4.4 C). Presence of the C-terminal peptide of Hsp90 is able to compete with the complex formation between both proteins. These results confirm the current literature and the TPR domain dependent interaction of UNC-45 and Hsp90 (Barral et al, 2002; Gazda et al, 2013). Interestingly, testing the purified TPR domain of UNC-45 (aa1-114) in isothermal titration experiments could not detect any binding to the Hsp90 peptide (Figure 3.4.5 A). This construct is either impeded in its native fold or lacks decisive residues that are essential for the binding to Hsp90. Apparently, the interaction between the chaperone and UNC-45 is depending on contacts outside the TPR binding groove which may be a common feature of TPR cochaperones. Examples are PPH-5 and FKB-6 as discussed earlier.

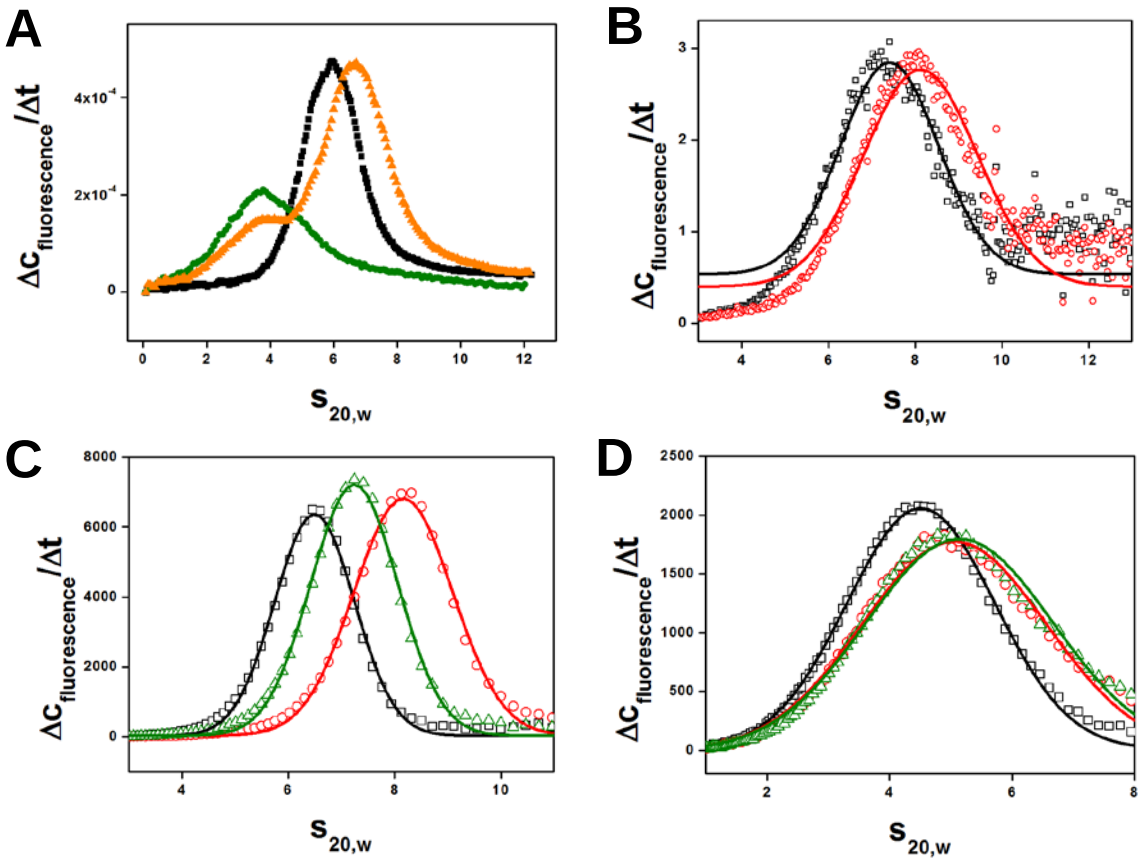

Figure 3.4.4. *A TPR-domain containing fragment of UNC-45 binds to Hsp90.* ***A****, The interaction of UNC-45(1-461) and Hsp90 is detected by UV detection in the AUC. 10 µM of UNC-45(1-461) (green) and 9 µM of Hsp90 (black) were sedimented alone and as a mixture (yellow).* ***B****, The sedimentation coefficient of Hsp90-YFP(li) (black) shifts in presence of 6 µM of UNC-45(1-461) (red).* ***C,*** *Using YFP-Hsp90 (black) as probe confirmed binding of UNC-45(1-461) (red), whereas presence of the C-terminal MEEVD-peptide induced a shift of the probe to a lower $s_{20,w}$ value (green).* ***D****, FAM-labeled Hsc70 (black) is shifted to a higher sedimentation coefficient in presence of UNC-45(1-461) (red). Presence of the C-terminal peptide of Hsc70 cannot compete the interaction (green).*

Applying the respective settings to a FAM-labeled Hsc70 probe could detect the complex formation between Hsc70 and UNC-45(1-461) (Figure 3.4.4 D). Addition of the C-terminal Hsc70-peptide, however, had no influence on the sedimentation coefficient of the protein complex. This demonstrates that interaction of the TPR domain of UNC-45 with the C-terminal end of Hsc70 is not essential for the interaction. Also titration of UNC-45(1-114) with the Hsc70-peptide did not detect binding in the ITC (Figure 3.4.5 B). Regarding the published results discussed above, it can be assumed that residues outside the TPR binding groove not only contribute to the interaction, but are in effect more specific than possible residual interactions between TPR domain and the IEEVD-

peptide of Hsc70. Presence of ATP could clarify whether the complex formation is rather a chaperone-client interaction in the case of Hsc70.

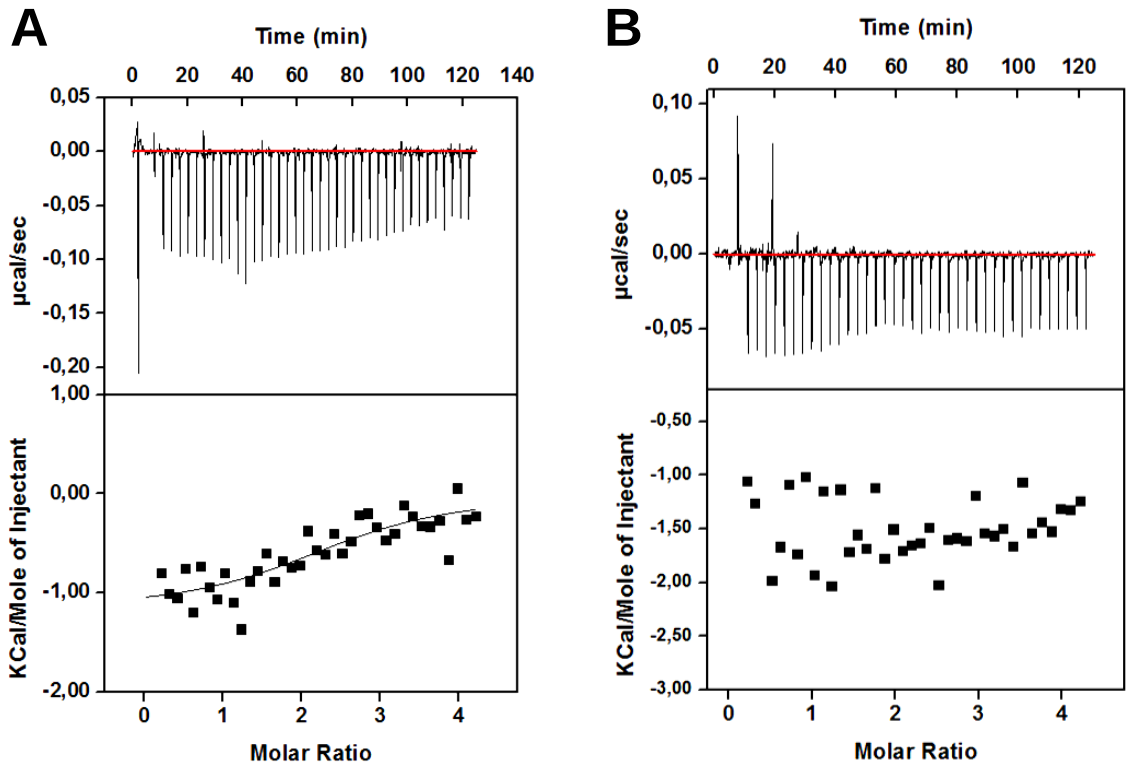

Figure 3.4.5. *The TPR-domain of UNC-45, UNC-45(1-114) is not sufficient to bind the C-terminal peptides of Hsp90 or Hsp70.* ***A****, 20 µM UNC-45(1-114) in the ITC cell was titrated with 400 µM Hsp90-peptide in the syringe.* ***B,*** *20 µM UNC-45(1-114) in the ITC cell was titrated with 400 µM Hsc70-peptide in the syringe.*

3.4.3 *In vivo* analysis of the cochaperone UNC-45

C. elegans is a suitable model organism to study protein interaction *in vivo*. Therefore, the respective proteins need to be labeled with different fluorescent dyes. To investigate the subcellular localization of Hsp90 and UNC-45, constructs of the fusion protein Hsp90-YFP(li) and a C-terminally CFP tagged UNC-45 were cloned to the 3' end of the muscle specific UNC-54 promotor and transgenic nematode lines were generated for each construct by injection of plasmid-DNA into the gonads of adult N2 worms. In collaboration with Christoph J. O. Kaiser and Andreas M. Gaiser the localization pattern of Hsp90 and UNC-45 in the myofibrillar lattice of these worms was analyzed by confocal microscopy (Gaiser et al, 2011). These studies suggested a differentiated localization pattern for Hsp90 and UNC-45. While Hsp90 seems to be preferably

associated to the I-band of the muscle fibers and is freely diffusible, UNC-45 shows various patterns and the strength of the association differed in FRAP assays as published (Gaiser et al, 2011). This suggests specialized roles for Hsp90 and UNC-45 in the muscular tissue despite their tight interplay *in vitro*.

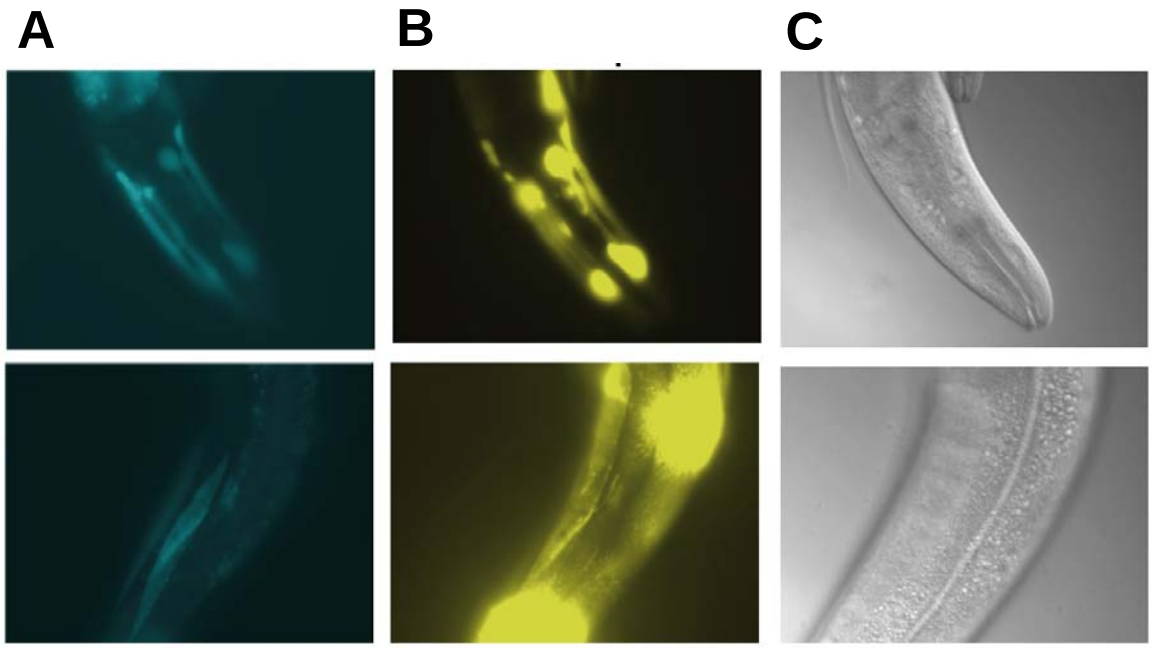

Figure 3.4.7. *Individual muscle cells can be analyzed with a two-colored stable transgenic nematode line expressing UNC-45-CFP and Hsp90-YFP(li) under the muscle promotor.* ***A****,UNC-45 is visible in the CFP channel.* ***B,*** *Hsp90-YFP(li) is visible in the YFP channel.* ***C,*** *DIC images.*

To study the interplay of Hsp90 and UNC-45 in the living muscle tissue a two-colored transgenic line was generated that expesses both proteins with fluorescent labels under the muscle promotor of UNC-54 (Figure 3.4.7). Hsp90-YFP(li) is visible in different muscle cells of the head and the body wall muscle cells under a Zeiss Axiovert 200 inverted microscope. An overlapping pattern can be observed when exciting C-terminal CFP-tagged UNC-45. However, both proteins are not equally expressed in the same cells resulting in cells that only express either Hsp90 or UNC-45. The specific muscle pattern can be detected in both channels. Further analysis, however, will require confocal microscopy and are under way.

The *C. elegans* mutant e286 characterized by Sydney Brenner expresses a temperature-sensitive *unc-45* allele. To visualize the temperature sensitivity and the plasticity of the effect, the motility of the corresponding strain CB286 was analyzed after incubation at

different temperatures. As a read-out the number of body bends per minute of N2 and CB86 worms (n = 10) when swimming in a M9 drop was counted and plotted.

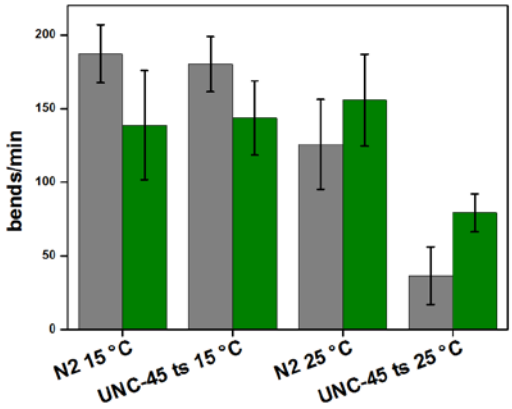

Figure 3.4.6. *The motility defects of CB286 caused by high temperature are reversible. Eggs were placed on OP50 seeded NGM plates and incubated at the indicated temperature for 4 days (grey) and the body bends per minute was counted. Subsequently, the incubation temperature was shifted to 25 °C in case of 15 °C incubation and to 15 °C in case of 25 °C incubation. After 24 h body bends per minute were analyzed (green).*

At a temperature of 15 °C both wild type N2 worms as well as temperature-sensitive UNC-45 mutant worms (CB286) showed full motility (Figure 3.4.6). When incubated at the restrictive temperature of 25 °C the ability to bend along the body wall was drastically decreased in CB286 worms. When the worms were incubated at the respective other temperature, worms started to move slower in case of incubation at 25 °C. Interestingly, a lower incubation temperature of 15 °C after 4 days of 25 °C could ameliorate the impaired motility of both worm strains. To validate these experiments where a batch of worms was used, a thorough analysis would have to be performed with identical worms before and after temperature shift.

4. Conclusions

4.1 Validation of a proteome wide approach enables the identification of new TPR cochaperones

The TPR domain is known to work as a protein-protein interaction tool bringing together different parts of a certain network like in the case of the Hsp90-TPR cochaperone complexes (Rohl et al, 2013), scaffolding protein assemblies as for the anaphase-promoting complex (Schreiber et al, 2011) or regulating enzymes like PP5 or OGT (Iyer & Hart, 2003; Kreppel & Hart, 1999; Yang et al, 2005). Searching whole proteomes for TPR domains by the algorithm described in this study revealed that during the evolution of higher eukaryotes the number of TPR proteins increased steadily from yeast to nematodes and humans. The first part of this thesis used a global approach to identify chaperone interacting TPR proteins amongst the whole TPRome of *C. elegans*.

A sample set of known TPR cochaperones from yeast, human and *C. elegans* was compiled and aligned to build a search model for the bioinformatics tool HMMER3.0. Examination of this alignment reveals not only the strict conservation of certain positions in the TPR-motifs, but also a close homology of the loops connecting the helix-turn-helix-motifs of certain proteins. As such, the TPR2A domain of human Hop/STIP1 contains a characteristic loop between TPR-motif 2 and 3 that is highly conserved in the respective yeast and nematode proteins. Also the peptidyl-prolyl-isomerases of all three organisms display conservation of a long loop between TPR-module 1 and 2. Interestingly, the muscular isoform of human Unc45, Unc45B, contains a short extension between module 1 and 2 that resembles those of nematode UNC-45 and the uncharacterized yeast protein Cns1, whereas the general cell isoform Unc45A differs in these residues. Such specific loop regions may serve for a first classification of uncharacterized TPR cochaperones. It would be interesting to analyze whether other classes of TPR cochaperones also exert characteristic loops that indicate their specific function. Applying a HMMER3.0 search on the *C. elegans* proteome using this alignment as search model ranked the TPRome according to the homology to the sample set. The fact that well-established TPR cochaperones concentrated on top of the ranking was a first indication that this approach is valid to search for new unidentified TPR cofactors of Hsp90 and Hsc70. The protein product of two highly ranking ORFs, C34B2.5 and ZK370.8, was purified and analyzed for physical interaction with the chaperones. Both proteins showed TPR domain

dependent interaction with the chaperone systems without clearly favoring either Hsp90 of Hsc70. Characterization of the expression pattern and intracellular localization suggested that these proteins represent the nematode homologs of human TTC1 in case of C34B2.5 and TOM70 in case of ZK370.8. A third, lower ranking TPR protein, F52H3.5, did not directly bind to the chaperones. Four residues of the TPR domain were analyzed more closely. In case of positive interaction with the chaperone systems, positions 5/12/13/74 displayed high conservation regarding the physical properties of the respective amino acids. This conservation was largely lost for F52H3.5 and proteins ranked below.
The rationale behind such a proteome wide approach was to first establish and validate an algorithm using the model system *C. elegans* and to extend this method in a second step on the TPRome of other species. Therefore, the human TPRome was ranked and a sample of purified TPR proteins analyzed for their ability to interact with Hsp90 and Hsc70. TTC9 and the TPR domains of two other human proteins, TTC12 and WDTC1, could be purified and identified as putative cofactors of the Hsp90 system. Developing better purification protocols for TTC12(99-225) and WDTC1(346-490) would allow thorough characterization of these proteins. Nevertheless, this part of the thesis describes a promising approach to identify new members of the presumably huge TPR cochaperone network whose diversity may have become necessary with the high level of differentiation in cell types and tissues during evolution. Furthermore, this study serves as an example how to classify whole parts of proteomes in respect of a specific biological question.

4.2 The P5SAs act selectively on the PP5 autoinhibitory mechanism and may represent lead candidates to target neurogenerative diseases

PP5 is able to dephosphorylate the human tau protein which is a major effector in the progression of Alzheimer's disease in its hyperphosphorylated form (Mandelkow & Mandelkow, 2012). In addition, the enzyme certainly plays an important role in cell signaling and cell cycle arrest, as it is involved in the regulation of steroid hormone receptors, check point kinases and DNA repair cascades (Hinds & Sanchez, 2008). Evaluating the current literature regarding PP5 imposes the conclusion that this protein represents a therapeutically very interesting target. However, the fact that there are only a few, highly homologous protein phosphatases in the cell may challenge the development

of selective drugs targeting the dephosphorylation of a specific clientele. Despite the relevance of PP5 different screening efforts have so far not discovered any highly selective and potent activators of PP5 with considerable *in vivo* efficacy (Cher et al, 2010; Ni et al, 2007). The screen performed in this study is based on the pNPP dephosphorylation reaction which allowed the identification of five activators out of a library of 15,000 substances. The compounds termed P5SAs feature K_Ds in the low micromolar range and activation potentials up to 22-fold. The success of the screen depended greatly on the library which was designed to contain small molecules with chemical characteristics according to the Lepinski's Rule of Five. Matching these requirements is a good starting point for further development as orally active drug (Lipinski et al, 2001). Characterization of the five activators revealed high selectivity for PP5 which is the only phosphatase in the PPP family with a tightly regulated autoinhibitory mechanism. PP5's outstanding domain composition and mode of activation already suggests that the interface between the regulatory domains (TPR and αJ-helix) with the catalytic domain play a role in the selective activation by the P5SAs. Attacking the highly conserved phosphatase domain and its active site would be rather unlikely given that the activators leave the activity of the phosphatases PP1, PP2A and PP2B/PP3 unchanged. According to this hypothesis, crystallizing rat PP5 in presence of the activator P5SA-2 revealed additional electron density in a pocket of the enzyme located between phosphatase domain and TPR domain. This residual density could not be observed in crystals produced without the compound and may represent parts of the activator in a newly identified binding cleft. The structure of the PP5:P5SA-2 complex was solved with a resolution of 2.0 Å, but displays a high degree of disorder in the last amino acids of the αJ-helix. In contrast to enzyme inhibitors that lock a protein in a tense or trapped state, the crystallization of an activated or relaxed enzyme would render an increase in flexibility. As a consequence, the activator does not arrest completely and is not fully resolved. However, the TPR domain is remodeled markedly and, even more strikingly, a channel to the active site opens up in presence of P5SA-2. Enzymatic tests using rat PP5 and fragments thereof confirmed that the activators all bind to the phosphatase domain despite their structural heterogeneity. Thereby, they act in a newly identified allosteric way independent of the TPR domain. Four of the five substances proofed beneficial in an Alzheimer mouse model in further studies together with the Lab of Frank Striggow (DZNE, Magdeburg, Germany). The activators could reduce tau phosphorylation in

neurons of the hippicampus and prevented severe structural misorganisation of this area despite the expression of the variant tau-P301L. These results demonstrated that they have certain *in vivo* efficacy and further efforts using cell culture or animal model systems should be made to analyze their mode of action in the cell as well as bioavailability and possible toxicity. Thorough analysis of the compounds' NMR spectra in response to addition of PP5 can lead to identification of parts of the compounds which are interacting with the proteins and which can be randomized by chemical synthesis. By competition experiments these NMR experiments could also be used to identify overlapping binding sites of the different P5SAs. Subsequently, high-throughput derivatization of the identified compounds should be performed and used to find high affinity binders in the low nanomolar range or below. The pNPP assay would allow such an analysis in a 96-well format at low costs. In summary, the P5SAs and their mode of action may represent a novel way to target neurodegenerative diseases.

4.3 The Hsp90-dedicated phosphatase PPH-5 may act only at certain steps of the chaperone cycle

The activation that Hsp90 imposes on the PP5 was discovered 11 years ago (Ramsey & Chinkers, 2002). Since then different groups found that the C-terminal MEEVD-motif of the chaperone is sufficient to activate its cochaperone (Ramsey et al, 2000; Yang et al, 2005). In the same studies, a dictinct activation potential of full-length chaperone versus the Hsp90-peptide had been observed suggesting that residues N-terminal to the MEEVD-motif are necessary to successfully compete with the autoinhibitory αJ helix of PP5. This thesis provides new insights into the complex interplay of both proteins by a thorough analysis of PPH-5 activity in presence of different Hsp90 fragments. Studying the nematode homologs of phosphatase and Hsp90 revealed that the chaperone is able to inhibit phosphatase activity under saturating substrate concentrations. The substrate inhibition is caused by the C-terminal domain of Hsp90 excluding, however, the well-characterized MEEVD-motif. In addition, the newly identified contacts seem to bind independently on the phosphatase, as the last 12 amino acids of nematode Hsp90 act in effect opposite to an Hsp90 variant lacking the MEEVD-motif. Hence, additional contacts between Hsp90 and PPH-5 are not only necessary to increase affinity for displacing the inhibitory αJ helix, but to modulate turnover and substrate specificity. It may be the case

that using other homologs or substrates would have not allowed these observations. Indeed, dephosphorylation of the substrate KRpTIRR was not activated by the Hsp90-peptide implying that complex formation between TPR domain and MEEVD-motif is not necessarily sufficient to enhance the turnover of a specific substrate where another step in the catalytic cycle may be rate limiting. Regarding the *in vivo* relevance of these findings, one can assume that Hsp90 is able to alter the substrate specificity of PPH-5 in the cellular environment. As a consequence, complexes of Hsp90 and PPH-5 would recognize and process a different set of phosphatase substrates and with distinct effectiveness than the enzyme would in its apo state. Applying phosphorylated peptide arrays would allow the analysis of the composition of possible substrate peptides under the influence of Hsp90.

Many phosphoproteins are among the Hsp90 clientele that might be possible substrates of PPH-5. However, during the maturation cycle of a certain client different TPR cochaperones have to bind to the Hsp90 platform apart from the phosphatase to contribute their specific function. It is still unclear whether the TPR cofactors bind in a certain order and how this order might be maintained. Addressing this question revealed that STI-1 and PPH-5 can build ternary complexes with Hsp90 while FKB-6 prefers the phosphatase free chaperone. Regarding the proposed Hsp90 cycle, PPH-5 and STI-1 could work together at a certain step during the maturation, but are displaced by peptidyl-prolyl-isomerases which are thought to act in a late stage of chaperoning an Hsp90 client. It would be interesting to analyze whether the long loop between TPR modules 1 and 2 that is characteristic for the PPIases, plays a role in this TPR protein regulation. Independent methods were applied in this study to examine the secondary binding site of PPH-5 that is involved in TPR cochaperone regulation. PPH-5 can connect the monomers of Hsp90 and impede exchange of single chaperone subunits. Crosslinking experiments identified interactions between the C-terminal dimerization domain of Hsp90 and the phosphatase domain. These contacts may explain why Hsp90 is able to impose effects like substrate inhibition onto the phosphatase apart from releasing the autoinhibitory mechanism. Concerning the mode of action of PPH-5 in the chaperone complex it could be observed that the phosphatase only processes phosphorylated CDC-37 when bound to the same Hsp90 monomer, although PPH-5 interacts and crosslinks both chaperone subunits of Hsp90.

During the search for new physiological substrates of PPH-5 a novel interaction partner of Hsp90 was found. Smad4 is a key player in TGFβ signalling and was first identified as a potential interaction partner of Hsp90 and PPH-5 in a genome wide yeast-two-hybrid screen performed in *C. elegans* (Li et al, 2004). This transcription factor bound to nematode Hsp90 together with the phosphatase in a nucleotide sensitive manner. Radioactive phosphatase assays showed that Smad4 can be dephosphorylated by mammalian PP5 independent of Hsp90. In addition, nematode AHA-1, the kinase PMK-1, HIP and the heat shock transcription factor HSF-1 were also identified as possible substrates of the Hsp90-PPH-5 phosphorylation machinery.

In summary, PPH-5 contributes phosphatase activity to the Hsp90 chaperone platform, but acts there under specific regulation of the chaperone. Further evidence has been found that PPH-5 acts only at certain PPIase-free complexes during the client maturation and is likely displaced by competing TPR proteins or specific posttranslational modifications of the chaperone machinery (Xu et al, 2012). Whether the phosphatase is fully dedicated to Hsp90 or also plays a significant role *in vivo* in absence of Hsp90 would be an important issue to address in the future.

4.4 The Hsp90-UNC-45 complex is based on TPR domain interactions in contrast to Hsp70 binding

The interaction of Hsp90 with its TPR cochaperone UNC-45 has been studied since many years, but the mode of binding between the cofactor and the chaperones Hsp90 and Hsp70 is still not fully understood (Etard et al, 2007; Gazda et al, 2013; Liu et al, 2008). Results obtained in this thesis clearly demonstrate that UNC-45 interacts with Hsp90 predominantly by recognition of the MEEVD-motif via its TPR domian. As Hsp90 and Hsp70 share the conserved EEVD-motif at the C-terminus, UNC-45 had also been analyzed for physical interaction with the general Hsp70 chaperone, but the results were contradictory (CELL2013, Barral2002). This study provides AUC analyses that let conclude a TPR independent interaction of UNC-45 with Hsc70, although it cannot be excluded that weak interaction between the IEEVD-peptide contribute to the formation of the complex. It is possible that Hsc70 undergoes a chaperone-substrate association with UNC-45 regarding the fact that a deletion construct of the cochaperone was used. UNC-45(1-461) might fold only partially into its native fold and further analyses using the full-length protein will help to scrutinize this interaction. A great advantage of the nematode

model system is that fluorescently labeled protein can be studied *in vivo* in their respective tissues. The generation of a transgenic *C. elegans* line expressing YFP-tagged Hsp90 and CFP-labeled UNC-45 in the same cell types, as reported in this thesis, enables a thorough examination of the protein interplay under various conditions. As such, gene knock-down of several members of the Hsp90 network or other induction of stress will allow the analysis of the spacial and temporal regulation of Hsp90 and UNC-45 on the muscular ultrastructure.

5. References

Ali A, Zhang J, Bao S, Liu I, Otterness D, Dean NM, Abraham RT, Wang XF (2004) Requirement of protein phosphatase 5 in DNA-damage-induced ATM activation. *Genes & development* **18:** 249-254

Anfinsen CB (1973) Principles that govern the folding of protein chains. *Science* **181:** 223-230

Anfinsen CB, Haber E, Sela M, White FH, Jr. (1961) The kinetics of formation of native ribonuclease during oxidation of the reduced polypeptide chain. *Proceedings of the National Academy of Sciences of the United States of America* **47:** 1309-1314

Ao W, Pilgrim D (2000) Caenorhabditis elegans UNC-45 is a component of muscle thick filaments and colocalizes with myosin heavy chain B, but not myosin heavy chain A. *The Journal of cell biology* **148:** 375-384

Bahl R, Bradley KC, Thompson KJ, Swain RA, Rossie S, Meisel RL (2001) Localization of protein Ser/Thr phosphatase 5 in rat brain. *Brain research Molecular brain research* **90:** 101-109

Ballinger CA, Connell P, Wu Y, Hu Z, Thompson LJ, Yin LY, Patterson C (1999) Identification of CHIP, a novel tetratricopeptide repeat-containing protein that interacts with heat shock proteins and negatively regulates chaperone functions. *Molecular and cellular biology* **19:** 4535-4545

Barral JM, Bauer CC, Ortiz I, Epstein HF (1998) Unc-45 mutations in Caenorhabditis elegans implicate a CRO1/She4p-like domain in myosin assembly. *The Journal of cell biology* **143:** 1215-1225

Barral JM, Hutagalung AH, Brinker A, Hartl FU, Epstein HF (2002) Role of the myosin assembly protein UNC-45 as a molecular chaperone for myosin. *Science* **295:** 669-671

Barstead RJ, Moerman DG (2006) C. elegans deletion mutant screening. *Methods in molecular biology* **351:** 51-58

Baumgrass R, Weiwad M, Erdmann F, Liu JO, Wunderlich D, Grabley S, Fischer G (2001) Reversible inhibition of calcineurin by the polyphenolic aldehyde gossypol. *Journal of Biological Chemistry* **276:** 47914-47921

Behra M, Cousin X, Bertrand C, Vonesch JL, Biellmann D, Chatonnet A, Strahle U (2002) Acetylcholinesterase is required for neuronal and muscular development in the zebrafish embryo. *Nature neuroscience* **5:** 111-118

Bell DR, Poland A (2000) Binding of aryl hydrocarbon receptor (AhR) to AhR-interacting protein. The role of hsp90. *The Journal of biological chemistry* **275:** 36407-36414

Bernick EP, Zhang PJ, Du S (2010) Knockdown and overexpression of Unc-45b result in defective myofibril organization in skeletal muscles of zebrafish embryos. *BMC cell biology* **11:** 70

Brenner S (1974) The genetics of Caenorhabditis elegans. *Genetics* **77:** 71-94

Brinker A, Scheufler C, Von Der Mulbe F, Fleckenstein B, Herrmann C, Jung G, Moarefi I, Hartl FU (2002) Ligand discrimination by TPR domains. Relevance and selectivity of EEVD-recognition in Hsp70 x Hop x Hsp90 complexes. *The Journal of biological chemistry* **277:** 19265-19275

Brunden KR, Trojanowski JQ, Lee VM (2009) Advances in tau-focused drug discovery for Alzheimer's disease and related tauopathies. *Nature reviews Drug discovery* **8:** 783-793

Bukau B, Deuerling E, Pfund C, Craig EA (2000) Getting newly synthesized proteins into shape. *Cell* **101:** 119-122

Bukau B, Weissman J, Horwich A (2006) Molecular chaperones and protein quality control. *Cell* **125:** 443-451

Carrello A, Allan RK, Morgan SL, Owen BA, Mok D, Ward BK, Minchin RF, Toft DO, Ratajczak T (2004) Interaction of the Hsp90 cochaperone cyclophilin 40 with Hsc70. *Cell stress & chaperones* **9:** 167-181

Chen MS, Silverstein AM, Pratt WB, Chinkers M (1996) The tetratricopeptide repeat domain of protein phosphatase 5 mediates binding to glucocorticoid receptor heterocomplexes and acts as a dominant negative mutant. *The Journal of biological chemistry* **271:** 32315-32320

Chen MX, McPartlin AE, Brown L, Chen YH, Barker HM, Cohen PT (1994) A novel human protein serine/threonine phosphatase, which possesses four tetratricopeptide repeat motifs and localizes to the nucleus. *The EMBO journal* **13:** 4278-4290

Cher C, Tremblay MH, Barber JR, Chung Ng S, Zhang B (2010) Identification of chaulmoogric acid as a small molecule activator of protein phosphatase 5. *Applied biochemistry and biotechnology* **160:** 1450-1459

Cliff MJ, Harris R, Barford D, Ladbury JE, Williams MA (2006) Conformational diversity in the TPR domain-mediated interaction of protein phosphatase 5 with Hsp90. *Structure* **14:** 415-426

Cliff MJ, Williams MA, Brooke-Smith J, Barford D, Ladbury JE (2005) Molecular recognition via coupled folding and binding in a TPR domain. *Journal of molecular biology* **346:** 717-732

Codina M, Li J, Gutierrez J, Kao JP, Du SJ (2010) Loss of Smyhc1 or Hsp90alpha1 function results in different effects on myofibril organization in skeletal muscles of zebrafish embryos. *PloS one* **5:** e8416

Cortajarena AL, Kajander T, Pan W, Cocco MJ, Regan L (2004) Protein design to understand peptide ligand recognition by tetratricopeptide repeat proteins. *Protein engineering, design & selection : PEDS* **17:** 399-409

Cortajarena AL, Regan L (2006) Ligand binding by TPR domains. *Protein science : a publication of the Protein Society* **15:** 1193-1198

Cortajarena AL, Wang J, Regan L (2010) Crystal structure of a designed tetratricopeptide repeat module in complex with its peptide ligand. *The FEBS journal* **277:** 1058-1066

Crevel G, Bennett D, Cotterill S (2008) The human TPR protein TTC4 is a putative Hsp90 co-chaperone which interacts with CDC6 and shows alterations in transformed cells. *PloS one* **3:** e0001737

D'Andrea LD, Regan L (2003) TPR proteins: the versatile helix. *Trends in biochemical sciences* **28:** 655-662

Davies TH, Ning YM, Sanchez ER (2005) Differential control of glucocorticoid receptor hormone-binding function by tetratricopeptide repeat (TPR) proteins and the immunosuppressive ligand FK506. *Biochemistry* **44:** 2030-2038

Dean DA, Urban G, Aragon IV, Swingle M, Miller B, Rusconi S, Bueno M, Dean NM, Honkanen RE (2001) Serine/threonine protein phosphatase 5 (PP5) participates in the regulation of glucocorticoid receptor nucleocytoplasmic shuttling. *BMC cell biology* **2:** 6

Dill KA, Chan HS (1997) From Levinthal to pathways to funnels. *Nature structural biology* **4:** 10-19

Du SJ, Li H, Bian Y, Zhong Y (2008) Heat-shock protein 90alpha1 is required for organized myofibril assembly in skeletal muscles of zebrafish embryos. *Proceedings of the National Academy of Sciences of the United States of America* **105:** 554-559

Dupuy D, Bertin N, Hidalgo CA, Venkatesan K, Tu D, Lee D, Rosenberg J, Svrzikapa N, Blanc A, Carnec A, Carvunis AR, Pulak R, Shingles J, Reece-Hoyes J, Hunt-Newbury R, Viveiros R, Mohler WA, Tasan M, Roth FP, Le Peuch C, Hope IA, Johnsen R, Moerman DG, Barabasi AL, Baillie D, Vidal M (2007) Genome-scale analysis of in vivo spatiotemporal promoter activity in Caenorhabditis elegans. *Nature biotechnology* **25:** 663-668

Duverger Y, Belougne J, Scaglione S, Brandli D, Beclin C, Ewbank JJ (2007) A semi-automated high-throughput approach to the generation of transposon insertion mutants in the nematode Caenorhabditis elegans. *Nucleic acids research* **35:** e11

Ebong IO, Morgner N, Zhou M, Saraiva MA, Daturpalli S, Jackson SE, Robinson CV (2011) Heterogeneity and dynamics in the assembly of the heat shock protein 90 chaperone complexes. *Proceedings of the National Academy of Sciences of the United States of America* **108:** 17939-17944

Eckl JM, Rutz DA, Haslbeck V, Zierer BK, Reinstein J, Richter K (2013) Cdc37 (Cell Division Cycle 37) Restricts Hsp90 (Heat Shock Protein 90) Motility by Interaction with N-terminal and Middle Domain Binding Sites. *The Journal of biological chemistry* **288:** 16032-16042

Edwards KA, Kiehart DP (1996) Drosophila nonmuscle myosin II has multiple essential roles in imaginal disc and egg chamber morphogenesis. *Development* **122:** 1499-1511

Epstein HF, Thomson JN (1974) Temperature-sensitive mutation affecting myofilament assembly in Caenorhabditis elegans. *Nature* **250:** 579-580

Etard C, Behra M, Fischer N, Hutcheson D, Geisler R, Strahle U (2007) The UCS factor Steif/Unc-45b interacts with the heat shock protein Hsp90a during myofibrillogenesis. *Developmental biology* **308:** 133-143

Etard C, Roostalu U, Strahle U (2008) Shuttling of the chaperones Unc45b and Hsp90a between the A band and the Z line of the myofibril. *The Journal of cell biology* **180:** 1163-1175

Etheridge L, Diiorio P, Sagerstrom CG (2002) A zebrafish unc-45-related gene expressed during muscle development. *Developmental dynamics : an official publication of the American Association of Anatomists* **224:** 457-460

Fairbanks G, Steck TL, Wallach DF (1971) Electrophoretic analysis of the major polypeptides of the human erythrocyte membrane. *Biochemistry* **10:** 2606-2617

Frydman J, Hohfeld J (1997) Chaperones get in touch: the Hip-Hop connection. *Trends in biochemical sciences* **22:** 87-92

Gaiser AM, Brandt F, Richter K (2009) The non-canonical Hop protein from Caenorhabditis elegans exerts essential functions and forms binary complexes with either Hsc70 or Hsp90. *Journal of molecular biology* **391:** 621-634

Gaiser AM, Kaiser CJ, Haslbeck V, Richter K (2011) Downregulation of the Hsp90 system causes defects in muscle cells of Caenorhabditis elegans. *PloS one* **6:** e25485

Gaiser AM, Kretzschmar A, Richter K (2010) Cdc37-Hsp90 complexes are responsive to nucleotide-induced conformational changes and binding of further cofactors. *The Journal of biological chemistry* **285:** 40921-40932

Galigniana MD, Harrell JM, Murphy PJ, Chinkers M, Radanyi C, Renoir JM, Zhang M, Pratt WB (2002) Binding of hsp90-associated immunophilins to cytoplasmic dynein: direct binding and in vivo evidence that the peptidylprolyl isomerase domain is a dynein interaction domain. *Biochemistry* **41:** 13602-13610

Gava LM, Goncalves DC, Borges JC, Ramos CH (2011) Stoichiometry and thermodynamics of the interaction between the C-terminus of human 90kDa heat shock protein Hsp90 and the mitochondrial translocase of outer membrane Tom70. *Archives of biochemistry and biophysics* **513:** 119-125

Gazda L, Pokrzywa W, Hellerschmied D, Lowe T, Forne I, Mueller-Planitz F, Hoppe T, Clausen T (2013) The myosin chaperone UNC-45 is organized in tandem modules to support myofilament formation in C. elegans. *Cell* **152:** 183-195

Gengyo-Ando K, Mitani S (2000) Characterization of mutations induced by ethyl methanesulfonate, UV, and trimethylpsoralen in the nematode Caenorhabditis elegans. *Biochemical and biophysical research communications* **269:** 64-69

Gething MJ, Sambrook J (1992) Protein folding in the cell. *Nature* **355:** 33-45

Guisbert E, Czyz DM, Richter K, McMullen PD, Morimoto RI (2013) Identification of a tissue-selective heat shock response regulatory network. *PLoS genetics* **9:** e1003466

Hajduk PJ, Olejniczak ET, Fesik SW (1997) One-dimensional relaxation- and diffusion-edited NMR methods for screening compounds that bind to macromolecules. *J Am Chem Soc* **119:** 12257-12261

Hartl FU (1996) Molecular chaperones in cellular protein folding. *Nature* **381:** 571-579

Haslbeck V, Eckl JM, Kaiser CJ, Lang J, Richter K (*Manuscript in preparation (b)*) The Hsp90-UNC-45 complex is regulated by the larger chaperone network.

Haslbeck V, Eckl JM, Kaiser CJ, Papsdorf K, Hessling M, Richter K (2013) Chaperone interacting TPR proteins in Caenorhabditis elegans. *Journal of molecular biology*

Haslbeck V, Eckl JM, Richter K (*Manuscript in preparation (a)*) The substrate interaction of PPH-5 is modified by two separate contact sites in the C-terminal domain of Hsp90.

Haslbeck V, Helmuth M, Alte F, Popowicz G, Schmidt W, Weiwad M, Fischer G, Gemmecker G, Sattler M, Striggow F, Groll M, Richter K (*Submitted manuscript*) Selective activation releases the autoinhibitory mechanism of protein phosphatase 5.

Haslbeck V, Kaiser CJ, Richter K (2012) Hsp90 in non-mammalian metazoan model systems. *Biochimica et biophysica acta* **1823:** 712-721

Hawkins TA, Haramis AP, Etard C, Prodromou C, Vaughan CK, Ashworth R, Ray S, Behra M, Holder N, Talbot WS, Pearl LH, Strahle U, Wilson SW (2008) The ATPase-dependent chaperoning activity of Hsp90a regulates thick filament formation and integration during skeletal muscle myofibrillogenesis. *Development* **135:** 1147-1156

Hessling M, Richter K, Buchner J (2009) Dissection of the ATP-induced conformational cycle of the molecular chaperone Hsp90. *Nature structural & molecular biology* **16:** 287-293

Hinds TD, Jr., Sanchez ER (2008) Protein phosphatase 5. *The international journal of biochemistry & cell biology* **40:** 2358-2362

Hohfeld J, Minami Y, Hartl FU (1995) Hip, a novel cochaperone involved in the eukaryotic Hsc70/Hsp40 reaction cycle. *Cell* **83:** 589-598

Hoppe T, Cassata G, Barral JM, Springer W, Hutagalung AH, Epstein HF, Baumeister R (2004) Regulation of the myosin-directed chaperone UNC-45 by a novel E3/E4-multiubiquitylation complex in C. elegans. *Cell* **118:** 337-349

Hutagalung AH, Landsverk ML, Price MG, Epstein HF (2002) The UCS family of myosin chaperones. *Journal of cell science* **115:** 3983-3990

Inoue H, Nojima H, Okayama H (1990) High efficiency transformation of Escherichia coli with plasmids. *Gene* **96:** 23-28

Iyer SP, Hart GW (2003) Roles of the tetratricopeptide repeat domain in O-GlcNAc transferase targeting and protein substrate specificity. *The Journal of biological chemistry* **278:** 24608-24616

Kabsch W (1993) Automatic Processing of Rotation Diffraction Data from Crystals of Initially Unknown Symmetry and Cell Constants. *Journal of applied crystallography* **26:** 795-800

Kachur T, Ao W, Berger J, Pilgrim D (2004) Maternal UNC-45 is involved in cytokinesis and colocalizes with non-muscle myosin in the early Caenorhabditis elegans embryo. *Journal of cell science* **117:** 5313-5321

Kachur TM, Audhya A, Pilgrim DB (2008) UNC-45 is required for NMY-2 contractile function in early embryonic polarity establishment and germline cellularization in C. elegans. *Developmental biology* **314:** 287-299

Kamath RS, Fraser AG, Dong Y, Poulin G, Durbin R, Gotta M, Kanapin A, Le Bot N, Moreno S, Sohrmann M, Welchman DP, Zipperlen P, Ahringer J (2003) Systematic functional analysis of the Caenorhabditis elegans genome using RNAi. *Nature* **421:** 231-237

Kang H, Sayner SL, Gross KL, Russell LC, Chinkers M (2001) Identification of amino acids in the tetratricopeptide repeat and C-terminal domains of protein phosphatase 5 involved in autoinhibition and lipid activation. *Biochemistry* **40:** 10485-10490

Khan LA, Nukina N (2004) Molecular and functional analysis of Caenorhabditis elegans CHIP, a homologue of Mammalian CHIP. *FEBS letters* **565:** 11-18

Kiefhaber T, Rudolph R, Kohler HH, Buchner J (1991) Protein aggregation in vitro and in vivo: a quantitative model of the kinetic competition between folding and aggregation. *Bio/technology* **9:** 825-829

Koren J, 3rd, Jinwal UK, Davey Z, Kiray J, Arulselvam K, Dickey CA (2011) Bending tau into shape: the emerging role of peptidyl-prolyl isomerases in tauopathies. *Molecular neurobiology* **44:** 65-70

Kreppel LK, Hart GW (1999) Regulation of a cytosolic and nuclear O-GlcNAc transferase. Role of the tetratricopeptide repeats. *The Journal of biological chemistry* **274:** 32015-32022

Laemmli UK (1970) Cleavage of structural proteins during the assembly of the head of bacteriophage T4. *Nature* **227:** 680-685

Lee CF, Melkani GC, Yu Q, Suggs JA, Kronert WA, Suzuki Y, Hipolito L, Price MG, Epstein HF, Bernstein SI (2011) Drosophila UNC-45 accumulates in embryonic blastoderm and in muscles, and is essential for muscle myosin stability. *Journal of cell science* **124:** 699-705

Li J, Richter K, Reinstein J, Buchner J (2013) Integration of the accelerator Aha1 in the Hsp90 co-chaperone cycle. *Nature structural & molecular biology* **20:** 326-331

Li S, Armstrong CM, Bertin N, Ge H, Milstein S, Boxem M, Vidalain PO, Han JD, Chesneau A, Hao T, Goldberg DS, Li N, Martinez M, Rual JF, Lamesch P, Xu L, Tewari M, Wong SL, Zhang LV, Berriz GF, Jacotot L, Vaglio P, Reboul J, Hirozane-Kishikawa T, Li Q, Gabel HW, Elewa A, Baumgartner B, Rose DJ, Yu H, Bosak S, Sequerra R, Fraser A, Mango SE, Saxton WM, Strome S, Van Den Heuvel S, Piano F, Vandenhaute J, Sardet C, Gerstein M, Doucette-Stamm L, Gunsalus KC, Harper JW, Cusick ME, Roth FP, Hill DE, Vidal M (2004) A map of the interactome network of the metazoan C. elegans. *Science* **303:** 540-543

Lipinski CA, Lombardo F, Dominy BW, Feeney PJ (2001) Experimental and computational approaches to estimate solubility and permeability in drug discovery and development settings. *Advanced drug delivery reviews* **46:** 3-26

Liu F, Grundke-Iqbal I, Iqbal K, Gong CX (2005a) Contributions of protein phosphatases PP1, PP2A, PP2B and PP5 to the regulation of tau phosphorylation. *The European journal of neuroscience* **22:** 1942-1950

Liu F, Iqbal K, Grundke-Iqbal I, Rossie S, Gong CX (2005b) Dephosphorylation of tau by protein phosphatase 5: impairment in Alzheimer's disease. *The Journal of biological chemistry* **280:** 1790-1796

Liu L, Srikakulam R, Winkelmann DA (2008) Unc45 activates Hsp90-dependent folding of the myosin motor domain. *The Journal of biological chemistry* **283:** 13185-13193

Lotz GP, Brychzy A, Heinz S, Obermann WM (2008) A novel HSP90 chaperone complex regulates intracellular vesicle transport. *Journal of cell science* **121:** 717-723

Luan CH, Qiu S, Finley JB, Carson M, Gray RJ, Huang W, Johnson D, Tsao J, Reboul J, Vaglio P, Hill DE, Vidal M, Delucas LJ, Luo M (2004) High-throughput expression of C. elegans proteins. *Genome research* **14:** 2102-2110

Mandelkow EM, Mandelkow E (2012) Biochemistry and cell biology of tau protein in neurofibrillary degeneration. *Cold Spring Harbor perspectives in medicine* **2:** a006247

Mayer MP, Bukau B (2005) Hsp70 chaperones: cellular functions and molecular mechanism. *Cellular and molecular life sciences : CMLS* **62:** 670-684

Mayer MP, Prodromou C, Frydman J (2009) The Hsp90 mosaic: a picture emerges. *Nature structural & molecular biology* **16:** 2-6

McConnell JL, Wadzinski BE (2009) Targeting protein serine/threonine phosphatases for drug development. *Molecular pharmacology* **75:** 1249-1261

McCoy AJ, Grosse-Kunstleve RW, Adams PD, Winn MD, Storoni LC, Read RJ (2007) Phaser crystallographic software. *Journal of applied crystallography* **40:** 658-674

Meissner B, Rogalski T, Viveiros R, Warner A, Plastino L, Lorch A, Granger L, Segalat L, Moerman DG (2011) Determining the sub-cellular localization of proteins within Caenorhabditis elegans body wall muscle. *PloS one* **6:** e19937

Mello CC, Kramer JM, Stinchcomb D, Ambros V (1991) Efficient gene transfer in C.elegans: extrachromosomal maintenance and integration of transforming sequences. *The EMBO journal* **10:** 3959-3970

Moerman DG, Fire A (1997) Muscle: Structure, Function, and Development. In *C. elegans II*, Riddle DL, Blumenthal T, Meyer BJ, Priess JR (eds), 2nd edn. Cold Spring Harbor (NY)

Mondragon A, Griffith EC, Sun L, Xiong F, Armstrong C, Liu JO (1997) Overexpression and purification of human calcineurin alpha from Escherichia coli and assessment of catalytic functions of residues surrounding the binuclear metal center. *Biochemistry* **36:** 4934-4942

Moorhead GB, De Wever V, Templeton G, Kerk D (2009) Evolution of protein phosphatases in plants and animals. *The Biochemical journal* **417:** 401-409

Morita K, Saitoh M, Tobiume K, Matsuura H, Enomoto S, Nishitoh H, Ichijo H (2001) Negative feedback regulation of ASK1 by protein phosphatase 5 (PP5) in response to oxidative stress. *The EMBO journal* **20:** 6028-6036

Murata S, Minami Y, Minami M, Chiba T, Tanaka K (2001) CHIP is a chaperone-dependent E3 ligase that ubiquitylates unfolded protein. *EMBO reports* **2:** 1133-1138

Ni L, Swingle MS, Bourgeois AC, Honkanen RE (2007) High yield expression of serine/threonine protein phosphatase type 5, and a fluorescent assay suitable for use in the detection of catalytic inhibitors. *Assay and drug development technologies* **5:** 645-653

Otero JH, Lizak B, Hendershot LM (2010) Life and death of a BiP substrate. *Seminars in cell & developmental biology* **21:** 472-478

Prasad BD, Goel S, Krishna P (2010) In silico identification of carboxylate clamp type tetratricopeptide repeat proteins in Arabidopsis and rice as putative co-chaperones of Hsp90/Hsp70. *PloS one* **5:** e12761

Price MG, Landsverk ML, Barral JM, Epstein HF (2002) Two mammalian UNC-45 isoforms are related to distinct cytoskeletal and muscle-specific functions. *Journal of cell science* **115:** 4013-4023

Prodromou C, Siligardi G, O'Brien R, Woolfson DN, Regan L, Panaretou B, Ladbury JE, Piper PW, Pearl LH (1999) Regulation of Hsp90 ATPase activity by tetratricopeptide repeat (TPR)-domain co-chaperones. *The EMBO journal* **18:** 754-762

Ramsey AJ, Chinkers M (2002) Identification of potential physiological activators of protein phosphatase 5. *Biochemistry* **41:** 5625-5632

Ramsey AJ, Russell LC, Chinkers M (2009) C-terminal sequences of hsp70 and hsp90 as non-specific anchors for tetratricopeptide repeat (TPR) proteins. *The Biochemical journal* **423:** 411-419

Ramsey AJ, Russell LC, Whitt SR, Chinkers M (2000) Overlapping sites of tetratricopeptide repeat protein binding and chaperone activity in heat shock protein 90. *The Journal of biological chemistry* **275:** 17857-17862

Richardson JM, Dornan J, Opamawutthikul M, Bruce S, Page AP, Walkinshaw MD (2007) Cloning, expression and characterisation of FKB-6, the sole large TPR-containing immunophilin from C. elegans. *Biochemical and biophysical research communications* **360:** 566-572

Richter K, Haslbeck M, Buchner J (2010) The heat shock response: life on the verge of death. *Molecular cell* **40:** 253-266

Rohl A, Rohrberg J, Buchner J (2013) The chaperone Hsp90: changing partners for demanding clients. *Trends in biochemical sciences* **38:** 253-262

Rual JF, Ceron J, Koreth J, Hao T, Nicot AS, Hirozane-Kishikawa T, Vandenhaute J, Orkin SH, Hill DE, van den Heuvel S, Vidal M (2004) Toward improving Caenorhabditis elegans phenome mapping with an ORFeome-based RNAi library. *Genome research* **14:** 2162-2168

Russell LC, Whitt SR, Chen MS, Chinkers M (1999) Identification of conserved residues required for the binding of a tetratricopeptide repeat domain to heat shock protein 90. *The Journal of biological chemistry* **274:** 20060-20063

Schafer H, Nau K, Sickmann A, Erdmann R, Meyer HE (2001) Identification of peroxisomal membrane proteins of Saccharomyces cerevisiae by mass spectrometry. *Electrophoresis* **22:** 2955-2968

Scheufler C, Brinker A, Bourenkov G, Pegoraro S, Moroder L, Bartunik H, Hartl FU, Moarefi I (2000) Structure of TPR domain-peptide complexes: critical elements in the assembly of the Hsp70-Hsp90 multichaperone machine. *Cell* **101:** 199-210

Schmid AB, Lagleder S, Grawert MA, Rohl A, Hagn F, Wandinger SK, Cox MB, Demmer O, Richter K, Groll M, Kessler H, Buchner J (2012) The architecture of functional modules in the Hsp90 co-chaperone Sti1/Hop. *The EMBO journal* **31:** 1506-1517

Schnorrer F, Schonbauer C, Langer CC, Dietzl G, Novatchkova M, Schernhuber K, Fellner M, Azaryan A, Radolf M, Stark A, Keleman K, Dickson BJ (2010) Systematic genetic analysis of muscle morphogenesis and function in Drosophila. *Nature* **464:** 287-291

Schreiber A, Stengel F, Zhang Z, Enchev RI, Kong EH, Morris EP, Robinson CV, da Fonseca PC, Barford D (2011) Structural basis for the subunit assembly of the anaphase-promoting complex. *Nature* **470:** 227-232

Silverstein AM, Galigniana MD, Chen MS, Owens-Grillo JK, Chinkers M, Pratt WB (1997) Protein phosphatase 5 is a major component of glucocorticoid receptor.hsp90 complexes with properties of an FK506-binding immunophilin. *The Journal of biological chemistry* **272:** 16224-16230

Sivils JC, Storer CL, Galigniana MD, Cox MB (2011) Regulation of steroid hormone receptor function by the 52-kDa FK506-binding protein (FKBP52). *Current opinion in pharmacology* **11:** 314-319

Sklenar V, Piotto M, Leppik R, Saudek V (1993) Gradient-Tailored Water Suppression for H-1-N-15 Hsqc Experiments Optimized to Retain Full Sensitivity. *J Magn Reson Ser A* **102:** 241-245

Song HO, Lee W, An K, Lee HS, Cho JH, Park ZY, Ahnn J (2009) C. elegans STI-1, the homolog of Sti1/Hop, is involved in aging and stress response. *Journal of molecular biology* **390:** 604-617

Srikakulam R, Liu L, Winkelmann DA (2008) Unc45b forms a cytosolic complex with Hsp90 and targets the unfolded myosin motor domain. *PloS one* **3:** e2137

Stafford WF, 3rd (1992) Boundary analysis in sedimentation transport experiments: a procedure for obtaining sedimentation coefficient distributions using the time derivative of the concentration profile. *Analytical biochemistry* **203:** 295-301

Toi H, Fujimura-Kamada K, Irie K, Takai Y, Todo S, Tanaka K (2003) She4p/Dim1p interacts with the motor domain of unconventional myosins in the budding yeast, Saccharomyces cerevisiae. *Molecular biology of the cell* **14:** 2237-2249

Tung HY, Alemany S, Cohen P (1985) The protein phosphatases involved in cellular regulation. 2. Purification, subunit structure and properties of protein phosphatases-2A0, 2A1, and 2A2 from rabbit skeletal muscle. *European journal of biochemistry / FEBS* **148:** 253-263

Vagin AA, Steiner RA, Lebedev AA, Potterton L, McNicholas S, Long F, Murshudov GN (2004) REFMAC5 dictionary: organization of prior chemical knowledge and

guidelines for its use. *Acta crystallographica Section D, Biological crystallography* **60:** 2184-2195

Vaughan CK, Mollapour M, Smith JR, Truman A, Hu B, Good VM, Panaretou B, Neckers L, Clarke PA, Workman P, Piper PW, Prodromou C, Pearl LH (2008) Hsp90-dependent activation of protein kinases is regulated by chaperone-targeted dephosphorylation of Cdc37. *Molecular cell* **31:** 886-895

Venolia L, Ao W, Kim S, Kim C, Pilgrim D (1999) unc-45 gene of Caenorhabditis elegans encodes a muscle-specific tetratricopeptide repeat-containing protein. *Cell motility and the cytoskeleton* **42:** 163-177

Venolia L, Waterston RH (1990) The unc-45 gene of Caenorhabditis elegans is an essential muscle-affecting gene with maternal expression. *Genetics* **126:** 345-353

Wandinger SK, Suhre MH, Wegele H, Buchner J (2006) The phosphatase Ppt1 is a dedicated regulator of the molecular chaperone Hsp90. *The EMBO journal* **25:** 367-376

Wang Z, Chen W, Kono E, Dang T, Garabedian MJ (2007) Modulation of glucocorticoid receptor phosphorylation and transcriptional activity by a C-terminal-associated protein phosphatase. *Molecular endocrinology* **21:** 625-634

Wechsler T, Chen BP, Harper R, Morotomi-Yano K, Huang BC, Meek K, Cleaver JE, Chen DJ, Wabl M (2004) DNA-PKcs function regulated specifically by protein phosphatase 5. *Proceedings of the National Academy of Sciences of the United States of America* **101:** 1247-1252

Wegele H, Wandinger SK, Schmid AB, Reinstein J, Buchner J (2006) Substrate transfer from the chaperone Hsp70 to Hsp90. *Journal of molecular biology* **356:** 802-811

Wesche S, Arnold M, Jansen RP (2003) The UCS domain protein She4p binds to myosin motor domains and is essential for class I and class V myosin function. *Current biology : CB* **13:** 715-724

Wohlgemuth SL, Crawford BD, Pilgrim DB (2007) The myosin co-chaperone UNC-45 is required for skeletal and cardiac muscle function in zebrafish. *Developmental biology* **303:** 483-492

Worrall LJ, Wear MA, Page AP, Walkinshaw MD (2008) Cloning, purification and characterization of the Caenorhabditis elegans small glutamine-rich tetratricopeptide repeat-containing protein. *Biochimica et biophysica acta* **1784:** 496-503

Xu W, Mollapour M, Prodromou C, Wang S, Scroggins BT, Palchick Z, Beebe K, Siderius M, Lee MJ, Couvillon A, Trepel JB, Miyata Y, Matts R, Neckers L (2012) Dynamic tyrosine phosphorylation modulates cycling of the HSP90-P50(CDC37)-AHA1 chaperone machine. *Molecular cell* **47:** 434-443

Yang J, Roe SM, Cliff MJ, Williams MA, Ladbury JE, Cohen PT, Barford D (2005) Molecular basis for TPR domain-mediated regulation of protein phosphatase 5. *The EMBO journal* **24:** 1-10

Zhang Y, Leung DY, Nordeen SK, Goleva E (2009) Estrogen inhibits glucocorticoid action via protein phosphatase 5 (PP5)-mediated glucocorticoid receptor dephosphorylation. *The Journal of biological chemistry* **284:** 24542-24552

6. Publication and patent list

Indicated chapters or parts of chapters contribute to these publications which are accepted or submitted for publication:

(1) Gaiser* AM, Kaiser* CJ, Haslbeck* V, Richter K (2011) Downregulation of the Hsp90 system causes defects in muscle cells of Caenorhabditis elegans. *PloS one* **6:** e25485

(2) Haslbeck V, Eckl JM, Kaiser CJ, Papsdorf K, Hessling M, Richter K (2013) Chaperone interacting TPR proteins in Caenorhabditis elegans. *Journal of molecular biology*

(3) Eckl JM, Rutz DA, Haslbeck V, Zierer BK, Reinstein J, Richter K (2013) Cdc37 (Cell Division Cycle 37) Restricts Hsp90 (Heat Shock Protein 90) Motility by Interaction with N-terminal and Middle Domain Binding Sites. *The Journal of biological chemistry* **288:** 16032-16042

(4) Haslbeck V, Kaiser CJ, Richter K (2012) Hsp90 in non-mammalian metazoan model systems. *Biochimica et biophysica acta* **1823:** 712-721

(5) Haslbeck V, Helmuth M, Alte F, Popowicz G, Schmidt W, Weiwad M, Fischer G, Gemmecker G, Sattler M, Striggow F, Groll M, Richter K (*Submitted manuscript*) Selective activation releases the autoinhibitory mechanism of protein phosphatase 5.

(6) Haslbeck V, Eckl JM, Richter K (Manuscript in preparation (a)) The substrate interaction of PPH-5 is modified by two separate contact sites in the C-terminal domain of Hsp90.

(7) Haslbeck V, Eckl JM, Kaiser CJ, Lang J, Richter K (*Manuscript in preparation (b)*) The Hsp90-UNC-45 complex is regulated by the larger chaperone network.

* These Authors contributed equally to this work.

The following patent has been sent to BayPat, DZNE and Max-Planck Innovation. In the next weeks this patent will be filed as a formal patent application to the European Patent Office.

Haslbeck V, Richter K, Groll M, Helmuth M, Werner S, Striggow F, Weiwad M, Fischer G. PP5-modulating Compounds.

7. Danksagung

Ich möchte mich an erster Stelle bei Johannes Buchner bedanken, der mir erlaubt hat, meine Arbeit an seinem Lehrstuhl anzufertigen, welcher durch seine Vielfalt und Größe eine enorme Produktivität zulässt.
Großer Dank gebührt Klaus Richter, der mir die Doktorarbeit in dieser Form erst ermöglicht hat und mir eine nicht selbstverständliche Freiheit in der Gestaltung und Ausarbeitung verschiedenster Fragestellungen gelassen hat, sowie den Raum, eigene Lösungsansätze zu entwickeln und zu testen. Es war ein großartiger Rahmen, um eigene Kreativität zu verwirklichen und gleichzeitig fokussiert zu bleiben. Vielen Dank für die uneingeschränkte fachliche Unterstützung und die Möglichkeit, mit anderen hervorragenden Gruppen zusammenzuarbeiten.
Bei diesen Gruppen möchte ich mich für die produktive Kollaboration bedanken, unter anderem Michael Groll und Ferdinand Alte, Frank Striggow und Martin Helmuth, Grzegorz Popowicz, Matthias Weiwad und Miriam Linnert für die Unterstützung in Halle, aber auch Bettina Schmid, Frauke van Bebber und Barbara Solchenberger für den Ausflug in die Zebrafisch-Forschung.
Ich danke auch meinen Praktikanten, die mich während meiner Doktorarbeit unterstützt haben.
Christoph, vielen Dank für tausend gute Ideen, uneingeschränkte Hilfe und dein Verständnis! Julia, team work forever, du bist die Beste und morgen lösen wir die Weltformel! Katha, vielen Dank für deine unerschütterliche gute Laune! Alina, Lars, Maike, Danae, Tilly, vielen Dank Büro 4 für diese unvergessliche Zeit im Asyl! Und tausend Dank an die vielen großartigen Leute des Lehrstuhls, como tu, Natalia, die das Arbeiten so entspannt und produktiv gemacht haben! Meine Crews aus Bachelor und Master, ohne euch wäre das Studium nicht so eine exzellente Zeit geworden! Unendlichen Dank an Anna und dem Rest der home base, ihr habt mich durch die Schule gebracht und seid einfach grandios! Martin, deine enorme Geduld, dein Verständnis und Beistand und die geteilte Freude an der Forschung haben diese Doktorarbeit so gelingen lassen, ich danke dir von Herzen, und - Ich will Pizza!
Der größte Dank gebührt meinen Eltern und ihren Partnern, die mich in allem uneingeschränkt und stets bedingungslos unterstützt haben. Vielen Dank für dieses Vertrauen.

8. Eidesstattliche Erklärung

Hiermit erkläre ich, dass ich die vorliegende Arbeit selbstständig verfasst und keine anderen als die angegebenen Quellen und Hilfsmittel verwendet habe. Diese Arbeit wurde bisher keiner Prüfungskommission vorgelegt. Teile dieser Arbeit wurden oder werden in wissenschaftlichen Journalen veröffentlicht.

München,

_____

Veronika Haslbeck